UC Santa Barbara

UC Santa Barbara Electronic Theses and Dissertations

Title

Tracing Molecules Through Oligotrophic Marine Ecosystems: Microbial Hydrocarbon Cycling and Coral Trophic Ecology

Permalink

https://escholarship.org/uc/item/7b03n1s7

Author

Love, Connor

Publication Date

2023

Peer reviewed|Thesis/dissertation

eScholarship.org Powered by the California Digital Library
University of California

UNIVERSITY OF CALIFORNIA

Santa Barbara

Tracing Molecules Through Oligotrophic Marine Ecosystems: Microbial Hydrocarbon Cycling and Coral Trophic Ecology

A dissertation submitted in partial satisfaction of the

requirements for the degree Doctor of Philosophy

in Marine Science

by

Connor R. Love

Committee in charge:

Professor David L. Valentine, Chair

Professor Alyson E. Santoro

Professor Craig A. Carlson

Professor Holly V. Moeller

June 2023

The dissertation of Connor Robert Love is approved.

_____
Alyson E. Santoro

_____
Craig A. Carlson

_____
Holly V. Moeller

_____
David L. Valentine, Committee Chair

March 2023

ACKNOWLEDGEMENTS

This work would not have been possible without the love and support of those close to me. It takes a village. To David Valentine, thank you for believing in me and giving me an opportunity to do science in your lab when I was just a recent graduate looking for a technician job. To Craig Carlson, Alyson Santoro, and Holly Moeller, thank you for the guidance in project design and data interpretation as well as opportunities to conduct field work.

To Kelsey Gosselin – from the *R/V Armstrong* cruise you have since become one of my best friends, collaborators, and lab mates. Thank you for your support in the shared troubles of analytical chemistry, the joy of cooking, and navigating the scientific and non-scientific worlds. I am so lucky to have had you as a friend in Woods Hole and now in Santa Barbara!

To the MSI Analytical Laboratory crew: Georges Paradis, Ken Marcus, Christie Yorke – thank you all for the great conversations about chemistry/ life and helping me run the EA-IRMS and GC/C-IRMS. None of these chapters would have been possible without your help.

To the Folger family – Bret and Janet thank you for housing me in Woods Hole and making me feel integrated in the community there. Bret, you have become one of my best friends and your support throughout my whole dissertation has been invaluable.

To Donovan, Kavi, and Fable – thank you for providing endless smiles, dance parties and philosophical discussions about biology. Time with you all truly nourished my soul and excitement about the natural world.

To Veronica Radice and Michael Fox – thank you for both believing in me and taking a vested interest in my growth as an early career researcher entering the world of coral trophic ecology. Mike, I'm grateful to have met you at IsoEcol in Chile in 2018; thank you for helping me design my feeding experiment in Israel, guiding me through collaborations and editing my grant proposals that enabled much of Chapter 2. Veronica, thank you for guiding me in fatty acid analysis and helping with data interpretation.

To Logan Kozal and Marie Strader – thank you for contacting me after seeing the bleaching patterns during the 2019 bleaching event. Logan, thanks for remembering that I was studying coral trophic ecology from our Schmidt meeting, Chapter 3 wouldn't have been possible without you. Marie thank you for the help in collaboration and constructing interpretation of the data.

To Clarissa Teixeira – it was so amazing to meet you at IsoEcol 2018, you have become a great friend and my favorite isotope ecologist. Thank you for showing me around Brasil, it was so great to meet your family and friends and experience the true local life in Curitiba and Florianópolis.

To Marleen Stuhr – thank you for collaborating with me on Chapter 2, showing me around Eilat and Bremen and housing me during 2022 ICRS! Both Germany and Israel were such amazing experiences because of you.

To the Valentine Lab – thank you for feedback and support throughout my time at UCSB. We all are doing such different projects, but I think it is so cool that we have the freedom to do so. Ellie, thank you for all the science and life conversations and the great times working on boats and in Woods Hole. Frank, thank you with all the help in ordering supplies and getting what I needed. Thank you Jon for the great conversations.

To the Fine Lab- thank you Dror, Guillehm, Na'ama, Chen, Julia and Maoz, Chapter 2 would not have been possible with all your help in Eilat! Dror thank you for the fun dives and laughs, Guillehm for project design guidance, Julia for helping me PAM corals late into the night, Chen and Na'ama for guidance around IUI and Maoz for taking me into your lab.

To the researchers, graduate students, and staff at Inter University Institute of Marine Sciences in Eilat – my work in Israel was successful because of the amazing community you have all created there. Thank you for taking me in while I was there.

To Gilad Antler, Orit Sivan and Effrat Russel – thank you for the help in getting samples all the way across Israel for preliminary isotope analysis Gilad, and thank you Orit and Effrat for running the samples.

To Chris Reddy – you are the coolest scientists I know. It was great getting to work in your lab and share an office space with you on my second visit.

To Ben Van Mooy – thank you for letting me use your lab space for extractions and helping guide data interpretation of the manuscript.

To Dylan and Michaela – thank you both for being my best friends during this PhD. Dylan I'm so lucky we wound up being roommates in my first year of grad school, your love and support and ability to crack dad jokes helped me stay light through my dissertation. Thank you Michaela for the soulful conversations and endless love.

To Robert, Alan, and Jake – to you three that know me better than anyone else. Thank you all of you for the endless love since we were kids. Times back home in the Bay are so great because of you three.

To my Family – thank you Mom and Dad for the endless support and believing in me. Thank you, Mom, for taking me out on the water at Lake Erie and teaching me how to clean fish. Thank you, Dad, for taking me boogie boarding at Stinson Beach. Thank you, Dylan and Brendan, for always letting me stay with you guys in SF.

To my late Grandpa Robert and Grandma Renée – thank you Grandma for showing me and Mom Lake Erie. Thank you for being the waterman that you were Grandpa, maintaining the old two-stroke Mercury engine that somehow worked 60 years later to go fishing, leaving behind your beloved Jacques Cousteau books, your life provided me with an endless fascination with the water.

VITA OF CONNOR R. LOVE

DECEMBER 2022

EDUCATION

Bachelor of Science in Biochemistry, University of California, Santa Barbara, June 2016
Doctor of Philosophy in Marine Science, University of California, Santa Barbara, June 2022 (expected)

PROFESSIONAL EMPLOYMENT

2016-2022: Graduate Student Researcher, Marine Science Institute, University of California Santa Barbara
2016-2022: Teaching Assistant, Department of Earth Science, University of California Santa Barbara

PUBLICATIONS

Love, C.R., Arrington, E.C., Gosselin, K.M., Reddy, C.M., Van Mooy B.A., Nelson, R.K., and Valentine D.L. Microbial production and consumption of hydrocarbons in the global ocean. *Nat Microbiol* 6, 489–498 (2021).

Love, C., Cziesielski, M.J., Hughes, H., Nowakowski, C., Rosa Marín, A. and Wilkins, K.W. (2021), Rethinking Collaboration for Coral Reef Science. Limnology and Oceanography Bulletin, 30: 16-18.

Wilkins, K.W , Rosa Marín, A., Cziesielski, M.J., Hughes, H., Love, C., Nowakowski, C. (2021), Short and long-term visions for protecting coral reefs. Limnology and Oceanography Bulletin, 30: 13-15.

Nowakowski, C., Hughes, H., Love, C., Marin, A.R., Wilkins, K. and Cziesielski, M.J. (2021), Communicating Hope for Coral Reefs. Limnology and Oceanography Bulletin, 30: 15-16.

Cziesielski, M., Hughes, H., Love, C., Marin, A.R., Nowakowski, C. and Wilkins, K.W. (2021), Channeling Hope for Reefs: A Series of Perspectives from Young Coral Reef Scientists. Limnology and Oceanography Bulletin, 30: 12-13.

Hughes, H., Cziesielski, M.J., Love, C., Nowakowski, C., Marín, A.R. and Wilkins, K.W. (2021), LOOKING TO THE FUTURE. Limnology and Oceanography Bulletin, 30: 18-19.

C. Love. Coccolithophores Respond Unexpectedly to OA. *Ocean Acidification Report* (2018)

C. Love. Pebble Mine Project Advances. *Ocean Acidification Report* (2018)

C. Love. Acidic Waters Reach Deep-Ocean Ecosystems. *Ocean Acidification Report* (2018)

AWARDS

Graduate Division Dissertation Fellowship (2022)
Schmidt Family Foundation Research Accelerator Award (2020)
Limnology and Oceanography Research Exchange (LOREX) Program Award (2018)
Wendell Phillips Woodring Memorial Graduate Fellowship (2018)
Ancillary Project position on Hawaiian Oceanographic Time Series Cruise (2017)

FIELDS OF STUDY

Major Field: Biological and Chemical Oceanography

Studies in Coral Trophic Ecology with Professor Michael Fox and Dr. Veronica Radice

Studies in Organic Geochemistry with Professor Christopher Reddy and Dave Valentine

Studies in Microbial Oceanography with Professors Craig Carlson and Alyson Santoro

ABSTRACT

Tracing Molecules Through Oligotrophic Marine Ecosystems: Microbial Hydrocarbon Cycling and Coral Trophic Ecology

by

Connor R. Love

The creation, movement, and consumption of distinct biomolecules by marine organisms has far reaching implications regarding ecosystem material and energy flow and how we manage the marine environment. Lipids are ubiquitous, energy rich biomolecules that are essential for all life and are used for cell membrane structure, energy storage and serve as useful indicators for ecosystem and food web dynamics. In this dissertation, the flow of specific lipid biomolecules through multiple marine environments is measured, explored, and clarified to better understand biogeochemical cycles, marine food webs and ecosystem connectivity.

In the first chapter of my dissertation, I measure, quantify, and close the loop of the open ocean microbial hydrocarbon cycle, with implications for priming effects of the ocean microbiome to oil spills. It is estimated that seeps, spills, and other oil pollution introduce ~ 1.3 million tons (1.3 Tg) of hydrocarbons into the ocean each year. Additionally, it is known that globally abundant marine cyanobacteria *Prochlorococcus* and *Synechococcus* which account for ~25% of ocean net primary production also produce hydrocarbons from fatty acids. But little is known about the size, turnover and fate of these cyanobacterial hydrocarbons and the implications for the ocean's microbiome response to future oil spills. From a research expedition in the North Atlantic, I report that cyanobacteria in an oligotrophic gyre mainly produce *n*-pentadecane which correlates tightly with fluorescence and

Prochlorococcus abundance in oligotrophic waters. Using chemical and isotopic tracing I find that pentadecane production and diel dynamics mainly occurs in the lower euphotic zone at the deep chlorophyll maximum. I estimate the global flux of cyanobacteria-produced pentadecane exceeds total oil input in the ocean by 100 to 500-fold, with cyanobacteria producing ~ 130-650 million tons of pentadecane per year. Analysis of sinking particles at the base of the euphotic zone show that nearly all pentadecane (< 0.001 % remaining) is consumed within the euphotic zone, suggesting near complete consumption of these hydrocarbons by hydrocarbon degrading microbes. These findings characterize a wide-spread microbial hydrocarbon cycle that selectively primes the ocean's microbiome with long-chain alkanes.

In the second chapter of my dissertation, I conduct a large-scale feeding experiment on a symbiotic reef-building coral (*Stylophora pistillata*) in the Red Sea to clarify fatty acid and isotopic biomarker patterns of coral heterotrophy for use in the field. Coral heterotrophy is an often-overlooked facet of coral nutrition that provides essential nutrients that help corals resist and recover from thermally induced bleaching that is degrading reef ecosystems around the world due to rising global ocean temperatures. Yet, methods for measuring coral mixotrophy, the balance between organic matter contributions to the coral host from autotrophic photo endosymbionts and heterotrophy on particles and plankton have typically been too coarse to elucidate source contributions. Through my experiment I show that fatty acids and isotopic biomarkers reliably separate experimental and reef nutritional source groups (heterotrophic or autotrophic). I show that heterotrophic fatty acid biomarkers are reliably recorded into coral host and symbiont tissues, with a divergent metabolic pattern of autotrophic biomarkers as feeding increases due to positive feedback of heterotrophy on the *in hospite* photo symbiont population. Additionally, I show that nitrogen and essential fatty

acids are preferentially recorded into coral tissue while most heterotrophic carbon is respired or exuded as mucous; this shows that the use of bulk carbon isotopes as a feeding proxy for the last ~ 40 years is largely underestimating the contribution of heterotrophy to the trophic ecology of reef building corals. Overall, this finding underscores a connectivity between oceanic phyto- and zooplankton and reef-building coral.

In the third chapter of my dissertation, I explore the mixotrophic differences of divergent bleaching responses of *Acropora hyacinthus* colonies on the forereef of Mo'orea during the 2019 mass bleaching event. During this bleaching event, all colonies of *A. hyacinthus* on the deep forereef (14 m) bleached and recovered, while colonies on the shallow forereef (5 m) near the reef crest resisted bleaching entirely, despite the same temperature stress. Using fatty acid and isotopic biomarkers I show through several lines of evidence that bleaching resistant colonies near the reef crest were likely consuming more particulate organic matter than deep forereef colonies. This conclusion is supported by isotopic feeding proxies, less isotopic niche overlap of the host and symbiont of resistant colonies, and larger proportions of putative POM fatty acid biomarkers in the host of resistant colonies relative to recovered colonies. This interpretation is in line with observations that benthic communities on the reef crest are a net sink of oceanic POM and that increased reliance on heterotrophy is associated with bleaching resistance. These data show the vital importance of reef environment, coral heterotrophy, and planktonic subsidies in structuring bleaching response of corals in a warming ocean and ultimately show that the reef crest may serve as a potent zone for reseeding coral populations after marine heat waves.

TABLE OF CONTENTS

CHAPTER 1

Microbial Production and Consumption of Hydrocarbons in the Global Ocean

This chapter was published in Love et al., 2021. I will discuss only my work on the production, dynamics, and geochemical budget of the microbial hydrocarbon cycle but the paper includes contributions and discoveries on microbial hydrocarbon consumption by Eleanor Arrington who included her work in greater detail in her dissertation.

1.1 Abstract

Seeps, spills and other oil pollution introduce hydrocarbons into the ocean. Marine cyanobacteria also produce hydrocarbons from fatty acids, but little is known about the size and turnover of this cyanobacterial hydrocarbon cycle. We report that cyanobacteria in an oligotrophic gyre mainly produce *n*-pentadecane and that microbial hydrocarbon production exhibits stratification and diel cycling in the sunlit surface ocean. Using chemical and isotopic tracing we find that pentadecane production mainly occurs in the lower euphotic zone. With a multifaceted approach, we estimate that the global flux of cyanobacteria produced pentadecane exceeds total oil input in the ocean by 100 to 500-fold. We show that rapid pentadecane consumption sustains a population of pentadecane-degrading bacteria, and possibly archaea. Our findings characterize a microbial hydrocarbon cycle in the open ocean that dwarfs oil input. We hypothesize that cyanobacterial hydrocarbon production selectively primes the ocean's microbiome with long-chain alkanes whereas degradation of other petroleum hydrocarbons is controlled by factors including proximity to petroleum seepage.

1.2 Introduction

1.2.1 Marine Hydrocarbons

Hydrocarbons are ubiquitous in the marine environment and can come from a variety of sources including natural seepage, anthropogenic spills, and biological production. Natural seepage and spills typically release a complex mixture of hydrocarbons known as petroleum whereas biological production typically produces only a handful of different hydrocarbons.

Petroleum (or crude oil) is formed over millions of years via geo-thermal chemical reactions that act on biological debris from sinking organic matter in the ocean. In these reactions biological molecules such as lipids, amino acids, carbohydrates, and nucleic acids get stripped of their functional groups (nitrogen, oxygen, phosphorus) via sustained pressure and heat to form hydrocarbons. Petroleum contains a complex mixture of thousands of hydrocarbons that are highly reduced and energy rich. These hydrocarbons are then released from their reservoirs by human extraction and natural seepage. Estimates of oil input to the ocean via natural seeps and industrial spills associated with extraction, transportation and consumption of oil total ~1.3 Tg per year (National Research Council, 2003). The anthropogenic release of petroleum hydrocarbons to the marine environment has garnered significant attention due to ecologically catastrophic and often preventable events like the Deepwater Horizon blowout, the Exxon Valdez tanker spill, and the Kalamazoo River pipeline breach. Consequently, the ability of native ocean microbes to catabolically break down hydrocarbons to carbon dioxide (Prince et al., 2018) and what controls this has also gathered significant attention and research as a potential solution to clean-up marine oil spills.

While petroleum is composed of thousands of different compounds, marine microorganisms naturally produce a much smaller subset of hydrocarbon compounds (at

geochemically significant levels) such as methane (Repeta et al., 2016; Saunois et al., 2020), isoprene (McGenity et al., 2018) and ethylene (Seifert et al., 1999) as well as phytoplankton producing C15-C19 alkanes and alkenes (Coates et al., 2014; Han et al., 1968; Li et al., 2010; White et al., 2019). While the production of small molecular weight hydrocarbons such as methane, isoprene and ethylene have been studied extensively, the production, consumption, and fate of medium chain (C15-C19) alkanes and alkenes produced by phytoplankton has scarcely been studied. It is known that medium chain hydrocarbons (C_{15}-C_{19}) are produced by cyanobacteria in a two-step decarboxylation of fatty acids (Coates et al., 2014) and predominantly localize to the thylakoid and cytoplasmic membranes due to their hydrophobic properties. Through membrane modeling and empirical observations hydrocarbons are shown to help promote membrane curvature for tightly packed membrane structures in cyanobacteria (Lea-Smith et al., 2016). This suggests a fundamental physiochemical role of these compounds in cyanobacteria physiology and photosynthetic function.

To estimate the production of hydrocarbons by cyanobacteria and contribution to the global marine hydrocarbon budget Lea-Smith et al. (2015) measured the dry weight percent of hydrocarbons of laboratory cultures for two globally abundant marine cyanobacteria *Prochlorococcus* and *Synechococcus* (known to account for ~25% of global ocean net primary productivity; Flombaum et al., 2013) and scaled these estimates by known doubling times of these cyanobacteria. The authors estimated primary production of hydrocarbons from these two cyanobacteria, in which pentadecane ($n$$C_{15}$) comprised ~ 85 % of total hydrocarbons, exceeds total petroleum input to the ocean from natural and anthropogenic sources per year (~ 1.3 Tg) by ~ two orders of magnitude (308-771 Tg; Lea-Smith et al., 2015). Importantly, the authors note that cyanobacteria lack metabolic degradation pathways for these

hydrocarbons (Lea-Smith et al., 2015) and since these hydrocarbons are not accumulating in the ocean, this suggests external degradation of these hydrocarbons (Valentine & Reddy, 2015).

1.2.2 Prevalence of Marine Hydrocarbon Degrading Bacteria

Hydrocarbon degrading bacteria have been found in almost every environment in the ocean, even in waters minimally polluted by petroleum (Nie et al., 2014; Yakimov et al., 2007). Yakimov et al. hypothesized that many obligate hydrocarbon degrading bacteria (principally *Alcanivorax*, *Marinobacter*, *Thallassolituus*, *Cycloclasticus* and *Oleispira)* exist in relatively low abundance or undetectable levels and then bloom when there is a significant source of hydrocarbons present (oil or specific compounds; Yakimov et al., 2005). The prevalence of hydrocarbon degrading bacteria in unpolluted waters appears to be supported by the constant primary production of hydrocarbons by marine phytoplankton (Lea-Smith et al., 2015; Love et al., 2021). As such, this short term hydrocarbon cycle was termed the "cryptic" marine hydrocarbon cycle (Lea-Smith et al., 2015; Valentine & Reddy, 2015) due to low concentrations of hydrocarbons (Gschwend et al., 1980; Love et al., 2021) and hydrocarbon degrading microbes (Yakimov et al., 2007), but one fundamental to the role of the oceans native ability to degrade hydrocarbons.

It has been shown clearly in the North Atlantic oligotrophic gyre that water and particles of marine snow harbor *n*-alkane degrading specialists bacteria that bloom readily when fed pentadecane (nC$_{15}$), a known hydrocarbon produced by *Prochlorococcus* (Arrington, 2021; Love et al., 2021). Furthermore, Arrington (2021) shows through analysis on the North Atlantic region within the Tara Oceans dataset (Sunagawa et al., 2015) that there is a higher abundance of *alkB*-like genes (which catalyzed the first step of medium-chain

alkane degradation) in the surface ocean and deep chlorophyll maximum where *Prochlorococcus* resides over genes that catalyze oxidation of petroleum hydrocarbons such as C_1-C_5 alkanes, phenanthrene, benzene, toluene, naphthalene, xylene, cymene, and biphenyl. Ultimately, Arrington shows the ubiquitous nature of native ocean microbes to degrade long-chain *n*-alkanes made by cyanobacteria whereas model petroleum hydrocarbon degradation of short chain alkanes, ring structures and aromatics is controlled by proximity to natural seepage due to biogeographic priming of the native microbial populations (Love et al., 2021).

1.2.3 The Marine Hydrocarbon Cycle

The hypothesis of the latent (hidden) marine hydrocarbon cycle states that the photosynthetic production of hydrocarbons, namely C_{15}-C_{19} alkanes and alkenes sustains hydrocarbon degrading bacteria in regions where there is no natural seepage that can then respond to oil input like a spill (Lea-Smith et al., 2015). While Arrington clearly shows the oceans inherent ability to consume medium chain alkanes produced by cyanobacteria, the biogeochemical production, dynamics and controls of the marine hydrocarbon cycle have not been directly observed or closed.

In this chapter, I directly measure hydrocarbon stock and production in an oligotrophic gyre which comprise ~ 40% of the Earth's surface (Karl & Church, 2014; Polovina et al., 2008). I show that pentadecane tightly correlates with cyanobacterial abundance and fluorescence and explore the oceanographic controls of production due to dissolved nutrients and *Prochlorococcus* physiology at the deep chlorophyll maximum. Lastly, I report two different geochemical estimates derived from oceanographic measurements that both confirm annual production of hydrocarbons by cyanobacteria exceeds total oil input from seeps, spills and extraction by ~ two orders of magnitude.

1.3 Methods

1.3.1 *in situ* Sampling and Quantification of Hydrocarbon Production

Water was collected with a rosette equipped with 12 L Niskin bottles just after sunrise (~ 8 AM) for all sampling except for the diel experiment. Salinity, density, temperature, fluorescence, and percent photosynthetically active radiation (% PAR) were measured semi-continuously for each hydrocast. For diel sampling, a Lagrangian framework was used by following deployed particle traps set just below the DCM (150 m) and sampled at six-hour intervals through a full 24-hour cycle. Sampling targeted six light-penetration levels with depths held constant following initial collection, plus the DCM, which is a depth-variable feature. Water was collected from the Niskin into 2 L polycarbonate bottles via a polyvinyl chloride tube equipped with a 200 μm mesh to filter out large zooplankton. Precautions were taken to avoid contamination from the vessel and validated with controls. For example, the entire CTD rosette was cleaned with a brush and MilliQ water before the cast and was moved into a secure bay for sampling. To avoid exhaust and fumes, the vessel was oriented into the wind during sampling and certain activities were disallowed during sampling (i.e. smoking and painting). Control samples were collected by pouring clean MilliQ water into the Niskin bottles and letting it sit for 30 minutes and then filtering the water using the same procedure for all samples. No pentadecane of considerable quantity (> 2 ng L^{-1}) was found in control samples and thus validated efforts to minimize contamination. As a secondary check, we also collected diesel from the vessel and extracted and ran the extract on the Gas Chromatograph. This diesel had a distinct multi-hydrocarbon fingerprint that we did not observe in any of our chromatograms. For *in situ* hydrocarbon concentration measurements, water in the 2 L polycarbonate bottles was immediately filtered through a 0.22 μm Teflon filter under gentle

vacuum with an oil-less vacuum pump. Captured particles (sediment trap deployed for 24 hr at 150 m) were also filtered onto 0.22 μm Teflon filters. For the hydrocarbon production experiment ^{13}C-bicarbonate tracer solution (with 45 g L^{-1} NaCl to sink the tracer to the bottom of the bottle) made from ^{13}C-sodium bicarbonate (Cambridge Isotope Laboratories Inc., ^{13}C 99%) was added to the 2L polycarbonate bottles to achieve a 480 ‰ enrichment in seawater DIC. Dark control bottles were covered completely beforehand with aluminum foil before tracer addition and kill control bottles were treated with Zinc Chloride to 2% $ZnCl_2$ (m/v) before tracer addition. 2 L bottles were then immediately placed into black mesh bags to attenuate light to the value from which it was collected (either 30%, 10% or 1% PAR) and placed into on-board seawater incubators with a continuous flow of surface water; this was marked as the start of incubation. No artificial light was used. Black mesh bags were made by stitching together rolls of commercial-grade neutral-density window screen material(Reshkin & Knauer, 1979) and photosynthetically active radiation attenuation by the bags was quantified using a spherical quantum sensor (Licor). Bottles were harvested at 0-hour (initial), 5, 10, 20 and 30-hour (final) time points for the 30% PAR light bags and at t = 0 hour and t = 30-hour final for the 10% and 1% light levels, care was taken to reduce light exposure in the ship-board laboratory when preparing for incubation by placing bottles into covered tubs. A 2 mL aliquot was taken for ^{13}C-DIC prior to filtration. Filters were placed into pre-combusted aluminum foil packets and immediately frozen at -20° C for later analysis.

A preliminary culture experiment was conducted to assess the percent of all cyanobacterial hydrocarbons within membranes, i.e. what percent of total cyanobacterial hydrocarbons our extraction protocol was capturing. We compared two types of extractions, the modified Bligh and Dyer used in this study (described below) to extract membrane lipids

from cells filtered on a 0.22 μm Teflon filter and an extraction of frozen cell culture that includes cells and the culture medium. A comparison of these results provides the proportion of hydrocarbons found within cell membranes versus total hydrocarbons inclusive of those interior and exterior to cells. We conducted a triplicate measurement of this ratio from a culture of *Synechocystis*. Of the two hydrocarbons that *Synechocystis* makes in abundance (*n*-heptadecane and 8-heptadecene), we found that 98 ± 17 % of total *n*-heptadecane and 82 ± 9 % of 8-heptadecene were cell associated. We interpret this to mean that the majority of hydrocarbons, particularly saturated *n*-alkanes, reside within the biological membranes of cyanobacteria or adsorb to particulate matter including cellular necromass. This is further supported by work done by Lea-Smith et al., 2016 and the low solubility of straight chain hydrocarbons 15-17 carbons in length.

1.3.2 Hydrocarbon Extraction and Analysis

A modified Bligh-Dyer (Van Mooy et al., 2008) was used to extract hydrocarbons from membranes of frozen cells collected on Teflon filters. Dodecahydrotriphenylene (internal standard) and C23 ethyl ester (secondary internal standard and transesterification standard if needed) were added to the dry filter before extraction. Two-thirds of the amounts of each solvent was used according to Van Mooy et al. 2008 and a 10-minute sonication step was added after addition of the first solvents. An additional extraction into 1.0 mL of DCM was conducted after the first lower organic phase was removed to extract any remaining hydrocarbons from the filter, this was added to the first DCM extract for a final extract volume of 3.0 mL of DCM. Once extracted into dichloromethane, sodium sulfate was added for drying, ~40 μL of toluene was added to prevent complete dryness of the extracts and then the solution was rotary evaporated to ~30 μL and placed into a 2 mL GC-vial with a combusted

glass insert. Before analysis, a small volume of C23 methyl ester (external standard) was added. All glassware and solid chemicals were pre-combusted before use. Concentration analysis was done on a gas chromatograph flame ionization detector (GC-FID) HP-Agilent 6890 GC FID. Chromatography was performed with a 30 m x 0.25 mm ID, 0.25 μm pore size, fused silica Restek 13323 Rxi-1 MS Capillary Column with a splitless 2 μL injection. Initial oven temperature was at 70 °C held for 2 minutes, a 3 °C min^{-1} ramp to 120 °C, then a 6 °C min^{-1} ramp to the final temperature of 320 °C. A standard mix of pentadecane, heptadecane, internal standard, external standard and transesterification standard was run to calibrate response factors for every batch of samples (~20 per batch). Blanks were run every ~ six samples and peaks were manually integrated, there were no co-eluting peaks for pentadecane or heptadecane in oligotrophic samples (all stations but station 1 on continental shelf). Comprehensive two-dimensional chromatography, GCxGC-FID and GCxGC-TOF (Time of Flight), was used on select samples to check for other hydrocarbons, contaminants, and quality of blank filters run through the extractive process.

GC×GC-FID and –TOF chromatographic analyses were performed on Leco systems consisting of an Agilent 7890A GC configured with a split/splitless auto-injector (7683B series) and a dual stage cryogenic modulator (Leco, Saint Joseph, Michigan). Samples were injected in splitless mode. The cold jet gas was dry N_2 chilled with liquid N_2. The hot jet temperature offset was 15 °C above the temperature of the main GC oven and the inlet temperature was isothermal at 310 °C. Two capillary GC columns were utilized in this GC×GC experiment. The first-dimension column was a Restek Rxi-1ms, (60-m length, 0.25 mm I.D., 0.25 μm df) and second-dimension separations were performed on a 50% phenyl polysilphenylene-siloxane column (SGE BPX50, 1.2-m length, 0.10 mm I.D., 0.1 μm df). The

temperature program of the main oven was held isothermal at 50 °C (15 min) and was then ramped from 50 to 335 °C at a rate of 1.5 °C min^{-1}. The second-dimension oven was isothermal at 60 °C (15 min) and then ramped from 60 to 345 °C at a rate of 1.5 °C min^{-1}. The hot jet pulse width was 0.75 seconds, while the modulation period between stages was 7.50 seconds and a 3.00 second cooling period, for the FID method, and 10.00 seconds and a 4.25 second cooling period for the TOF method. FID data was sampled at an acquisition rate of 100 data points per second, while the TOF data was sampled at an acquisition rate of 50 spectra per second in the mass range of 40 to 500 atomic mass units (amu). Different modulation periods were used due to differences in the GC×GC instrument, for example, the GC×GC-FID combusts the column effluent at atmospheric pressure while in the GC×GC-TOF instrument, column effluent must move through a heated transfer line into the ion source. Since the total distance between detector and secondary oven is different between these two instruments, optimization of the chromatographic plane requires slight modifications to the GC×GC methods.

1.3.3 Compound-specific and Dissolved Inorganic Carbon Isotope Measurements

Compound-specific isotope analysis was performed after concentration analysis on a gas chromatograph combustion isotope ratio mass spectrometer (GC/C-IRMS) with a Trace GC (Thermo Finnigan) set up to a GC-C/TC III (Finnigan™) interface and a Delta^{plus} XP isotope ratio mass spectrometer (Thermo Finnigan). A J & W Scientific DB-5 Capillary column (30 m, 0.25 mm, 0.25 μm) was used with 2 μL manual injections. Temperature ramp was conducted starting at 70 °C and held for 2 minutes, then a 3 °C min^{-1} ramp to 120 °C, hold for 0 minutes, then a 6 °C min^{-1} ramp to 185 °C, hold for 0 minutes then a 120 °C min^{-1} ramp to 290 °C, hold for 3 minutes. Inlet temperature was 260 °C, flow rate was held at 2.2

mL He min^{-1} with a splitless injection held for 0.5 minutes after injection. Isotope ratio accuracy was calibrated with a C_{14} fatty acid methyl ester Schimmelmann reference material to Vienna PeeDee Belemnite. Precision was accounted for with a standard mix of nC_{15}, nC_{16} and nC_{17} at ~1.2 ng µL $^{-1}$ and was run between every batch of ~20 samples. Peaks were manually integrated after establishing the baseline, analytical precision was ~0.9 ‰ $\delta^{13}C$ for pentadecane.

Dissolved inorganic carbon ^{13}C isotope ratio measurements were made on a Gas Bench II (Thermo Finnigan) interfaced to the same Delta^{plus} XP isotope ratio mass spectrometer (Thermo Finnigan) used for the compound-specific analysis. Sample preparation and analysis were followed closely to the protocol outlines by the University of California, Davis, Stable Isotope Facility (https://stableisotopefacility.ucdavis.edu/dictracegas.html).

1.3.4 Cell Counts and Dissolved Nutrient Analysis

Sampling for nutrients and cell counts was conducted on the CTD cast immediately before the casts for hydrocarbon sampling (~ 1-hour difference), these casts were all at ~sunrise. Parallel sampling was conducted with the same cast water for the diel sampling. Flow cytometry analysis was performed by the Bigelow Laboratory for Ocean Sciences using a slightly modified protocol from Lomas et al., 2010. Samples were fixed with paraformaldehyde (0.5% final concentration) and stored at ~4 °C for 1-2 hours before long term storage in liquid nitrogen. An Influx cytometer was used with a 488 nm blue excitation laser, appropriate Chl-a (692 ± 20 nm) and phycoerythrin (585 ± 15 nm) bandpass filters, and was calibrated daily with 3.46 µm Rainbow Beads (Spherotech Inc. Lake Forest, Illinois, USA). Each sample was run for 4–6 min (~0.2–0.3 ml total volume analyzed), with log-

amplified Chl-a and phycoerythrin fluorescence, and forward and right-angle scatter signals recorded. Data files were analyzed from two-dimensional scatter plots based on red or orange fluorescence and characteristic light scattering properties (Durand & Olson, 1996) using FlowJo 9.8 Software (Becton Dickinson, San Jose, CA). Pico-autotrophs were identified as either *Synechococcus* or *Prochlorococcus*, pico-eukaryotes or nano-eukaryotes based upon cell size and the presence or absence of phycoerythrin. Nutrients were analyzed by the University of Washington Marine Chemistry Laboratory.

1.3.5 Calculations and Analyses, Statistics and Reproducibility

All statistics and points within figures were conducted with distinct samples (not replicated measurements of the same sample). Pentadecane production from compound-specific isotope enrichment measurements were calculated using a published equation (López-Sandoval et al., 2018). The time duration used in the equation was from complete set up of the incubation to completion of filtering the water through the filter. The value used for ^{13}C-DIC was the average of the whole dataset ($\delta^{13}C$ = 480‰) and the value used for unlabeled pentadecane was from a non-enriched sample ($\delta^{13}C$ = -20‰) because of variations in the time zero values from a slight but inevitable enrichment when bottles were filtered in the laboratory (roughly one hour to filter the whole bottle in a well-illuminated laboratory space).

Considering that 30% and 10% PAR waters were at a steady state with respect to pentadecane concentration, we used a modified primary production calculation using ^{13}C enrichment from López-Sandoval et al., 2018, to calculate the production of pentadecane. The concentration of pentadecane for the 1% PAR incubation increased over the 30-hour incubation for most oligotrophic stations (Extended Data Figure 2), violating an assumption outlined by López-Sandoval et al (2018). We thus chose to compare two approaches:

calculation of production via concentration data only and calculation using ^{13}C from López-Sandoval et al., 2018. Ultimately, we chose to use the isotope-predicted production rates of pentadecane because loss processes were clearly evident from the comparison of the two approaches.

Statistical analyses were conducted using R within RStudio version 1.2.1335. Statistical analyses of single linear models were done using the R base stats package. Relative importance of regressors in multiple linear models were found using the R package 'relaimpo' and the function 'calc.relimp()'. Source data is provided. Reproduction of experiments at the same station was not possible due to time constraints, space on-board and resources.

1.3.6 Quantification of global stock and production for cyanobacterial alkanes: Method 1

Method 1 draws from direct observations of water column pentadecane stock and production rates encountered in the North Atlantic subtropical gyre. We integrated the depth profiles of pentadecane concentration for stations 4, 6 and 8 to calculate a mean water column integrated stock of pentadecane with standard deviation and further integrated primary production rates of pentadecane for stations 4, 5 and 8 from our isotope enrichment incubation experiments, to obtain a mean water column production rate with standard deviation. Calculation of pentadecane stock results in an average water column integrated stock of pentadecane of 3.42 ± 0.83 mg m^{-2}, and when scaled by the mean areal extent of the oligotrophic ocean (estimated at 204×10^6 km^2) results in a standing stock of 0.70 ± 0.17 Tg (Table 1). Calculation of pentadecane production rate results in 1.76 ± 0.17 mg pentadecane m^{-2} d^{-1}, which multiplied by the areal extent of the oligotrophic ocean yields 131 ± 13 Tg pentadecane per year (Table 1).

To integrate pentadecane stock in the water column we integrated station 4, 6 and 8 depth profiles because of suitable data coverage. Integration was performed by taking a data point to be the center of a rectangle, with the ends of rectangles meeting halfway between data points on the depth axis. For the data closest to the surface, we assume that the stock stays at that value from the depth of collection to the surface. If the deepest data is shallower than 200 m (station 4) we assume that the pentadecane concentration attenuates to 0 ng L^{-1} at 200 m depth and thus integrated the area from the deepest rectangle to 200 m as a triangle. If the deepest data goes to 200 m or deeper (station 6 and 8), we integrated the height of the deepest rectangle as the value of the data found beyond 200 m, and chose this data to be the deepest endmember of our integration.

To integrate pentadecane production rate throughout the water column we used "typical" oligotrophic stations that had production measurements at 30%, 10% and 1% PAR (stations 4, 5 and 8). All three stations had a very similar trend in productivity (Figure 2A). We integrated by taking the data to be the height (pentadecane productivity) of the rectangle and the width of the rectangle (depth) to be the depth halfway between data points. Integration to the surface was done by assuming that productivity remained the same from the shallowest data point to the surface. For the deep endmember we chose to retain the distance between the middle (10%) and deepest (1%) data points and carry the rectangle this same distance below the 1% PAR data point depth.

1.3.7 Quantification of global stock and production for cyanobacterial alkanes: Method 2

Method 2 draws from all samples with co-occurring measured pentadecane concentrations as well as *Prochlorococcus* and *Synechococcus* abundance (n = 67) to establish

average per cell quantities of pentadecane across all our stations. We then used previously modeled global populations of *Prochlorococcus* ($2.9 \pm 0.1 \times 10^{27}$) and *Synechococcus* ($7.0 \pm 0.3 \times 10^{26}$) (Flombaum et al., 2013) to scale our estimates for a global stock and utilized known doubling rates (1-2 days for *Prochlorococcus*, 1-6 days for *Synechococcus*) (Field et al., 1998; Liu et al., 1995; Mann & Chisholm, 2000; Vaulot et al., 1995; Zubkov, 2014) to scale the average per cell pentadecane content from our data to estimate a global production rate.

To differentiate the pentadecane contributions from each genus in our data, we created a multiple linear model using *Prochlorococcus* and *Synechococcus* cell counts as separate independent variables, yielding values of 0.47 ± 0.42 fg cell^{-1} for *Prochlorococcus* and 0.60 ± 0.35 fg cell^{-1} for *Synechococcus* ($R^2 = 0.768$). These values are similar to those from pure cultures of three ecotypes of *Prochlorococcus* (0.49 ± 0.23 fg/cell) and are slightly higher than reported of four strains of *Synechococcus* (0.25 ± 0.04 fg/cell), also from culture (Lea-Smith et al., 2015). From this approach we estimate the global standing stock of pentadecane from *Prochlorococcus* to be 1.4 ± 1.2 Tg and *Synechococcus* to be 0.42 ± 0.25 Tg, for a total of 1.78 ± 1.24 Tg. See Table 1 for estimates and comparisons to Lea-Smith et al. 2015.

1.4 Results & Discussion

1.4.1 Pentadecane is abundant and vertically structured in the oligotrophic ocean

Our efforts focus on the North Atlantic subtropical oligotrophic gyre for which productivity is dominated by hydrocarbon-producing cyanobacteria *Prochlorococcus* and *Synechococcus* (Chisholm et al., 1988), genera estimated to account for ~25% of the global ocean's net primary production (Field et al., 1998; Flombaum et al., 2013). Subtropical oligotrophic gyres comprise ~40% of the planet's surface (Karl & Church, 2014; Polovina et al., 2008), tend to host predominantly cyanobacterial productivity (Flombaum et al., 2013) (Figure 7), and are far from the continents and associated petroleum sources that could mask the signal of cyanobacterial hydrocarbons. Here we target the primary production of hydrocarbons by cyanobacteria in oligotrophic settings and the associated consumption by hydrocarbon-oxidizing microbes to establish the spatial context, flux and controls on the cycle.

To investigate the abundance pattern of cyanobacterial alkanes we quantified their depth distribution at seven locations in the western North Atlantic, five of which represent oligotrophic conditions and two that were more nutrient replete (Figure 1). In total, we quantified alkane concentration in 441 particulate samples ($\geq$ 0.2 μm), mainly in triplicate. It is important to note that we measured particulate samples from a filter and pentadecane (and heptadecane) is interpreted to reside primarily in the membranes of cells in the particulate phase (Lea-Smith et al., 2016, see Methods section 1.3.1). Thus, these units do not represent a truly dissolved chemical compound.

Pentadecane (nC$_{15}$) was the most abundant hydrocarbon in each sample from the five stations located in oligotrophic waters (Figure 1). Concentrations of pentadecane ranged from

2-65 ng L^{-1} in the subtropical gyre, with maximum values of ~80 ng L^{-1} for the Gulf Stream (station 3) and ~130 ng L^{-1} for a *Synechococcus* bloom (station 9). Heptadecane (nC_{17}) was found at concentrations up to 12 ng L^{-1} but was often near our detection limit of ~ 2 ng L^{-1}; additionally, heptadecane was always lower in abundance than pentadecane in waters off the continental shelf. No other hydrocarbons of measurable concentration were found in these samples.

Depth profiles of pentadecane concentration in oligotrophic waters reveal a distinctive subsurface maximum that coincides with both fluorescence and cyanobacteria cell counts (Figure 1), aligning with the deep chlorophyll maximum (DCM). Concentrations above the DCM at the surface are lower but detectable (10-15 ng L^{-1} in *Prochlorococcus* dominated waters), while they become undetectable below the DCM (Figure 1) near the base of the euphotic zone (150-200 m). The observed coupling of pentadecane concentration with cell abundance is consistent with pentadecane occurrence primarily within cyanobacterial cells (Lea-Smith et al., 2016) (> 98%), a finding further supported by observations of diel cycling (Figure 2c, d; Figure 5) and cultivation work (see Methods section 1.3.1). Heptadecane shows no coherent spatial patterns or relationships with other variables likely due to the inability of our analytical procedure to measure concentrations < 2 ng L^{-1} with suitable precision.

The geographic and vertical distribution of pentadecane is consistent with the ecology of *Prochlorococcus* and *Synechococcus.* The subsurface pentadecane maximum exhibits a decrease in magnitude and a deepening from ~50 m in the Gulf Stream, to ~100 m at the most southerly station in the North Atlantic subtropical gyre, which is reflective of *Prochlorococcus* and *Synechococcus* cell abundance distributions (Cavender-Bares et al., 2001) (Figure 1). Pentadecane was slightly decoupled from cyanobacteria cell abundance at

stations 6 and 7 (Figure 1), possibly due to differential cell specific hydrocarbon content for *Prochlorococcus* ecotypes at different parts of the photic zone (Johnson et al., 2006; Lea-Smith et al., 2015).

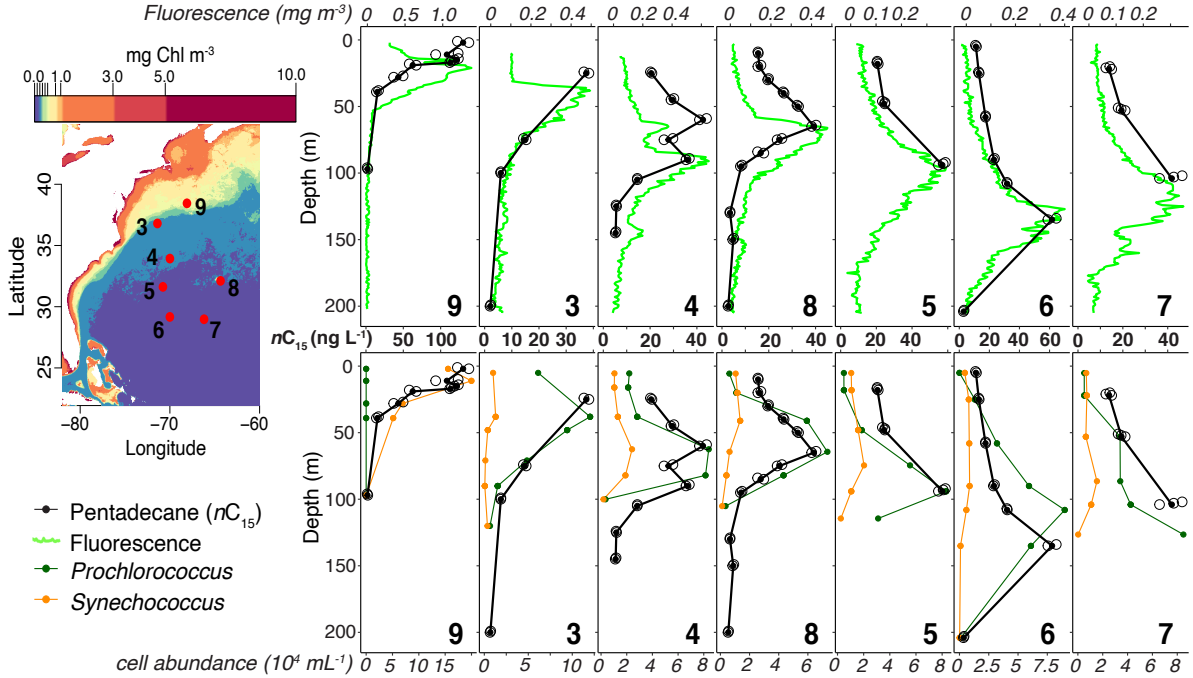

Figure 1. Pentadecane maps onto trends in ocean fluorescence and cyanobacteria abundance. Study area (at left) shows station coordinates mapped onto 4-km resolution MODIS-Aqua chlorophyll concentration for 2017. Station 3 was located in the Gulf Stream and station 9 targeted a *Synechococcus* bloom, all other stations captured more "typical" *Prochlorococcus* dominated oligotrophic water. Pentadecane depth distributions for each station are displayed with fluorescence (top row) and cyanobacterial abundance (bottom row). Depth distributions are organized by descending latitude with pentadecane distribution and station number duplicated for ease of comparison. Open black circles show biologically independent pentadecane measurements, each data represents the contents of one distinct sample bottle (see Methods). Replicates are sequentially moved 1-meter below the other for visualization (water was taken from same depth, depth of top replicate), solid black circles indicate mean of n = 2 at stations 9, 4, 8 and 6 and represent mean of n = 3 for stations 3, 5 and 7.

1.4.2 Rapid pentadecane production in the lower euphotic zone

To quantify production patterns of cyanobacterial alkanes, we amended shipboard incubations with ^{13}C-enriched dissolved inorganic carbon (DIC) to 480‰ and quantified changes in hydrocarbon concentration (Figure 3 and 4) and ^{13}C enrichment of pentadecane. Incubations were conducted shipboard at ambient temperature and light level (see Methods). In total, we quantified alkane production in 31 samples, from five of the seven stations, mainly in triplicate. Pentadecane production varies between ~ 3-30 ng nC_{15} L^{-1} d^{-1} within oligotrophic gyre waters (Figure 2a) and has a higher maximum (~ 50 ng nC_{15} L^{-1} d^{-1}) in the Gulf Stream at the DCM. For each of the (four) oligotrophic stations tested (stations 4, 5, 7 and 8), volumetric pentadecane production is greatest near the DCM, where approximately 1% of photosynthetically active radiation penetrates (1% PAR) (Figure 2a). Three of these stations (stations 4, 5 and 8) exhibit pentadecane production of 5-8 ng nC_{15} L^{-1} d^{-1} at 30% PAR depths, increasing with depth to ~30 ng nC_{15} L^{-1} d^{-1} at 1% PAR. (Figure 2a). Diel variability in pentadecane concentration is also greatest at the DCM and 1% PAR, further consistent with hotspot production there (Figure 2c, Figure 5).

By normalizing volumetric pentadecane production to cyanobacteria abundance (*Pro.* + *Syn.*), we find that 1% PAR has a higher average cellular production rate of pentadecane (0.37 ± 0.13 fg cell^{-1} d^{-1}) compared to 30% and 10% PAR (0.26 ± 0.05 and 0.13 ± 0.05 fg cell^{-1} d^{-1}, respectively) (Figure 2b), indicating that cyanobacteria at or near the DCM produce more pentadecane per cell per unit time. Furthermore, steady state pentadecane replenishment time (production rate divided by concentration) calculated from ^{13}C incorporation and pentadecane concentration, is approximately twice as rapid at 1% PAR compared to 10% and 30% PAR (Figure 2f). It is notable that we consistently observed greater production of pentadecane in

the lower photic zone (1% PAR, near the DCM) than the upper photic zone (30% PAR) because depth profiles of primary production in oligotrophic gyres typically have greater production closer to the surface (Grande et al., 1989; Karl & Church, 2017). The reason underlying this productivity inversion is unclear, but is potentially related to a role for pentadecane in low-light and cold adaption of cyanobacteria (Knoot & Pakrasi, 2019; Lea-Smith et al., 2016).

Our findings of increased cell-specific pentadecane production and variability in the lower euphotic zone for the North Atlantic subtropical gyre are informed by differences in per-cell pentadecane content (nC$_{15}$/[*Pro*. + *Syn*.]) and dissolved nitrite concentrations. Relative importance analysis for physicochemical parameters ammonium, nitrite, depth, light and cyanobacterial pentadecane content (stations 4, 5, 7 and 8) in determining cell-specific production rate of pentadecane revealed that per-cell pentadecane content and nitrite are the most powerful and only significant predictors at 33% and 34% respectively (nC$_{15}$/[*Pro*. + *Syn*.]: $p < 0.001$, nitrite: $p < 0.001$; ANOVA). In addition, ammonium, depth and light have 6%, 5% and 4% predictive power respectively for a total predictive power of 80% ($R^2 = 0.80$). A similar predictive capacity is found when the number of predictor variables was reduced to only per-cell pentadecane content and dissolved nitrite concentration (Figure 2e). Given a constant cell growth rate, the cell-specific production rate of pentadecane would be dependent on cell-specific pentadecane content, logically explaining its predictive power. The reason underlying nitrite's predictive power is less clear, but it is possible that low-light *Prochlorococcus* ecotypes can utilize nitrite more effectively than high-light ecotypes (Martiny et al., 2009) driving production of pentadecane at the DCM via shoaling of the nitricline.

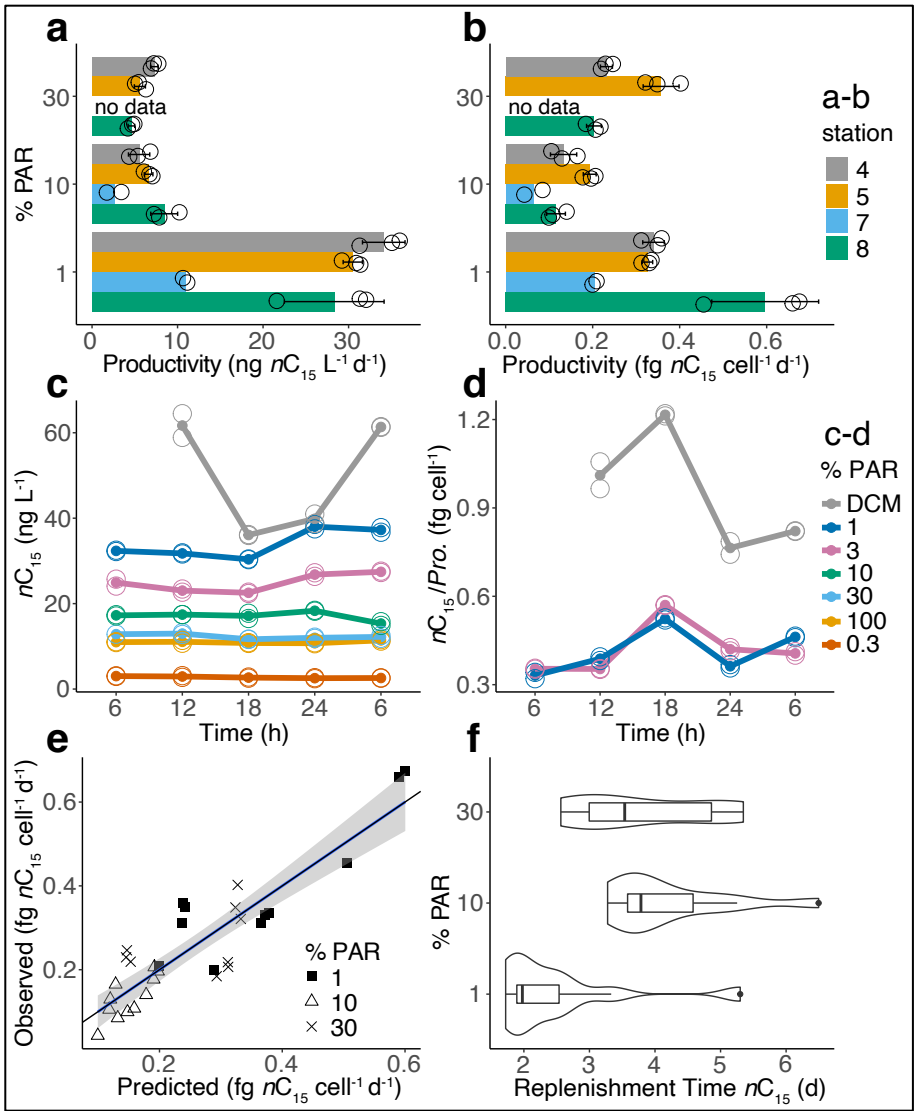

Figure 2. Most pentadecane production in lower euphotic zone. Pentadecane production and diel dynamics from ^{13}C-DIC enrichments and diel sampling grouped by light penetration depth. **a-b** Volumetric and cellular (cell = *Pro.* + *Syn.*) pentadecane production were calculated using pentadecane concentration and ^{13}C enrichment from incubation experiments (see Methods). Data displayed as open black circles with bar representing mean production rate, error bars show standard deviation for n = 3. **c-d** Diel change in pentadecane concentration and pentadecane per *Prochlorococcus* cell show the lower euphotic zone and particularly the Deep Chlorophyll Maximum (DCM) is most dynamic (see Figure 5-5), data are plotted as open circles, mean of replicates are plotted as solid circles (n = 2). **e** Results of a multiple linear regression (n = 31) using nitrite and per-cell pentadecane content (nC_{15}/[*Pro.* + *Syn.*]) to predict cell-specific production (blue line), gray shadings indicate 95% confidence intervals; black line is 1:1. **f** A density plot overlaid on a box and whisker plot of pentadecane replenishment time, grouped by light depth (center line, median; box limits, upper and lower quartiles; whiskers, 1.5x interquartile range; points, outliers); replication by light depth is as follows: 30 PAR (n = 9), 10 PAR (n = 11), 1 PAR (n = 11). For all panels, "n" describes the number of biologically independent pentadecane measurements.

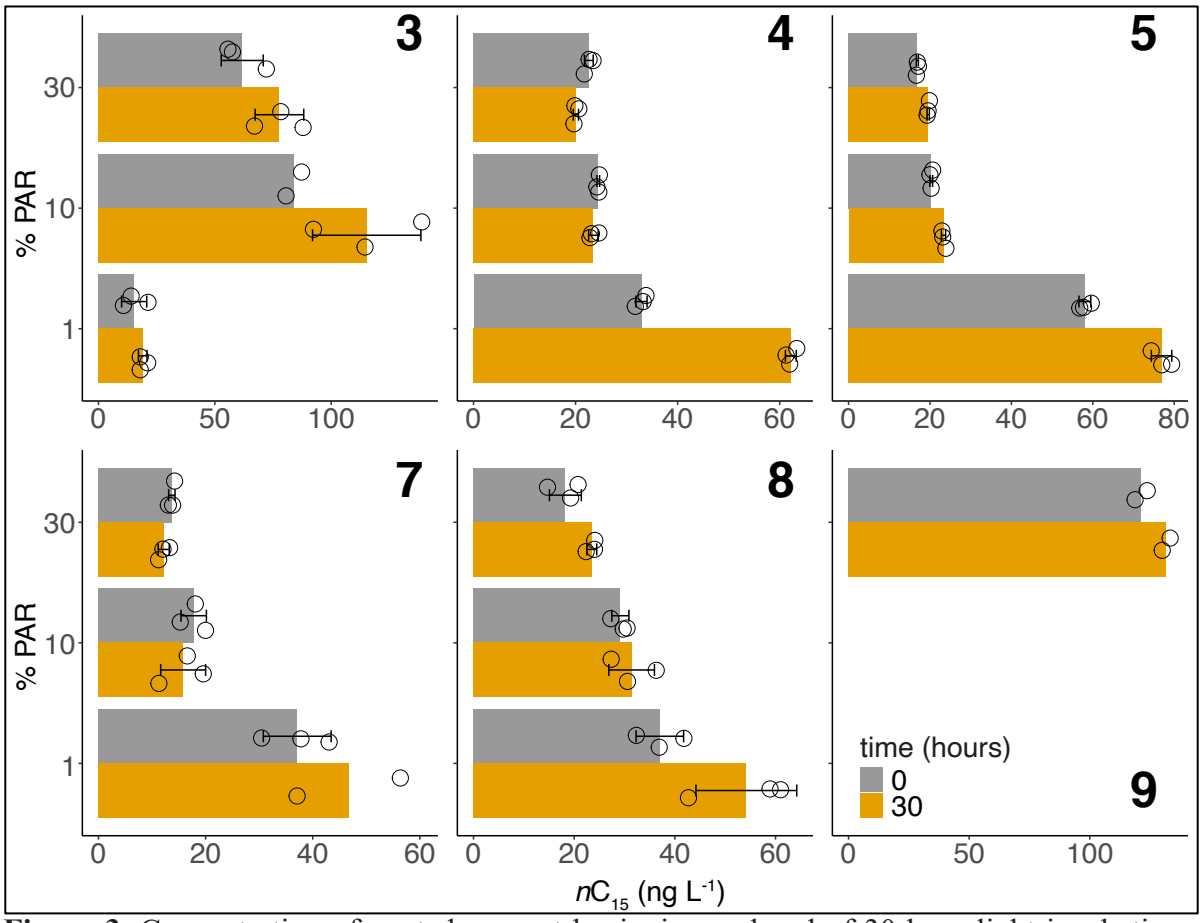

Figure 3. Concentration of pentadecane at beginning and end of 30-hour light incubations (time = 0 and 30 hours) at three light penetration depths for stations 3, 4, 5, 7, 8, 9 (indicated by number at right of each panel). Water was incubated at the light level from which it was collected. Data are plotted as black open circles and represent biologically independent measurements; bar indicates mean of replicates at that light depth, error bars indicate standard deviation of n = 3 replication.

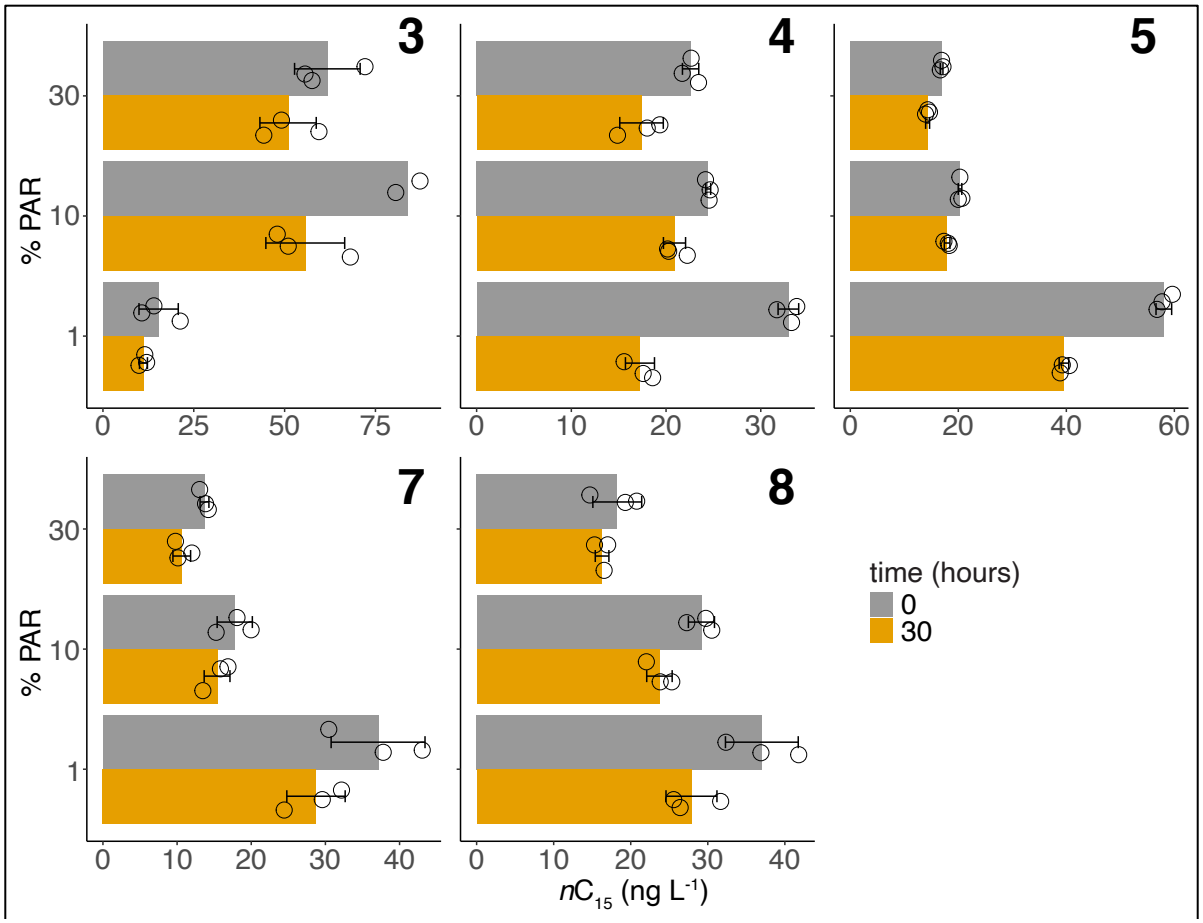

Figure 4. Concentration of pentadecane at beginning and end of 30-hour dark control incubations (time = 0 and 30 hours) at three light penetration depths for stations 3, 4, 5, 7, 8 (indicated by number at right of each panel). Data are plotted as black open circles and represent biologically independent measurements; bar indicates mean of replicates at that light depth, error bars indicate standard deviation of n = 3 replication.

1.4.3 Hydrocarbon production in the Gulf Stream and Continental Shelf

The sampling station located in the Gulf Stream exhibited high production at 10% PAR (50 ng nC_{15} L^{-1} d^{-1}), which aligned with the DCM at ~50 m (Figure 1). In contrast, the "true" oligotrophic stations exhibited a 1% PAR depth usually aligning close to the DCM (within ~ 15 m). Furthermore, a large *Prochlorococcus* population was seen with higher nitrite concentrations at 10% PAR in the Gulf Stream compared to the "true" oligotrophic stations. Station 7 exhibited lower production at 1% PAR (10 ng nC_{15} L^{-1} d^{-1}) compared to other oligotrophic stations (Fig. 3a) likely due to a comparatively smaller *Prochlorococcus*

population at this depth and extremely low nutrients. These anomalies are well reconciled in the multiple linear model predicting cell-specific production rates from dissolved nitrite and cellular pentadecane content (Figure 2e).

Station 1 was the sole station located in eutrophic waters on the continental shelf. These waters are dominated by eukaryotic phytoplankton and thus were not the focus of our study. Furthermore, we did not utilize a 200 μm mesh to catch large zooplankton at this station and as a result observed variable amounts of zooplankton in our 2L samples. Additionally, we observed a chromatographic coelution in these samples with both heptadecane and our internal standard, DDTP. We found that heptadecane was present at higher concentrations than in nutrient poor waters and was always higher in concentration than pentadecane at this station (although with a similar ~3:1 ratio), consistent with eukaryotic-derived octadecanoic acid (stearic acid) as the precursor. Additionally, heptadecane exhibited more variable concentrations between replicates which might be related to the presence of large zooplankton or other forms of heterogeneity in these waters. For these reasons we excluded this data from this study and refer to the results in qualitative terms.

1.4.4 Diel patterns for pentadecane, cells and fluorescence

Pentadecane concentrations were consistent over the diel cycle for shallower depths but not for the deep photic zone (DCM, 1% PAR and 3% PAR), which varied between 8-30%, with the DCM displaying the greatest change (Figure 5a). Density variations were minor for waters sampled at the DCM, 1% PAR and 3% PAR depths (Figure 6) supporting the interpretation that observed variations reflect biological process rather than sampling bias or physical processes.

Like pentadecane, the abundance of *Prochlorococcus* remained consistent in the upper portion of the photic zone throughout the diel cycle whereas it varied substantially (~ 50%) in the lower photic zone (DCM, 1% and 3% PAR depths) (Figure 5b). *Prochlorococcus* abundance in the lower photic zone was observed to decrease in the daylight hours by ~half, with replenishment beginning at dusk and continuing through the night, to meet the original concentration at dawn (Figure 5b). This behavior is reflective of previously reported doubling patterns of *Prochlorococcus* in both the laboratory and in the ocean (Ribalet et al., 2015; Zinser et al., 2009), with cell growth during the day and the peak of cell division occurring near dusk. *Synechococcus* abundance did not follow any discernable pattern over the diel cycle (Figure 5c) and was approximately an order of magnitude lower in abundance than *Prochlorococcus*, thus we interpret pentadecane dynamics to stem primarily from *Prochlorococcus*.

Combining pentadecane concentrations with *Prochlorococcus* abundance patterns enables an assessment of cell-specific pentadecane variability over a diel cycle at three depths (DCM, 1% PAR, 3% PAR). Accumulation of pentadecane preceded cell division (Figure 5e), consistent with diurnal growth preceding nocturnal division. This pattern is also in alignment with previous reports from laboratory knockout experiments of *Synechocystis* (a freshwater cyanobacterium) indicating that hydrocarbons promote membrane flexibility and optimal cell growth and division (Lea-Smith et al., 2016). Thus, it appears that the diel changes in the pentadecane per *Prochlorococcus* cell measured here are reflective of *Prochlorococcus'* cell physiology relative to day-night cycles of growth and division. Since *Prochlorococcus* abundance is a balance between cell death and cell division, cell-specific pentadecane production rates and average cell division rates may serve as reasonable scaling factors to

calculate hydrocarbon production in the ocean. The cell-specific content of pentadecane was notably higher in waters at the DCM at all times in the diel cycle, compared to other depths (Figure 5e). This observation further highlights our finding that pentadecane abundance is proportional to fluorescence and may shed light on utilization of hydrocarbons for photo-acclimation by cyanobacteria in low-light environments. Specifically, these results are consistent with a model in which increased membrane stacking serves as a low-light adaptation, housing more chlorophyll and requiring more alkane to minimize curvature stress.

We also find that 1% and 3% PAR waters exhibit an increase in pentadecane/fluorescence during the day (Figure 5f), with a decrease at night. This observation could be interpreted as an increase in internal membranes (scaffolding) and the need for tight membrane curvature preceding production of chlorophyll and division, however, an opposing trend was observed for the DCM and the topic warrants further investigation. Regardless, it is clear that pentadecane concentrations are stable in the upper photic zone and with lower concentrations as compared to the lower photic zone in which there is more rapid production and utilization of pentadecane by cyanobacteria, particularly *Prochlorococcus*. These results further bolster our finding that the DCM is a highly dynamic focal point for biogeochemical cycling of pentadecane.

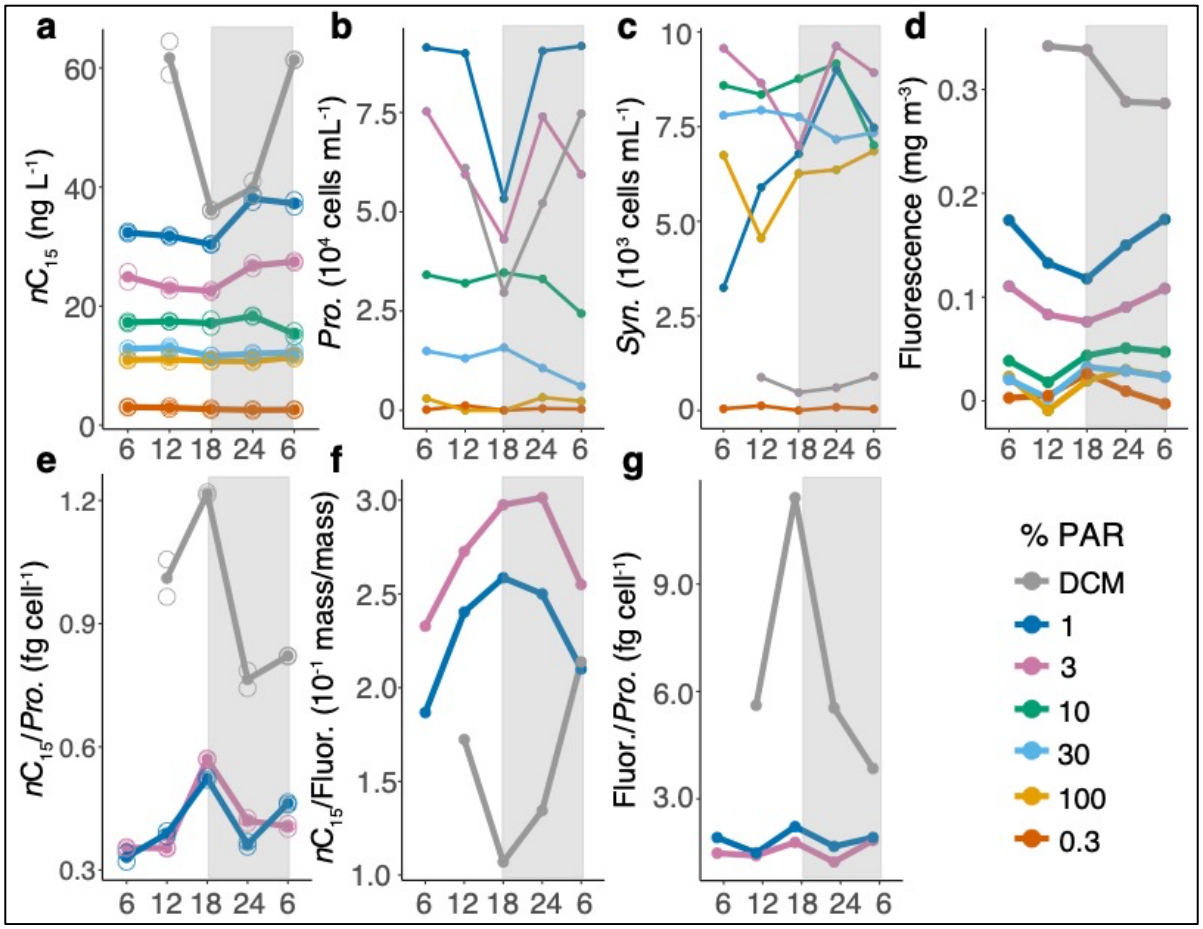

Figure 5. Light depths kept constant through Lagrangian sampling framework whereas the DCM is a depth variable feature throughout the diel cycle. The x-axis represents time of day in hours, with gray shading representing night. Diel patterns of **a** pentadecane, **b** *Prochlorococcus*, **c** *Synechococcus*, **d** fluorescence (averaged with 1-meter resolution data with 2 data points above and 2 data points below to smooth signal, n = 5) and **e-g** selected ratios. **a**, **e**, Data are plotted as open circles with n = 2 biologically independent pentadecane measurements, solid circles indicate mean.

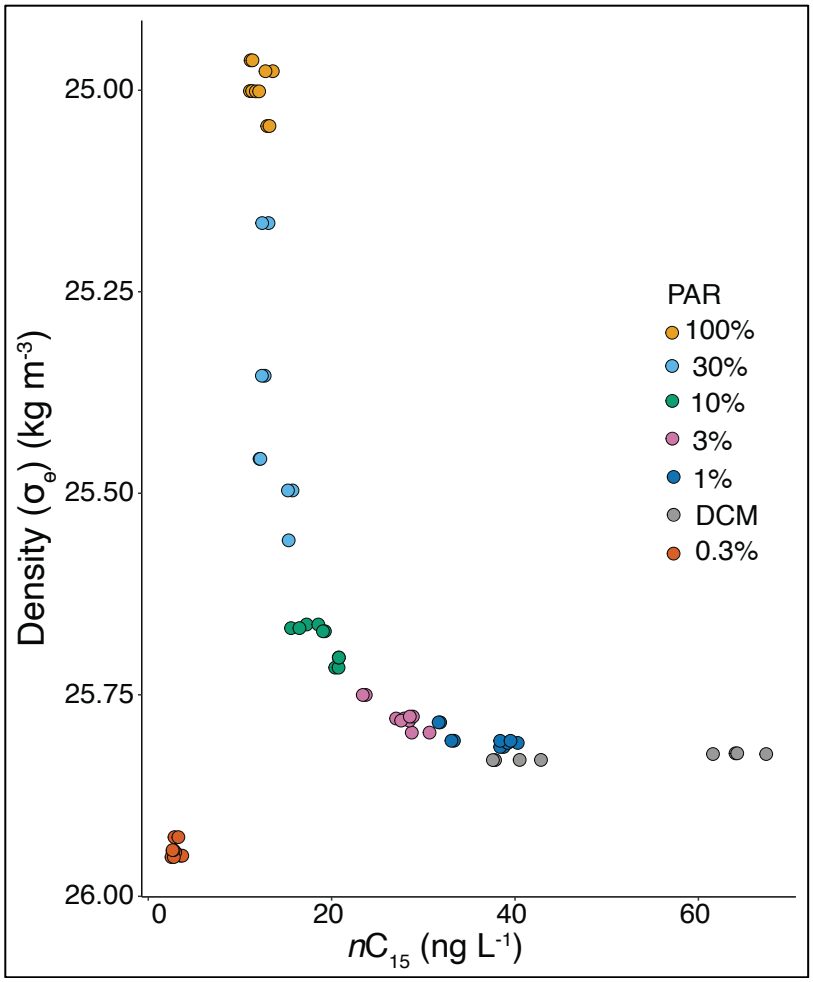

Figure 6. Seawater density plotted against pentadecane concentration colored by light penetration depth and feature (DCM). In this plot, seawater density acts as a proxy for water mass identity in diel sampling. The closer the vertical spread of points of the same color means that samples are more likely to have originated from the same water mass, whereas the further spread means that samples may have originated from different water masses. The horizontal spread of points of the same color represents different concentrations of pentadecane found in the diel cycle. 3% PAR, 1% PAR and particularly the DCM, have pronounced changes in pentadecane over the diel cycle with minimal shifts in seawater density. We conclude this to mean that pentadecane patterns at these depths can be attributed to biological origin, rather than sampling of different water masses.

1.4.5 Global geochemical budget of pentadecane

Based on our measures of productivity and concentration, we sought to quantify key terms in the geochemical budget of cyanobacterial pentadecane – namely global standing-stock (i.e., reservoir magnitude) and global production of pentadecane produced by *Prochlorococcus* and *Synechococcus* (i.e., turnover rate or input). Importantly, we assume consumption balances production (i.e., steady state) at the regional and global scale. We focus on pentadecane production by *Prochlorococcus* and *Synechococcus* because we found them to be the main drivers of the biological hydrocarbon cycle in the oligotrophic ocean (Figure 7). Two distinct approaches are applied for each budget term, low-end values based on pentadecane stock and production rates encountered in the study area (Figure 1 and Figure 2a) scaled by oligotrophic ocean area (method 1, representative of global oligotrophic ocean contribution), and higher values based on scaling of observed cellular properties (pentadecane content per cell) using a previous model (Flombaum et al., 2013) (method 2, representative of global cyanobacterial contribution, both outlined in Methods). The water column integrated approach (method 1) is representative of the pentadecane stock in the oligotrophic gyres insomuch as the locations (North Atlantic subtropical gyre) and season are scalable; considering population estimates (Flombaum et al., 2013) and time series data (see Figure 7) we note that the Atlantic tends to have relatively-low cyanobacterial abundance causing a potential low bias to method 1 (Figure 7). Additionally, method 1 does not consider regions outside the open-ocean oligotrophic gyres, particularly for *Synechococcus* which is found in both coastal oligotrophic waters and more eutrophic waters (Flombaum et al., 2013). We propose that our method using water column integration is a reasonable representation for the

North Atlantic subtropical gyre but our average estimate using modeled cell-specific concentrations may be more accurate for the global stock for oligotrophic ocean regions.

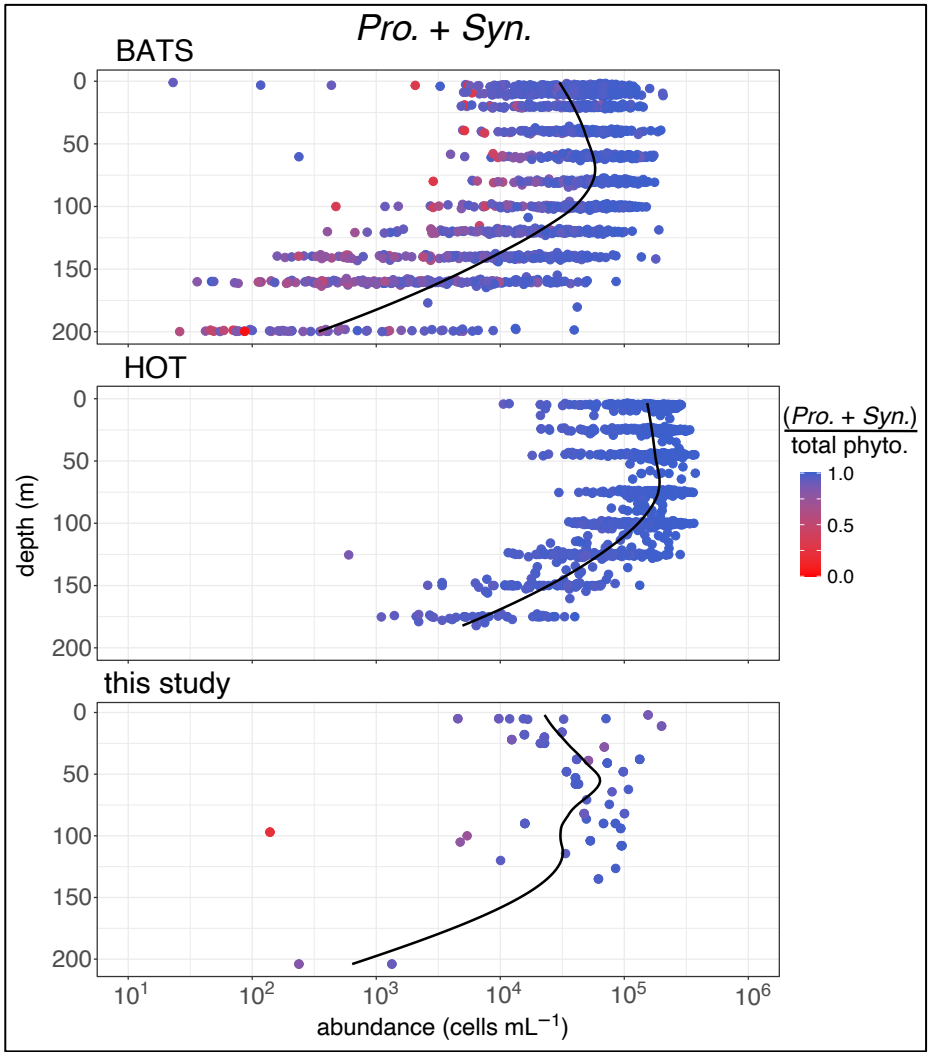

Figure 7. Depth profiles of ~20 years of data from the Bermuda Atlantic Time-series (BATS, at top, data obtained from Bermuda Atlantic Time-series Study http://bats.bios.edu/bats-data/), the Hawaii Ocean Time-series (HOT, in middle, data obtained from Hawaii Ocean Time-series HOT-DOGS application; University of Hawai'i at Mānoa, National Science Foundation Award #1756517), and this study (at bottom). Data points are colored on a gradient by the proportional contribution to the phytoplankton community by *Prochlorococcus* and *Synechococcus* (total phytoplankton community is calculated as *Pro.* + *Syn.* + pico- + nano-Eukaryotes for BATS and this study, and *Pro.* + *Syn.* + pico-Eukaryotes for HOT). BATS and HOT data are each from a single station measured nearly monthly for ~20 years whereas measurements from this study incorporate spatial variability (see Fig. 1) with minimal temporal variability (all measurements taken in May 2017). The proportional contribution of *Prochlorococcus* and *Synechococcus* is > 90 % of the phytoplankton community at BATS 84% of the time. At HOT, *Pro.* + *Syn.* is > 90 % of phytoplankton community ~100% of the time. For this study, *Pro.* + *Syn.* is > 90% of the

phytoplankton community (*Pro*. + *Syn*. + pico + nano-Eukaryotes) for 80% of the measurements, with most cases of lower proportional prokaryote abundance due to an anomalous nutrient pulse observed at station 9 (a *Synechococcus* bloom) or at low absolute abundance of *Pro*. + *Syn*.

We estimate the global standing stock of pentadecane to be 0.70 ± 0.17 Tg by method 1 and 1.78 ± 1.24 Tg by method 2, the latter of which is similar to an estimate based on laboratory cultivation (Lea-Smith et al., 2015). We further estimate the global production rate of pentadecane to be 131 ± 13 Tg pentadecane yr^{-1} by method 1 and 274-649 Tg pentadecane yr^{-1} by method 2 (Table 1). By comparison, the total quantity of petroleum estimated to reach the ocean annually from all sources is 1.3 Tg (National Research Council, 2003), indicating that biohydrocarbon input to the ocean exceeds petroleum input by a factor of ~100-500. Interestingly, the global production rate of pentadecane by cyanobacteria is similar in magnitude to the atmospheric release for two other important hydrocarbons: methane (Saunois et al., 2020) and isoprene (Guenther et al., 2012; McGenity et al., 2018).

In order to assess the reasonableness of our measurements and global scaling we further check the replenishment time of pentadecane relative to known population turnover for wild *Prochlorococcus* and *Synechococcus*. Replenishment time of pentadecane was calculated from independent measures of water-column integrated stock and production at 3 oligotrophic stations (see Methods), yielding a value of 1.9 ± 0.5 d. This value is taken to represent the turnover time of cellular pentadecane and is within the range of cellular turnover time observed for environmental *Prochlorococcus* (1-2 days) – weighted slightly towards the slower environmental turnover of *Synechococcus* (1-6 days) (Field et al., 1998; Liu et al., 1995; Mann & Chisholm, 2000; Vaulot et al., 1995; Zubkov, 2014). Furthermore, since water column integrated turnover aligns with 1% PAR replenishment time (Figure 2f), this further

bolsters our finding that the low-light euphotic zone is driving most pentadecane flux, where elevated pentadecane concentrations and rapid turnover coincide.

1.4.6 Microbial productivity from pentadecane

Based on the assumption of steady state, we estimated the magnitude for the production rate of obligate alkane-degrading bacteria or archaea using cyanobacterial pentadecane as sole substrate in the oligotrophic ocean. Assuming a carbon conversion efficiency range (pentadecane to biomass) of 5-50% and a carbon mass of hydrocarbon degrading microbes of 120 fg C $cell^{-1}$ (Valentine et al., 2012), pentadecane in the lower photic zone (1% PAR) would support microbial production of the order of ~10-100 cells ml^{-1} d^{-1} with the upper photic zone (30% PAR) supporting ~2-20 cells ml^{-1} d^{-1}. The size of the supported community further depends on cellular turnover time, and an assumed turnover rate of 0.1 day^{-1} equates to a steady state population of ~10^2-10^3 cells ml^{-1} in the lower photic zone (1% PAR) and ~20-200 cells ml^{-1} in the upper photic zone (30 % PAR) of the oligotrophic ocean (Table 1). Additionally, geochemical analysis of sinking particles collected at the base of the euphotic zone (150 m) shows that only ~ 1 x 10^{-4} % of pentadecane production (1.76 mg nC^{15} m^{-2} d^{-1}) is exported below 150 m, which suggests rapid consumption of this hydrocarbon within the euphotic zone, further supporting the estimates in Table 1. These results underscore the depth dependency of cyanobacterial pentadecane production, and the potential for similar structuring for the microbial community of alkane degraders. Furthermore, we expect a secondary structuring of alkane degradation based on phase-state of the alkanes, with particles showing more consumption than surrounding waters, as we interpret in incubation experiments (Arrington, 2021) and sediment trap data.

	Method 1	Method 2	Lea-smith et al., 2015
Stock (Tg *n*C15)	0.70 ± 0.17	1.78 ± 1.24	1.59
Production (Tg *n*C15 yr^{-1})	131 ± 13	274-649	270-583
***n*C_{15} Consuming Cells (30% PAR)**	20-200 cells mL^{-1}		
***n*C_{15} Consuming Cells (1% PAR)**	100-1000 cells mL^{-1}		

Table 1. Global reservoirs and fluxes of pentadecane and estimates of a supported bacterial or archaeal community relying solely on pentadecane. We assume a conversion efficiency range (pentadecane to biomass) of 5-50%, a dry carbon mass of hydrocarbon degrading cells of 120 fg C/cell (Valentine et al., 2012), and a cellular turnover rate of 0.1 d^{-1}.

1.5 Conclusion

Oceanographic measurements in the North Atlantic Oligotrophic Gyre reveal that pentadecane is the dominant hydrocarbon produced by cyanobacteria, with pentadecane depth profiles closely mapping onto *Prochlorococcus* cell abundance and fluorescence, with peak pentadecane concentration at the Deep Chlorophyll Maximum (DCM). Through isotope tracer experiments and compound-specific isotope ratio measurements we find that the deep euphotic zone (1 % PAR) near the DCM produced the most pentadecane per unit time by volume and by cell, and that production is governed by pentadecane per cell content and dissolved nitrite. This highly dynamic production in the deep euphotic zone is also seen in diel dynamics that reveal the DCM as a hotspot of pentadecane production. Through isotopic and geochemical measurements, we find that pentadecane in the euphotic zone is completely turned over in ~ 1.9 days with negligible export below 150 m, which illustrates the rapid turnover and near complete utilization of this hydrocarbon by hydrocarbon degrading bacteria on sinking marine particles. We estimate through several methods that cyanobacterial hydrocarbon production dwarfs oil input into the ocean by 100 to 500-fold, supporting field observations of low-level alkane degrading specialists found in ocean waters unpolluted by

oil. The cryptic hydrocarbon cycling observed here is an important factor in understanding the metabolic response of the oceanic microbiome to oil inputs and should be incorporated as a predictive tool in oil spill response planning.

CHAPTER 2

Fatty acid and isotope biomarker response to coral heterotrophy in context of *in situ* sampling on reefs

2.1 Abstract

Reef-building corals are mixotrophic and obtain organic matter from their endosymbiotic dinoflagellates (*Symbiodiniaceae*; herein 'symbionts') or through heterotrophy on particulate organic matter (POM) and zooplankton in the water column. A body of work has shown an unexpected reliance of many corals on heterotrophy and the vital role heterotrophy plays in supplying corals with essential nutrients that help corals resist and recover from thermally induced bleaching that is threatening coral-reef ecosystems worldwide. Yet, we still have a limited understanding of coral feeding plasticity and trophic ecology of reef-building corals that would help predict survivorship patterns and inform management practices. Most current methods are either analytically or replication limited for interpreting coral trophic ecology patterns in nature which remains challenging due to the tight recycling of nutrients between the host and symbiont and the multi-trophic nature of corals (detritivores, herbivores, carnivores, etc.). Only a small number of controlled feeding experiments have been conducted to understand biomarker response to shifts in coral heterotrophy. To fill this knowledge gap, a high replication feeding experiment (n ~ 30 per treatment) was conducted on Red Sea *Stylophora pistillata* in which corals were fed along a gradient from full autotrophy to full heterotrophy on a distinct food source (*Artemia* nauplii) to better understand fatty acid (FA), isotopic and elemental biomarker response to shifts in coral mixotrophy. Both FA and isotope biomarkers are the most used analyses in trophic ecology studies and when combined provide the most cost and data effective measurements to advance understanding of coral mixotrophy and feeding ecology in nature.

It was found that increasing coral heterotrophy provided several physiological and molecular benefits to corals but did not offset detrimental bleaching effects and that bleached corals generally ate less than non-bleached corals when presented with the same prey density and feeding frequency. Experimental nutritional source groups (heterotrophic and autotrophic) showed strong FA and isotopic biomarker separation due to significant differences ($p < 0.01$) in 22 out of 30 biomarkers. Nearly all heterotrophic source biomarkers scaled with increasing heterotrophy in the host fraction while only a smaller subset increased in the symbionts, indicative of controlled metabolic gatekeeping by the host. A divergent metabolic pattern was seen for autotrophic biomarkers in both the host and symbiont fractions in which some autotrophic biomarkers were positively correlated with feeding, likely due to increased symbiont density and chlorophyll which increases with feeding, which represents of a "fast turnover" FA pool; while other autotrophy markers were negatively correlated with feeding, suggesting a dilution effect, or "slow turnover" symbiont biomarkers that were diluted with both fast turnover autotrophic biomarkers and heterotrophic biomarkers. Nitrogen isotope and essential fatty acid data showed clear integration of heterotrophic biomarkers in host and symbiont tissues while carbon isotope data revealed non-significant changes to heterotrophy, with ~ 10-60 heterotrophic nitrogen atoms recorded for every 1 heterotrophic carbon atom, depending on tissue fraction, and feeding regime. This shows that the decades long use of soft tissue bulk carbon isotope data to assess coral heterotrophy may be drastically underestimating the vital contribution of heterotrophy to reef-building corals because most heterotrophic carbon appears to be respired or exuded as mucous while nitrogen and essential molecules (fatty and amino acids) are retained. It was found that essential FA heterotrophic biomarkers and heterotrophic nitrogen turnover exhibit non-linear trends due to less

heterotrophic nitrogen integration by the host of bleached corals, which suggests that FA biomarkers may be the most responsive biomarkers on shorter time scales, particularly for bleached corals. Lastly, the results of this experimental feeding study and particular biomarkers are discussed in context of assessing coral mixotrophy and trophic level using just *in situ* nutritional source found in the Gulf of Aqaba. Overall, findings show reliable recording of FA, isotopic and elemental biomarkers from feeding in reef-building corals that can be used in the field, with unique fatty acid metabolism dynamics within the coral-dinoflagellate symbiosis with evidence that carbon isotope proxies may be vastly underestimating the reliance of coral heterotrophy in nature. This shows that reef-building corals and oceanographic patterns that control POM and zooplankton dynamics on reefs are likely more intimately linked than originally thought.

2.2 Introduction

2.2.1 The coral symbiosis and heterotrophy

The ecological success of reef-building corals in oligotrophic waters has been termed "Darwin's paradox" in which the flourishing, colorful and biodiverse areas of coral reefs stand in stark contrast to the low nutrient (oligotrophic) waters in which they reside. The success of tropical reef-building corals in oligotrophic water has largely been attributed their symbiosis with the photosynthetic dinoflagellate *Symbiodiniaceae* in which tight recycling of nutrients between the animal host and endosymbiont (herein 'symbiont') help the coral meet its metabolic needs. The coral animal and algal symbiont (together termed the 'holobiont') share energy and nutrients in the form of organic molecules like amino acids (Ferrier-Pagès et al., 2021; Krueger et al., 2018; Martinez et al., 2022; Wall et al., 2021), lipids (Chen et al., 2017; Radice, Brett, et al., 2019; Teece et al., 2011) and carbohydrates (Burriesci et al., 2012), as

well as inorganic catabolic waste products such as ammonium, phosphate and carbon dioxide that are transferred unidirectionally to the symbiont from the host (Yellowlees et al., 2008) to be fixed back into organic biomolecules by the symbiont (Figure 8). This tight recycling of nutrients between host and symbiont leads to a high retention, long turnover times, of essential nutrients like nitrogen (> 1 year; Tanaka et al., 2018) which gives corals a competitive edge in oligotrophic waters (Gustafsson et al., 2013; Muscatine & Porter, 1977) where dissolved nutrient concentrations are very low.

Yet, even with the tight and efficient recycling of nutrients between host and symbiont, corals do not rely entirely on their symbionts and often acquire essential biomolecules and elements by feeding (heterotrophy) in the water column (Fox et al., 2019; Teece et al., 2011). Corals are mixotrophic in nature and rely on a mix of autotrophy (photosynthetic products from symbionts) and heterotrophy (feeding on organic matter in the water column) to meet metabolic needs. While carbon acquired through photosynthesis of the endosymbionts is typically considered "junk food" (Falkowski et al., 1984) (low in nitrogen and phosphorus) and is turned over quickly via respiration, carbon acquired through heterotrophy is essential (Baumann et al., 2014; Tolosa et al., 2011b) and is typically incorporated into longer turnover pools, such as membranes and proteins (Bachar et al., 2007; A. D. Hughes et al., 2010). Indeed, carbon, nitrogen and phosphorus acquired through feeding is necessary for biomass growth and reproduction (Cox, 2007; Ferrier-Pagès et al., 2003) and accounts for a significant portion of a coral's metabolic demands (Houlbrèque & Ferrier-Pagès, 2009; Leal et al., 2014; Sorokin, 1991).

Corals feed heterotrophically on a variety of organic matter sources in the water using tentacles, mucous nets, and mesenterial filaments that enable capture of a variety of planktonic

and organic matter sources in the water column. Corals feed on zooplankton (Grottoli, 2002; Sebens et al., 1997), detritus (Mills et al., 2004; Mills & Sebens, 2004), diatoms (Radice, Brett, et al., 2019), bacteria (Sorokin, 1991), and flagellates (Ferrier-Pagès and Gattuso, 1998). It has been shown that some corals increase heterotrophy with primary production in the water column (Fox et al., 2018), showing that coral mixotrophy is linked with local oceanography such as internal waves and wind driven upwelling that drive new production (Leichter and Genovese, 2006; Fox *et al.*, 2018; Williams *et al.*, 2018; Radice *et al.*, 2019; Fox *et al., in review*). Given the physiological benefits of coral heterotrophy and it's link with local oceanography, it is paramount to understand how flexible coral trophic strategies are and if they can increase feeding when food is available to help remediate the effects of climate induced ocean warming (Anthony et al., 2009; Conti-Jerpe et al., 2020; Grottoli et al., 2006).

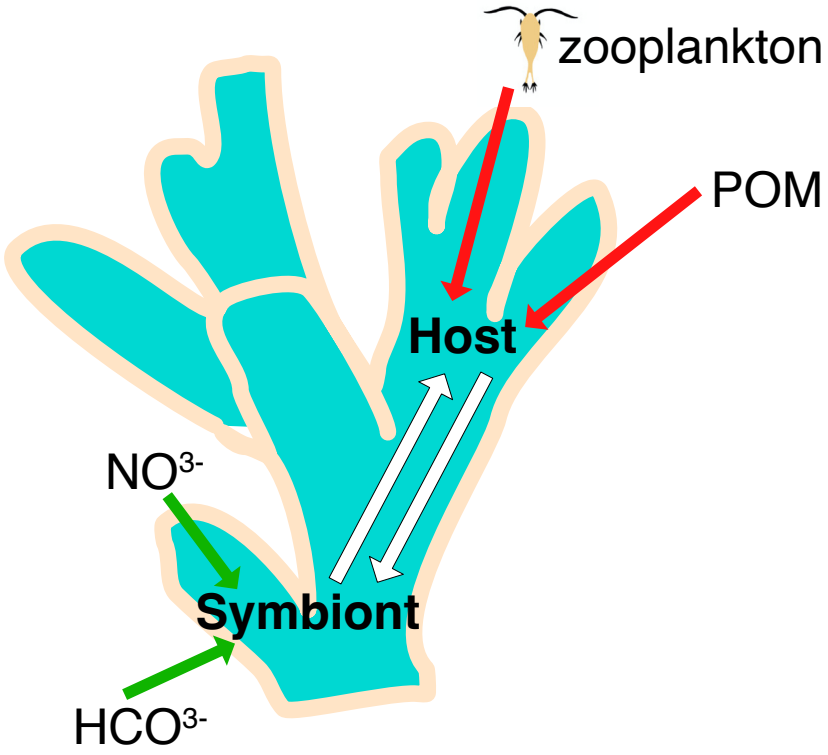

Figure 8. Schematic of coral mixotrophy and nutritional exchange of a symbiotic reef-building coral. The animal host can feed on detritus, phytoplankton, and bacteria (POM here) as well as zooplankton of various size classes, while the symbiont can access the dissolved inorganic carbon and nitrogen in reef waters. There is a bidirectional exchange of organic

molecules between host and symbiont and a unidirectional exchange from host to symbiont of catabolic waste products like ammonium to be fixed back into organic nitrogen.

2.2.2 Climate driven coral heat stress and bleaching

In the past ~40 years, regional scale coral bleaching has been observed with increasing regularity and severity (Hughes et al., 2018) due to global ocean warming (Levitus et al., 2005; Lyman et al., 2010) caused by anthropogenic greenhouse gases (Barnett et al., 2005). Bleaching occurs when high water temperatures destabilize the symbiosis between coral and their dinoflagellate symbionts, which causes corals to expel their symbionts, revealing their white skeleton (Hoegh-Guldberg, 1999). Once bleached, the coral animal no longer has a steady supply of organic carbon from the symbiont to fuel metabolism and must rely on body lipid reserves and/or heterotrophic feeding (Grottoli et al., 2006) to supply energetic demands until temperatures cool and they can regain their endosymbionts. A body of research has shown that heterotrophy is vital for the coral to meet metabolic requirements and recover from bleaching (Grottoli et al., 2006; A. D. Hughes & Grottoli, 2013; Schoepf et al., 2015; Tremblay et al., 2016). Additionally, Conti-Jerpe et al. show clear results that coral heterotrophy positively correlates with *resistance* to bleaching, suggesting that autotrophic corals will more readily bleach and lose their competitive edge as the ocean continues to warm. As the evidence stands, the future of coral reefs will hinge largely upon the ability of corals to *resist* and *recover* from thermally induced bleaching which is determined largely by coral feeding plasticity and the delivery of heterotrophic subsidies to reefs via physical oceanographic processes (Fox et al., *in review*; Skinner et al., 2021; Williams et al., 2018). However, coral feeding plasticity remains poorly understood and therein exists a crucial knowledge gap for understanding how reefs will survive climate change. The goal of this work is aimed to ground truth a chemical approach to measure coral mixotrophy on the reef, to

ultimately improve our understanding of coral trophic ecology, heterotrophic plasticity and thus coral thermal resistance and bleaching recovery potential.

2.2.3 History and advances of measuring coral trophic strategies in nature

Reef-building corals can be involved in multitrophic interactions simultaneously as primary producers, herbivores, carnivores, and detritivores (Goreau et al., 1971; Muscatine, 1973; Muscatine & Porter, 1977) which makes tracing of material flow and understanding reef food web connectivity difficult. In an experimental setting, stable isotope labelling (typically with enriched ^{13}C and/or ^{15}N) can be used effectively to trace autotrophy and heterotrophy into different tissue fractions of the coral holobiont (host and symbiont). However, isotopic labeling cannot be conducted on the reef and lacks applicability as a tool to understand complex reef systems. For several decades, the natural abundance ratios of bulk tissue carbon ($^{13}C/^{12}C$) and nitrogen ($^{15}N/^{14}N$) have been used to understand coral trophic strategies in nature.

The natural abundance of stable isotopes is used effectively in a variety of food webs to assess the source and abundance of assimilated nutrients (Fry, 2006). However, due to the tight recycling of material between the coral host and symbiont it is very difficult to disentangle what source the carbon (or nitrogen) came from, as compared to an organism without endosymbionts. The $\Delta^{13}C$ value ($\delta^{13}C_{host} - \delta^{13}C_{symbiont}$) has been used extensively as a proxy for coral heterotrophy (Grottoli et al., 2006; Muscatine et al., 1989) but is sensitive to many processes beyond heterotrophy that can influence this value and sometimes lead to erroneous interpretations. For instance, symbiont genotype can affect carbon contribution amounts to the host (Leal et al., 2015; Starzak et al., 2014) and variations in lipid assimilation or consumption can easily alter $\Delta^{13}C$ values (Alamaru et al., 2009) because lipids have a strong

(~ - 8 ‰) difference from bulk tissue $\delta^{13}C$ values (Wall et al., 2019). Some studies have used compound-specific amino acid isotope analysis (CSIA-AA) to clarify coral trophic strategies (Ferrier-Pagès et al., 2021; Fox et al., 2019; Martinez et al., 2022) but this approach is cost and time intensive with a high barrier to entry due to expensive instrumentation and set up and is thus limited to low-throughput sampling with only a small number of laboratories consistently generating this type of data.

It is becoming more common to rely on multiple biomarkers to study trophic ecology of organisms, often coupling fatty acids and bulk tissue stable isotopes to help enhance separation between source groups and clarify food web contributions into consumer tissues (Alfaro et al., 2006; Fey et al., 2021; Guerrero & Rogers, 2020; Madgett et al., 2019; Neubauer & Jensen, 2015). Both fatty acids and bulk tissue isotopes analysis together are the two most common type of analyses in trophic ecology based publications (Pethybridge et al., 2018) and together combined are still greatly more cost effective than CSIA-AA, yet provide a similar amount of data per sample (~32 for FA + bulk tissue isotope, ~ 35 for $\delta^{15}N$ and $\delta^{13}C$ of AA). Additionally, many more laboratories are conducting fatty acid and bulk isotope analyses at much higher volume than CSIA-AA. However, while fatty acids have been used consistently for marine ecology (Budge et al., 2006; Dalsgaard et al., 2003; Iverson et al., 2004; Thurber, 2007), there is a critical need for experimentation on the uptake and modification of these trophic biomarkers in controlled feeding experiments to better scale results to populations and ecosystems (Galloway & Budge, 2020). This is particularly true for reef-building corals in which the endosymbionts and mixotrophy greatly complicates the fatty acid response to feeding and in which very few feeding experiments have been conducted (Al-Moghrabi et al., 1995a; Tolosa et al., 2011a; Treignier et al., 2008). The second chapter of my dissertation

aims to experimentally clarify fatty acid and isotope biomarker uptake and modification due to variations in coral mixotrophy, and how these results can be used to interpret fatty acid and isotope biomarker data more accurately from the field to understand coral trophic ecology.

2.2.4 Fatty Acids as Trophic Biomarkers

Fatty acids (FA) are a major component of coral lipids (up to 73%, Tolosa et al., 2011a; Treignier et al., 2008) and are used for energy storage, membrane structure and chemical signaling. FA are composed of a long hydrophobic tail (usually 14-22 carbons long in the marine environment) with a carboxylic acid functional group that enables attachments to different headgroups. FA can be saturated with hydrogens at each carbon (SFA = saturated fatty acid, no double bonds) or have 1-6 or even more double bonds (unsaturation, MUFA = monounsaturated fatty acid, PUFA = polyunsaturated fatty acid) with a systematic nomenclature. For example, 18:2n6 would denote a fatty acid with 18 carbons and 2 double bonds with the first double bond located six carbons away from the terminal carbon in the hydrophobic tail (the omega carbon). FA are typically found in four main forms, triacylglycerols (TAG), wax esters (WE), phospholipids (PL) and free fatty acid (FFA); while TAG and WE are energy storage molecules, PL create the fundamental unit of cell membrane architecture and FFA can be used as signaling molecules and membrane energetic decouplers.

Fatty acids have been used extensively as qualitative (Dalsgaard et al., 2003) and sometimes quantitative (Guerrero & Rogers, 2020; Happel et al., 2016; Iverson et al., 2004) assessment of diet in the marine environment. In marine mammals this approach is particularly useful because of high fat diets which results in a high proportion of dietary fatty acids directly deposited into blubber with little biochemical modification before storage (Budge et al., 2006). FA have been used sparingly as a tool to qualitatively detect trophic strategy in reef-

building coral (Kim, Lee, et al., 2021; Mies et al., 2018; Radice, Brett, et al., 2019; Seemann et al., 2013; Teece et al., 2011) and even less so for quantitative assessments of diet, although Radice et al., 2019 show the potential of this tool in elucidating >2 diet sources for corals. Due to the sparse use of FA in coral trophic ecology, there is a variety of data normalization practices and disparity in using holobiont (Pupier et al., 2021) or separate host and symbiont fractions (Kim, Baker, et al., 2021; Radice, Brett, et al., 2019) that make comparisons across studies difficult.

In this second chapter I conducted a high replication feeding experiment on a common and well-studied reef-building coral in the Red Sea (*Stylophora pistilalta*) to understand fatty acid and isotopic response to a gradient in heterotrophy, from full autotrophy (unfed corals) to ~100% heterotrophic corals (bleached + fed). This work aims to build a framework to interpret biomarker response to a gradient in heterotrophy and better understand past and future coral biomarker (FA + isotope) field data and heterotrophic plasticity on the reef. Since it is known that heterotrophy aids resistance and recovery from thermally induced bleaching, it is paramount to understand coral heterotrophic plasticity and better prepare for coral survivorship patterns in a warming global ocean.

It is important to note that the food source used in this experiment, *Artemia* nauplii, is typically used in aquarium settings and is not what corals eat in nature. This heterotrophy source was chosen because it has a consistent biomarker "fingerprint" to clearly trace heterotrophic nutrition through the coral symbiosis from a distinct and unchanging source. Certainly, the distinct fatty acid and isotopic "fingerprint" of *Artemia* nauplii makes it such that not all the results of this experiment can be utilized to interpret coral biomarkers and heterotrophy in nature, however, there is considerable overlap between *Artemia* and natural

zooplankton (Figure 14) in nature and overlapping biomarkers will be discussed further in the final section of this work. This study provides, at a fundamental level, the shifts in fatty acid and isotopic biomarkers along a heterotrophy gradient given a distinct and singular heterotrophic source. The results from this study can be used to interpret coral mixotrophy as it occurs in the field so long as heterotrophic sources (zooplankton and particulate organic matter) are also collected and measured for their fatty acid and isotopic "fingerprints".

2.3 Methods

2.3.1 Coral collection, experimental setup and feeding rate measurements

Corals were collected from Interuniversity Institute for Marine Sciences underwater nursery on SCUBA on 11/20/19 and on 11/28/19 at ~5 m depth. Roughly sixteen ~5-8 cm length nubbins from *Stylophora pistillata* colonies were taken using clippers. Corals were taken to the Red Sea Simulator (Bellworthy & Fine, 2018) and laid into tanks, with three tanks per experimental condition and 10-12 coral fragments per tank. The same day of collection corals were glued to plastic bases using superglue and baking soda. Within ~2 hours of supergluing to bases corals were visibly extending and moving their polyps to feed. Coral fragments were randomly assigned to one of four treatments using a random number generator: 1) bleached and fed 6x per week, 2) fed 6x per week, 3) fed 2x per week, 4) unfed (control). The coral fragments were then left to acclimate for 10 days except for the bleached condition. After 3 days of tank acclimation the bleaching condition corals were bleached in 8 hr menthol (0.58 uM)/ 16 hr DCMU bath (10 uM) for 4 days with menthol condition during the 12 hr light period (as described by Matthews et al., 2016; Wang et al., 2012). Corals were gently shaken during bleaching to ensure homogenization of bleaching agent chemicals. After 4 days, coral fragments were visibly white and appeared to have polyps fully extended within

3 days after the last day of bleaching. Tanks were constantly circulated with seawater from the Gulf of Aqaba (filtered through a 130 μm) and a small pump was used to break surface tension of water and improve circulation in the tank. Two tanks were also left empty with flowing water and pumps to sample particulate organic matter that got into the RSS through the coarse sweater filters.

Artemia nauplii were hatched near daily from a singular source of eggs (sourced from the Eilat Underwater Observatory) at ~27.5 °C overnight and fed to corals at a density of ~1000 nauplii L^{-1} near dusk. During feeding, flow into and out of tanks was halted and five liters were removed to ensure that no water would spill out, however the pump remained on for water movement and evenly circulate nauplii around the tank. The corals were fed nauplii for one hour and checked to ensure feeding was occurring. After 2 hours of feeding the flow to the tanks was turned back on to circulate the nauplii out of the tank. Before the flow was turned back on, triplicate water samples were taken from each tank in which there was feeding and the abundance of remaining nauplii was counted. The difference between initial and final concentrations was used to calculate nauplii consumed per tank for each feeding day.

2.3.2 Particulate organic matter and zooplankton sampling

Particulate organic matter (POM) samples from the reef were sampled with 5 L Niskin bottles at the IUI coral nursery where coral fragments were taken from (~ 5 m depth) and filtered onto pre-combusted 0.7 um GF/F filter, with ~10 L filtered per filter. POM samples from two adjacent mesocosm tanks without coral were also taken to constrain the chemical and isotopic fingerprint of 130 μm filtered POM entering the tank from the 30 m depth that supplies the mesocosm, with ~10 L of total volume per filter as well.

Zooplankton was collected in two ways: one set of samples was collected from the IUI pier adjacent to the collection site of the underwater nursery and from net tows in deeper water

near the middle of the Gulf of Aqaba. Zooplankton collection from the pier involved a 200 µm pore size net. The pier experiences a prevailing north to south current and because the underwater nursery is just north of the pier, this would theoretically collect all the plankton that these corals would have been encountering. The collection of zooplankton from the pier was conducted overnight with samples collected the next morning to best mimic the known coral feeding times and high densities of plankton on the reef due to diurnal migration. Samples were not sorted due to time constraints but were typically red in color, likely revealing a majority of copepods captured during most sampling times. After collection, samples were immediately frozen at -80 °C for later lyophilization.

The second set of zooplankton samples were collected in the middle of the gulf to represent a pelagic plankton source. Net tows were conducted behind a boat using a 100 µm pore net at 350 m from the bottom, tows were done in 7–10-minute pulls at a depth of 20 m at ~ 2:00 PM. *Trichodesmium* colonies and pelagic foraminifera were picked out of these net tows before later freezing and lyophilization.

2.3.3 Coral Fragment Processing

Corals were flash frozen in liquid nitrogen and later airbrushed with 10 mL of cold phosphate buffer (0.1 M) with EDTA (0.1 mM) (pH = 7.0) at 4 °C and manually homogenized. Buffer volumes added and returned were recorded. A fraction of homogenized holobiont tissue (10%, 1 mL) was saved and stored in the freezer as backup, while another 10% (1 mL) of homogenate was allocated to physiology measurements including symbiont counting, Chlorophyll extraction and total soluble protein analysis. The remaining 80% of homogenate was used for fatty acid and isotope analysis. Separation of the host and symbiont fractions for physiology measurements and fatty acid and stable isotope analysis was conducted as follows:

the homogenate was centrifuged at 5,000 rpm for 5 min at 4 °C, the host fraction (supernatant) was decanted while the endosymbiont pellet was resuspended in 25% of the original volume of phosphate buffer and centrifuged again. The supernatant of this second centrifuge step was added to the host fraction and this was centrifuged again to remove any remaining endosymbiont cells. Both the endosymbiont and host fractions were immediately lyophilized at -80 °C until each sample was completely dry. These freeze-dried samples were then taken to UC Santa Barbara and later stored in a -80 °C freezer under N_2 gas for preservation of polyunsaturated fatty acids (PUFA).

2.3.4 Fatty Acid Extraction and Analysis

Fatty Acid extraction and analysis was performed on the previously freeze-dried host and symbiont fractions as separate samples (they were not extracted together as a holobiont). Symbiont samples were weighed out at ~3-5 mg per sample and host fraction samples were weighed out at ~15 mg per sample. Samples were extracted using a modified Folch method (Folch et al., 1957) following Taipale et al., 2013. The fatty acid extraction was followed closely to Radice et al., 2019 but with slightly different volumes for the final extract (500 uL for symbiont and 300 uL for host). For most samples, two internal standards were used: 2-methyldodecanoic acid (C12- methyl branched) and nonadecenoic acid (C19:1). Due to constraints, some samples only had 2-methyldodecanoic acid as an internal standard while others only had nonadeconic acid, although most had both. When available, the percent recovery of nonadecenoic acid was used to calculate percent recovery of total fatty acids and only samples with this internal standard were used to calculate mass normalized fatty acid concentrations because it represented a more realistic mass and degree of unsaturation of the fatty acids of interest (C14-C22 with varying degrees of unsaturation).

Fatty acids were analyzed with a Gas Chromatograph equipped with a Flame Ionization Detector (GC-FID, Hewlett Packard HP5890) and a Supelco Omegawax 250 Column (30 m x 0.25 mm ID x 0.25 um film thickness) with a 1 uL injection and a 30 second splitless hold time. Temperature ramp was conducted as follows: 50 °C hold start temp, hold for 1 minute, 10 °C/min ramp to 150 °C, hold for 0 min then a 4 °C/min ramp to 265 °C. Flow rates were as follows: 60 mL/min He flow into inlet, 3.5 mL/min He out of septum purge, 54 mL/min He out of split vent, 2.5 mL/min He flow through FID (column flow). Detector flow rates were 475 mL/min air, 60 mL/min N2, and 120 mL/min H2 at FID. Fatty acids were identified by a mixture of techniques; comparison of retention times and peak area to a certified reference material (Supelco 37 component FAME mix, FAME-37), spiking experiments with known compounds, and by analyzing a representative subset of samples on a gas chromatograph equipped with a mass spectrometer (GC-Ms) using similar GC run parameters. The mass of each fatty acid on column was calculated by dividing peak area by the response factor (area/ mass) for that fatty acid on that day (FAME-37 reference material was run on the GC-FID each morning to check the instrument and get response factors for each fatty acid). If the fatty acid of interest was not in the FAME-37 mix a response factor was generated by the next closest fatty acid with the same carbon length tail and the same or similar number of double bonds. This was possible because the response factor followed a linear trend, decreasing systematically throughout the chromatographic run time as carbon number and degree of unsaturation increased. Analytical precision for relative abundance data (calculated from FAME-37) was ± 0.04% and precision for mass normalized data was ~ 0.1 $\mu g\ g^{-1}$.

2.3.5 Isotope Ratio Measurements

Freeze-dried tissue samples were dried at 60°C for a minimum of 48 h to ensure dryness and later acidified with a minimum of 190 µl 6% sulfurous acid or more until bubbles ceased forming to remove any inorganic carbonates. Samples were analyzed for $\delta^{13}C$ and $\delta^{15}N$ using a Thermo Finnigan Delta-Plus Advantage isotope mass spectrometer coupled with a Costech EAS elemental analyzer in the University of California Santa Barbara Marine Science Institute Analytical Laboratory. Instrument calibration was conducted using acetanilide reference standards run at the beginning of each set of 35 samples and tested every 5 samples within each set. Instrument precision, determined using replicate analyses of L-glutamic acid USGS40, was ± 0.12 for ^{13}C and ± 0.06 for ^{15}N. The abundances of ^{13}C and ^{15}N are expressed in standard δ notation and calculated as follows for element X:

$$\delta X_n = 1000 \times \frac{R_{sample} - R_{standard}}{R_{standard}},$$

where $R = X_n/X_{n-1}$, expressed as per mil (‰) relative to the PDB standard for carbon and atmospheric N_2 for nitrogen.

2.3.6 Physiology Measurements

Skeletal growth measurements and Pulse Amplitude Fluorometry (PAM) measurements were taken during the experiment to non-destructively assess coral physiology. Skeletal growth measurements were taken using the buoyant weight method (Jokiel et al., 1978). Fragments were taken from their tanks and skeletal mass was measured three times during the experiment using water of a known temperature and salinity to calculate the mass difference when the coral fragment was dipped into the water on a mass balance. After the experiment was completed, brushed coral skeletons were dried and their surface area determined by wax dipping (Stimson & Kinzie, 1991).

For pulse amplitude fluorometry (PAM) measurements during the experiment, coral fragments were dark-acclimated for 20 min in their respective treatment and rapid light curves were generated (RLC, 0–701 μmol m−2s−1PAR, 20 s intervals), using an Imaging-PAM fluorometer (MI3, SI 10, gain 2, damp 2, saturating width 0.8 s; Heinz Walz GmbH, Effeltrich, Germany). All PAM measurements were conducted between 8:00 and 10:00 PM. Calculations for maximal photosynthetic yield and maximum relative electron transport rates were calculated according to Krueger et al., 2017.

For symbiont densities, 90 uL of homogenate (host + symbiont fraction) was fixed with paraformaldehyde to 4% and stored at 4 °C until counting. Symbiont density was determined by placing homogenate onto a hemocytometer grid and counting symbiont cells with a Zeiss Axioskop binocular microscope at 10-40x magnification. Cells were counted in 8 grids and total symbiont count for the coral fragment was calculated by multiplying by fractional volume used and any dilution factors. Measurements were conducted at 8x replication for each sample. Symbiont chlorophyll was analyzed by extraction of a portion of the symbiont fraction in 1 ml of 90% acetone in the dark (24 h, 4°C). Samples were centrifuged (5000×g, 4°C) and the concentration of chl a and c2 and total chlorophyll in the supernatant was spectrophotometrically determined (Jeffrey & Humphrey, 1975). The total soluble protein content of host and symbiont was determined with the improved Bradford protocol, using bovine serum albumin as the protein standard (Bradford, 1976).

2.3.7 Statistical Methods

Statistical analyses were conducted in R (version 4.2.1) and R studio (version 2022.12.0+353). ANOVA tests were run using the ‘aov()’ function within R and non-linear modes were fit using the ‘nls()’ function. Reef and pelagic zooplankton were assessed for

statistical differences in FA profile using PERMNOVA (non-parametric multivariate ANOVA) using the ‘adonnis2’ within the ‘pairwiseAdonnis’ package function in R and showed $p > 0.01$, thus we pooled both pelagic and reef zooplankton for the remainder of analyses.

2.4 Results & Discussion

2.4.1 Corals scale feeding with food availability, bleached corals eat at slower rates than unbleached counterparts

Experimental treatment coral fragments of *Stylophora pistillata* were fed freshly hatched nauplii at ~ dusk. Two treatments, Fed 6x (F_6x) and Bleached/Fed 6x (B_F_6x) were fed six times a week, while another treatment, Fed 2x (F_2x) was fed two times per week and the control treatment was unfed for the entirety of the acclimation and the experiment (~ 4 weeks). These treatments represent a gradient in heterotrophy where control corals represent a full autotrophic endmember (0% heterotrophy), F_2x and F_6x treatments represented sequential increases in heterotrophy (between 0-100% heterotrophy) and B_F_6x corals represent a fully heterotrophic endmember (100% heterotrophy). It is important to note that due to the level of experimental replication (n ~ 30 per treatment), with near daily feeding, it was not possible to measure feeding rate for each fragment and thus feeding rate was measured at the tank level (n ~10 per tank, 3 tanks per condition, Figure 9). We would expect some intra-specific variation in heterotrophy of different colonies, as has been shown for another branching coral, *Pocillopora meandrina* (Fox et al., 2019).

There was considerable variation in cumulative nauplii captured per tank within treatments (Figure 9), likely due to variation in cumulative feeding rates of the corals in each tank given that each tank was fed the same nauplii density on a given day (with variation between days). Control corals were fed no nauplii during the experiment and have a cumulative capture of 0 nauplii cm^{-2}, F_2x tanks fed on an average of 973 ± 260 nauplii cm^{-2}, while F_6x tanks fed on roughly double the nauplii of the Fed 2x corals, but with larger variation between tanks at 2066 ± 499 nauplii cm^{-2}. On average, B_F_6x tanks fed on less nauplii over the course of the experiment (1675 ± 329 nauplii cm^{-2}) although one tank did feed

on 2052 nauplii cm^{-2}. Although bleached corals fed on less nauplii than unbleached corals we would expect them to be more heterotrophic (acquiring a larger % of biomass from heterotrophy) than F_6x corals because of the significant loss in symbiont density and chlorophyll (Figure 11, Table 2) that reveals minimal autotrophic influence from the symbionts. Altogether, these results indicate that a gradient in heterotrophy was captured during the experiment.

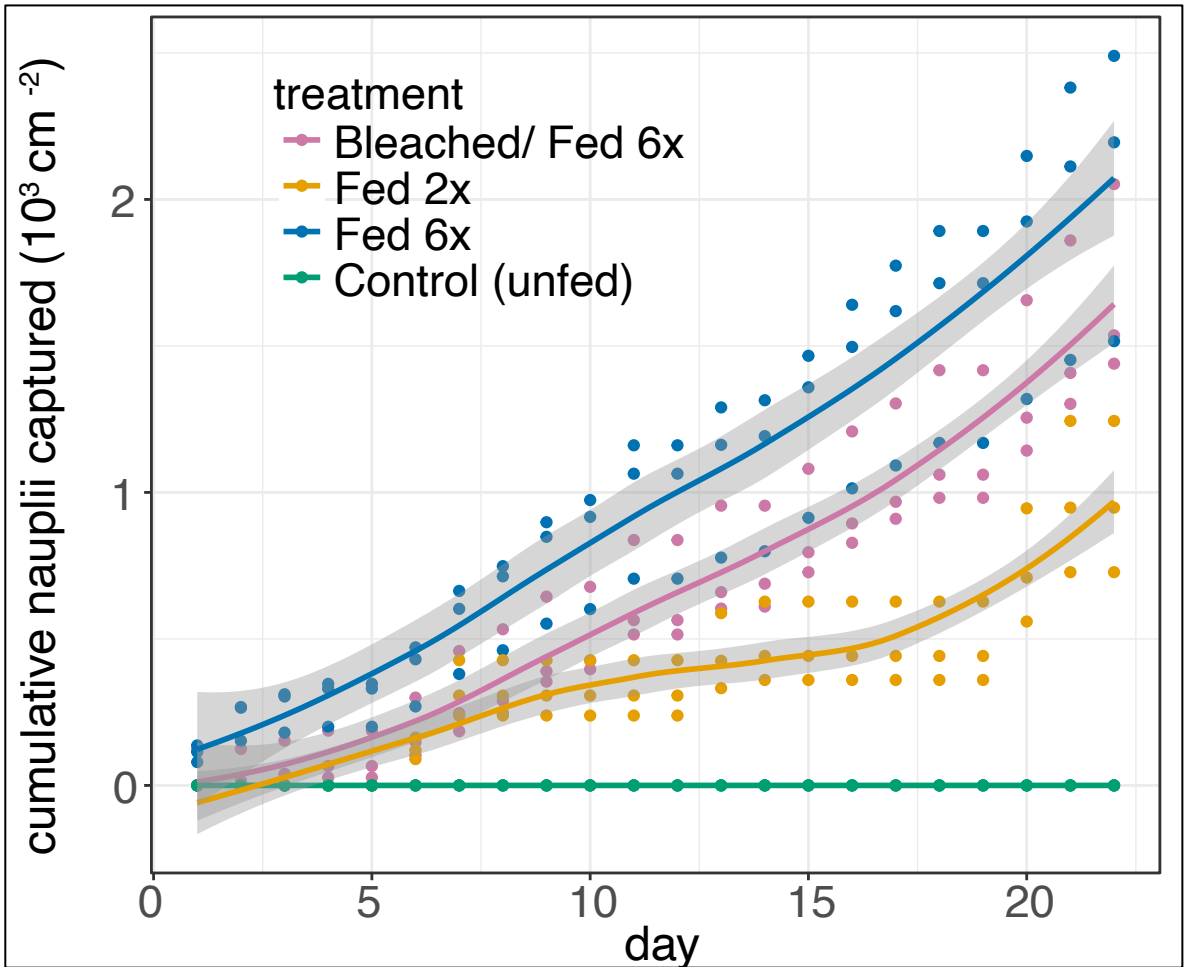

Figure 9. Cumulative nauplii capture per tank (n = 3 per condition), plot shows raw data and smoothed line with standard error for cumulative nauplii capture for each tank over the course of the experiment.

Due to slight variation in water temperatures during daily *Artemia* cyst hatching, corals were fed nauplii at a range of densities (between 175 – 1407 nauplii L^{-1}) throughout the experiment, this enabled a prey-density versus prey consumption rate plot to understand prey capture and consumption efficiency of the different experimental treatments (Figure 10), data were fit to a logarithmic equation with a non-zero intercept according to Ferrier-Pagès et al., 2003. Logarithmic regressions per treatment (y = a + b*x) show that F_2x corals exhibited the highest consumption rates (a = -275.7, $p < 0.001$; b = 54.4, $p < 0.001$; $F_{1, 16} = 40.61$; $R^2 = 0.70$), over the F_6x condition (a = -209.1, $p < 0.001$; b = 41.0, $p < 0.001$; $F_{1, 55} = 57.37$ $R^2 = 0.50$) suggesting that Red Sea *Stylophora pistillata* may reach a feeding "limit" in which feeding declines as number of prey captured per day increases, although this limit is likely not reached on in nature where planktonic densities are much lower (~ 1-2 orders of magnitude lower in biomass m^{-3} in oceanic water, ~ 2-3 orders of magnitude lower in lagoonal reef waters; Hamner et al., 2007). Interestingly, bleached corals (B_F_6x) exhibited the lowest feeding efficiency of all treatments (a = -177.1, $p < 0.001$; b = 33.8, $p < 0.001$; $F_{1, 55} = 41.09$; $R^2 = 0.42$; Figure 10) suggesting that there may be an energetic cost to feeding that is supplemented by the symbionts. It has been shown that *Stylophora pistillata* release hydrogen peroxide into the water at site of physical and chemical stimulus during feeding (the polyp) in bleached and non-bleached corals (Armoza-Zvuloni et al., 2016) which may require energy for maintenance and hydrogen peroxide generation due to inhibited symbiont photosynthesis (Lesser, 2006; Venn et al., 2008). This result has further implications for corals in the face of a warming global ocean such that if bleached corals consume less plankton than unbleached corals given the same heterotrophic supplies, their ability to supplement energetic reserves with feeding and recover from bleaching may be more hindered than previously thought.

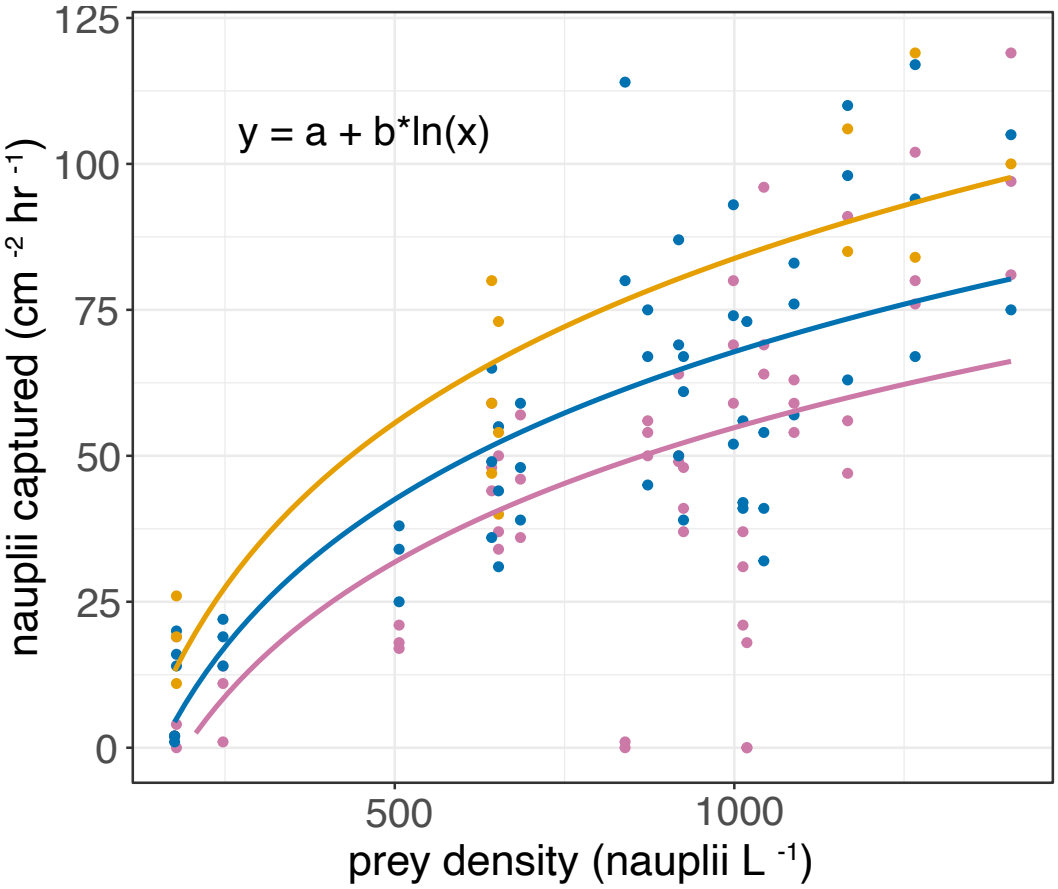

Figure 10. Logarithmic models of feeding rate as a function of prey density following the model function of Ferrier-pages 2003 et al. All logarithmic model coefficients (a and b) are significant to the $p < 0.001$ level. Bleached corals show lowest feeding rates, whereas unbleached corals fed six times a week show slightly faster feeding rates and corals fed twice a week show the fastest feeding rates, suggesting that there may be an energetic cost to feeding.

2.4.2 Feeding induces physiological and molecular benefits to corals but does not offset bleaching effects

During the feeding experiment, non-destructive measurements were taken to assess skeletal growth and photosynthetic efficiency of corals. Photo-physiological measurements taken every five days during the experiment revealed that bleached and fed corals (B_F_6x) had significantly reduced maximum photosynthetic yield and relative maximum electron transport through the duration of the experiment (Table 2, Figure 12, Figure 11 F and G; $p < 0.001$; ANOVA), revealing that bleaching was effective in drastically reducing symbiont density (Figure 11B and E) and chlorophyll (Figure 11A) and thus the photosynthetic contributions of symbionts to the host within these corals. Bleaching induced a significant decline of every holobiont physiology metric that was measured ($p < 0.001$, one-way ANOVA, Table 2). Interestingly, the high feeding treatment (F_6x) of non-bleached corals showed small but sometimes significant declines in photo-physiological parameters on certain days of the experiment (Figure 11G, Table 2, Figure 12). However, these changes were relatively subtle when considering the relative change between bleached and non-bleached corals.

Feeding increased mean treatment surface area normalized symbiont density and host protein, although non-significantly (Figure 11B and E, Table 2) and significantly increased chlorophyll a ($p < 0.001$; ANOVA), total chlorophyll (Figure 11A; $p < 0.001$; ANOVA) and aragonite growth (Figure 11C; $p < 0.01$; ANOVA). Feeding increased mean host protein per treatment (normalized to surface area or symbiont cell, Figure 11D, Table 2) and showed considerable variation within treatments. Across all treatments, skeletal growth rate plotted against total chlorophyll appears to fit a logarithmic function (Figure 11I; $R^2 = 0.66$; $p < 0.001$) exhibiting an upper limit reached at about 2.5 mg d^{-1} cm^{-2} for *S. pistillata.* This data suggests

that symbionts are facilitating holobiont skeletal growth and that even with high feeding and capture rates (Figure 9 and 10), bleached corals still struggle to grow their skeleton (Figure 11C and I). Overall, this data shows that feeding incurs physiological benefits to the coral holobiont and that even feeding on large amounts of nutritionally rich *Artemia* nauplii, bleached corals are unable to offset the detrimental effects of bleaching.

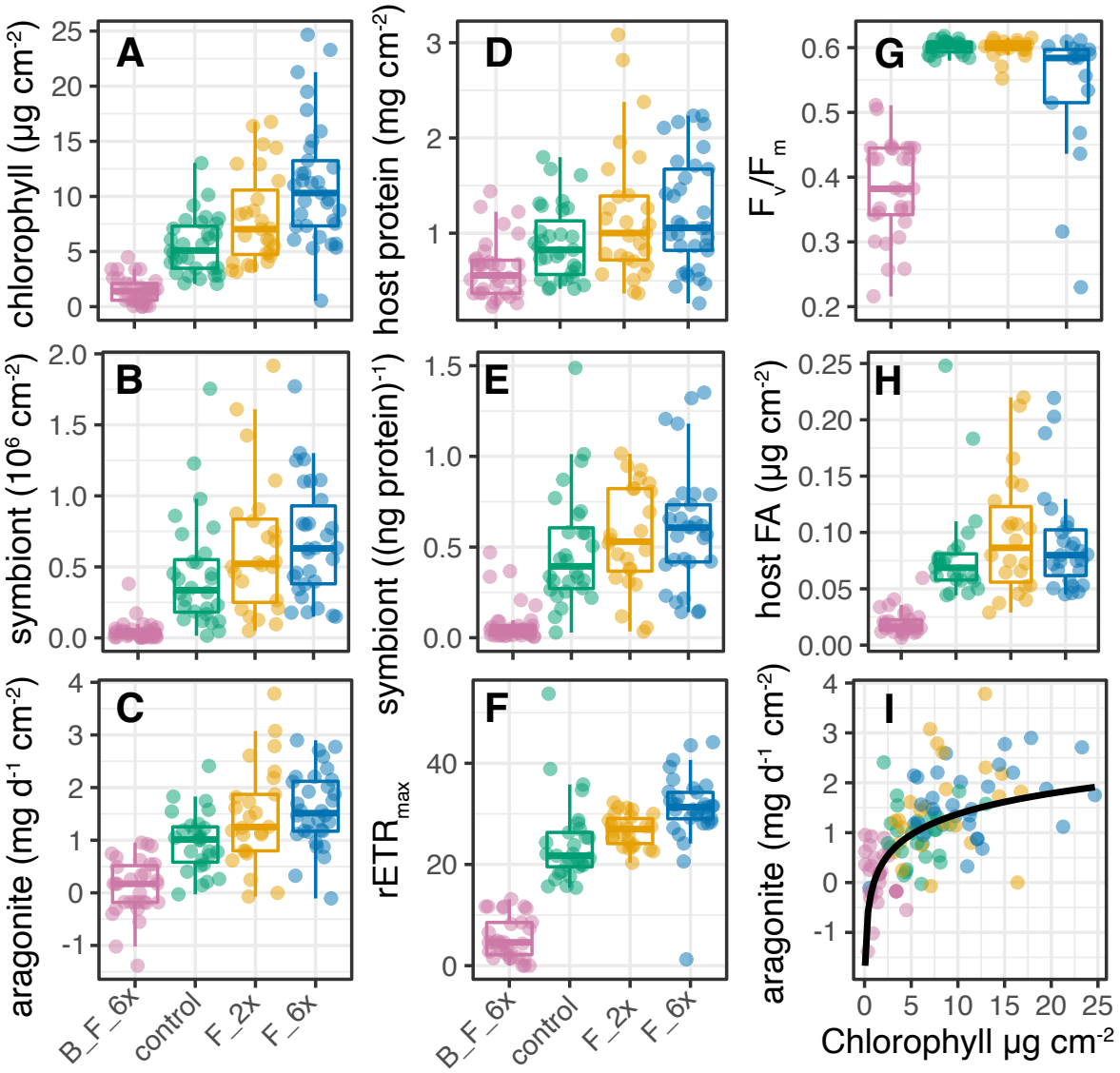

Figure 11. Physiology multiplot, all figures show physiological response variables from feeding experiment, with bleached and fed corals in pink, control corals (unfed) in green, corals fed twice a week in yellow, and corals fed six times a week in blue. **A** shows surface area normalized chlorophyll, **B** shows surface area normalized symbiont density, **C** shows aragonite (skeletal) growth throughout the experiment, **D** shows surface area normalized host protein, **E** shows symbiont count normalized to host protein, **F** shows relative

maximum electron transport rate calculated according to Krueger et al., 2017, **G** shows maximum photosynthetic yield (ref), **H** shows surface area normalized total fatty acid and **I** shows aragonite growth plotted with chlorophyll density fitted to a logarithmic curve of the equation $y = 0 + a*\ln(x)$.

Physiology metric	control	F_2x	F_6x	B_F_6x	feeding effect	bleach effect
symbiont density (x 10^5 cm $^{-2}$)	4.96 ±4.02	6.44 ±4.96	7.02 ±4.1	0.5 ±0.77		***
host protein (mg cm $^{-2}$)	0.91 ±0.37	1.18 ±0.74	1.19 ±0.59	0.63 ±0.31		***
Chlorophyll a (µg cm $^{-2}$)	4.32 ±1.81	6.29 ±2.88	8.55 ±4.03	0.69 ±0.58	***	***
Chlorophyll c2 (µg cm $^{-2}$)	1.56 ±1.26	2.6 ±2.05	2.59 ±2.01	0.68 ±0.71		***
Chlorophyll total (µg cm $^{-2}$)	5.88 ±2.69	8.89 ±4.25	11.14 ±5.51	1.37 ±1.15	***	***
aragonite growth (mg cm $^{-2}$ d^{-1})	0.98 ±0.54	1.54 ±0.96	1.62 ±0.73	0.11 ±0.58	**	***
F_v/F_m day 4	0.6 ±0	0.6 ±0	0.5 ±0.1	0.2 ±0.1	**	***
F_v/F_m day 9	0.6 ±0	0.6 ±0	0.6 ±0.1	0.3 ±0.1		***
F_v/F_m day 16	0.6 ±0	0.6 ±0	0.6 ±0.1	0.3 ±0.1		***
F_v/F_m day 21	0.6 ±0	0.6 ±0	0.6 ±0.1	0.4 ±0.1		***
$rETR_{max}$ day 4	23.5 ±5.2	27 ±5.7	27.8 ±8	1.6 ±1.9	*	***
$rETR_{max}$ day 9	24.7 ±7.5	36.8 ±25	33.8 ±13.9	4.1 ±7.2	*	***
$rETR_{max}$ day 16	24.3 ±8.5	26.8 ±2.9	30.6 ±7.3	5.7 ±4.1	**	***
$rETR_{max}$ day 21	29.8 ±14.7	31.9 ±11.7	30.9 ±6.7	8.4 ±5.4		***

Table 2. Physiology metrics summary table. Feeding effect significance results from one-way ANOVA between control condition, fed 2x per week and fed 6x per week condition [* ($p < 0.05$), ** ($p < 0.01$), ***($p<0.001$)]. Bleaching effect results from one-way ANOVA between fed 6x per week condition and bleached and fed 6x per week condition.

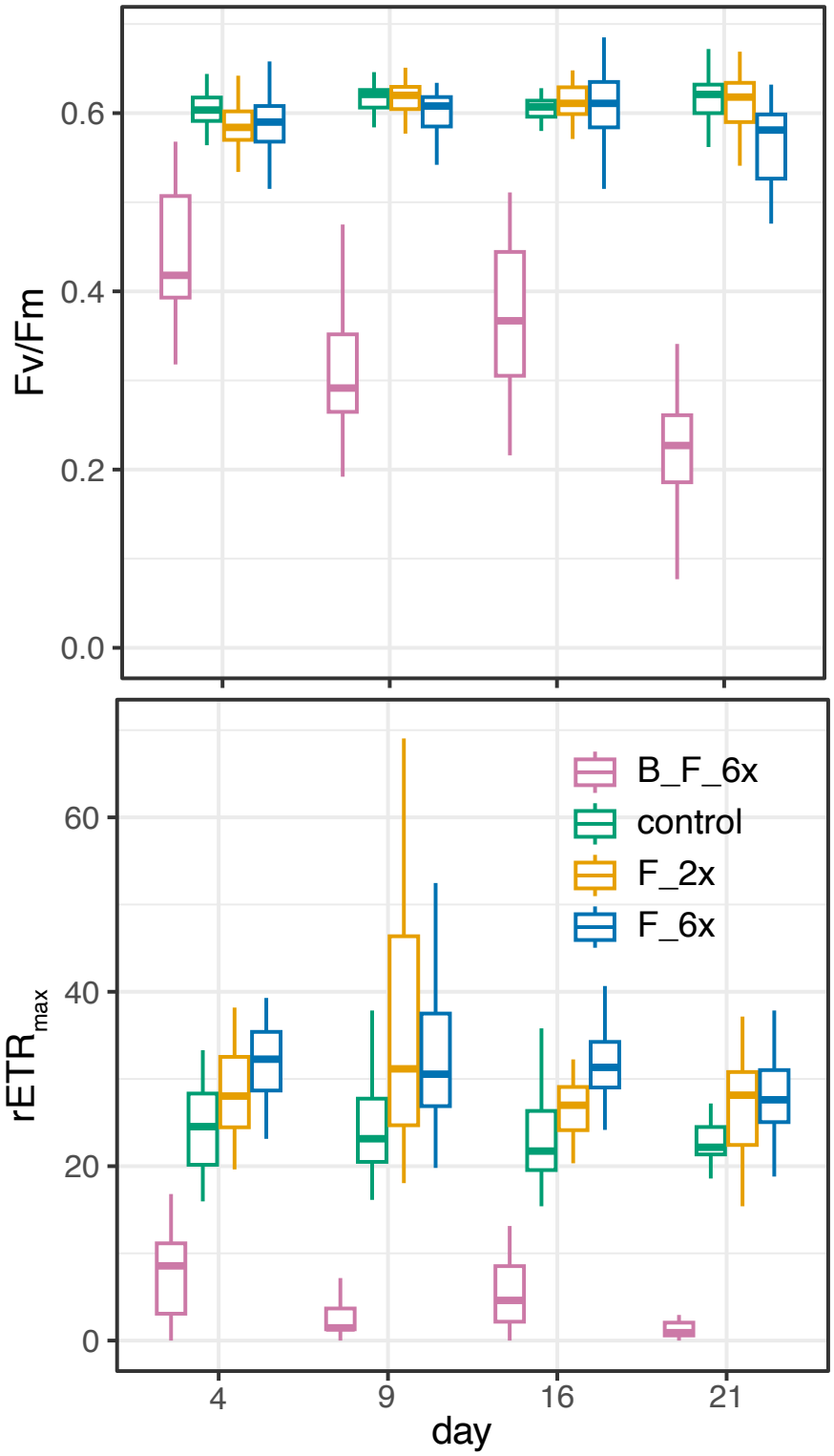

Figure 12. Boxplots of Coral photosynthetic measurements separated by treatment group from four equally spaced days during the 3-week experiment. Top plot shows maximum photosynthetic yield, bottom plot shows maximal relative electron transport rate calculated according to (Krueger et al., 2017).

2.4.3 Heterotrophy significantly alters biomarkers in both host and symbiont

Changes in coral heterotrophy of non-bleached corals (control, F_2x, F_6x) elicited significant changes in a larger number of fatty acids (FA) in both the host and symbiont fraction when considering relative abundance data (% of total fatty acids; for $p < 0.05$, one-way ANOVA; host = 20, symbiont = 16, Table 3) than mass normalized fatty acid data (μg g^{-1} dry tissue; for $p < 0.05$, one-way ANOVA; host = 3, symbiont = 9, Table 4) and showed more significant change (smaller p-values) than mass normalized data (Table 3 and 4). Although some argue that for corals, "calculating FA compositions … as a percentage risks greatly under- or overestimating their true amounts" (Kim, Lee, et al., 2021) these data suggest that relative abundance data best captures shifts in coral heterotrophy over a mass normalized calculation. Additionally, the coral animal-dinoflagellate symbiosis often exhibits positive feedback loops (Tremblay et al., 2016) in which the tight recycling of nutrients between the host and symbiont results in the symbiont benefiting from host heterotrophy (Figure 8). For example, feeding increases symbiont density and chlorophyll (Figure 11A and B) as well as symbiont photosynthesis (Dubinsky et al., 1990; Grottoli, 2002; Houlbrèque et al., 2003; E. Titlyanov et al., 2000; E. A. Titlyanov et al., 2001) and may increase symbiotic biomarker concentrations in the host (Seemann et al., 2013). Additionally, for *Stylophora pistillata*, mass normalized total fatty acid concentration remained unchanged with increased heterotrophy for non-bleached corals ($p = 0.861$; one-way ANOVA; Table 4). Total lipid content is known to also remain constant for *Stylophora subseriata* along eutrophication gradients in Indonesia in which heterotrophy increases with increasing eutrophication (Seemann et al., 2013), suggesting that these corals maintain tight levels of total FA via a balance of deposition, anabolism and catabolism (Chen et al., 2017). This may explain why mass normalized fatty

acid data does not perform as well in capturing shifts in coral heterotrophy as compared to a "fingerprinting" measurement (unitless) such as relative abundance data. Additionally, since fatty acid relative abundance is an internal metric within each sample extract these data are likely more robust to human error, normalization practices across laboratories and are more comparable across studies since relative abundance values have classically been used for fatty acid feeding and comparative studies (Al-Moghrabi et al., 1995b; Bachok et al., 2006; Imbs, Latyshev, et al., 2010; Iverson et al., 2004). Thus, moving forward, we will consider only fatty acid relative abundance data along with other frequently used biomarkers ($\delta^{13}C$, $\delta^{15}N$ and C:N) to strengthen source group separation and tissue level responses to changes in heterotrophy (biomass acquired through heterotrophy).

Corals were fed freshly hatched *Artemia* nauplii as their singular heterotrophic source which exhibited significant differences in most biomarkers (22 out of 30 biomarkers, $p < 0.01$, one-way ANOVA; Figure 13) when compared to the autotrophic source (symbionts of control, unfed, corals). These data show that for this experiment, there were significant chemical and isotopic differences between source groups that would enable capture of differences in relative heterotrophy of coral fragments. It is important to recognize two possible sources of variation in the experiment that may complicate the biomarker signal in coral tissues: 1) possible carryover of biomarker signals from heterotrophy on the reef before the experiment and 2) ingestion of non-nauplii sources during the experiment (i.e particulate organic matter in the tanks). Considering the possibility of carry-over of heterotrophy biomarkers into the experiment (biomarkers from feeding on the reef), some of this variation may in fact be captured by the vertical spread (PC2 axis) in the autotrophic source (i.e. more or less "heterotrophic" symbionts; Figure 13), while the horizontal axis (PC1) appears to capture

almost entirely the difference between autotrophic or heterotrophic source. To explore this further nauplii were plotted with *in-situ* food sources (Gulf of Aqaba zooplankton, pom, and control coral symbionts) using a principal component analysis which shows that *Artemia* nauplii still exhibit a unique biomarker "fingerprint" that enables tracking of this heterotrophy source into host tissues (Figure 14). While it is possible that some corals were feeding on particulate organic matter in the tanks during the experiment, it has been shown that *Stylophora pistillata* does not feed readily on microalgae (Leal et al., 2014), which is a significant mass fraction reef POM (~ 30-45% for pelagic/non-lagoonal POM, Wyatt et al., 2013). Additionally, corals scale heterotrophy with increased prey density (Ferrier-Pagès et al., 2003, Figure 10) and POM in the tanks exhibited a mass density 124.2 ± 43.7 μg C L^{-1} while *Artemia* nauplii was fed to corals at densities of ~ 10,000 prey L^{-1} for a mass density of 1.28 x 10^4 μg C L^{-1} (3.2 μg nauplii $^{-1}$; Peykaran et al., 2011; ~40% C nauplii^{-1}, this study), showing that *Artemia* nauplii carbon concentrations were roughly 1-2 orders of magnitude higher. This indicates that most change in biomarkers of coral tissues was from the symbiont fraction and/or feeding on *Artemia* nauplii (Figure 13).

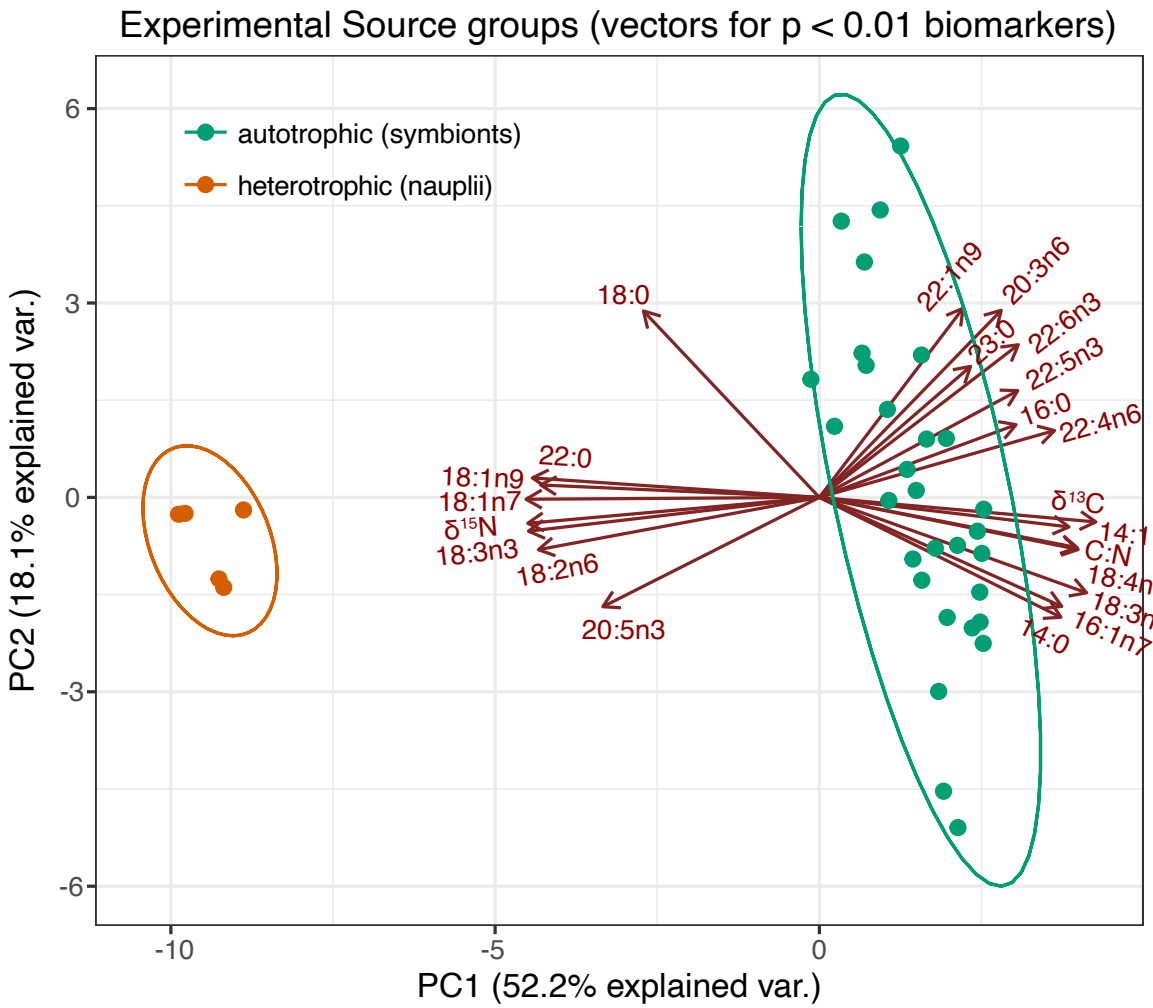

Figure 13. Principal component analysis of biomarkers of two nutritional sources during feeding experiment, autotrophic source represented by unfed coral symbionts in green and heterotrophic source represented by *Artemia* nauplii in orange, ellipses represent 95% confidence intervals. Vectors in which biomarker had $p > 0.01$ (one-way, ANOVA) significant difference between source groups were excluded. Biomarker vectors included in plot all have $p < 0.01$ (one-way, ANOVA) significant difference between source groups.

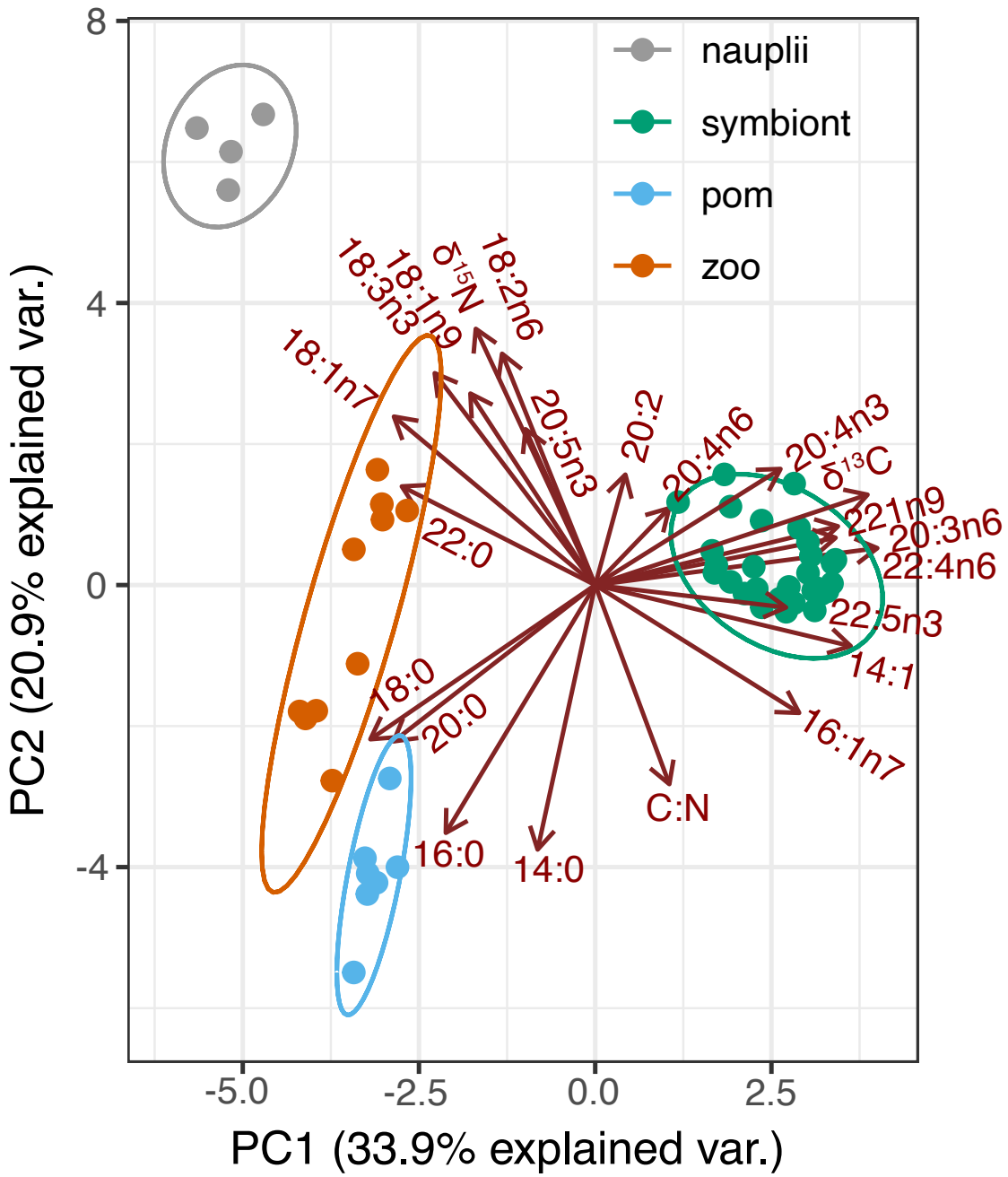

Figure 14. Principal component analysis of *in situ* nutritional sources (zooplankton, particulate organic matter [pom] and control coral symbionts) and experimental nauplii source showing complete separation and a distinct biomarker "signature" for artemia nauplii. Ellipses are 95% confidence ellipses showing complete separation of all in situ and experimental sources. Some biomarker vectors omitted for clarity.

Relative heterotrophy of non-bleached corals significantly altered the abundance of several FA and elemental biomarkers in both the host and symbiont fraction (Table 3, Figure 15). In the host fraction, 18:0, 18:2n6, 18:3n3, 20:5n3, 22:5n3 and $\delta^{15}N$ significantly increased ($p < 0.001$, one-way ANOVA) with several other biomarkers increasing at lower levels of significance ($p < 0.01$ or $p < 0.05$, one-way ANOVA; Table 3). Nauplii were significantly higher in a specific suite of FA and isotopic biomarkers compared to symbionts (cluster of PC1 negative vectors in Figure 13) that all exhibited significant ($p < 0.001$) increases in coral host tissue except for 22:0 and 18:1n7. Interestingly, increasing biomass sourcing from heterotrophy on nauplii elicited an increase in some fatty acids that were lower in the heterotrophic source and higher in the autotrophic source. For example, 22:5n3, a fatty acid that was higher in the autotrophic source (Figure 13), significantly increased in the host fraction with increased feeding ($p < 0.001$; one-way ANOVA). It is known that 22:5n3 is a diagnostic marker of dinoflagellates/ autotrophy (Mies et al., 2018; Papina et al., 2003; Treignier et al., 2008) and that heterotrophy tends to increase symbiont density, chlorophyll (Figure 11) and photosynthesis (Dubinsky et al., 1990; Grottoli, 2002; Houlbrèque et al., 2003; E. Titlyanov et al., 2000; E. A. Titlyanov et al., 2001), which is in alignment with 22:5n3 exhibiting significantly lower values in bleached corals ($p < 0.001$; one-way ANOVA; Table 3, Figure 15). Given that heterotrophy provides positive feedbacks on symbiont density and transfer of photosynthates like 22:5n3 from symbiont to host, considering singular biomarker field data in isolation may lead to erroneous interpretations of coral heterotrophy which may be misinterpreting increases in 22:5n3 as a relative increase in autotrophic source contribution when it may be due to increased heterotrophy. This underlines the importance of considering many biomarkers at once when considering coral mixotrophy. Overall, this data shows that

both essential (18:2n6 and 18:3n3; Table 3, Figure 16; Dunn et al., 2012) and non-essential fatty acids are reliably recorded into host tissues after feeding and would likely be of great use when considered alongside isotopic and elemental biomarkers.

While some biomarkers in the host fraction increased due to increased heterotrophy, several biomarkers in the host significantly decreased with increased heterotrophy, such as 18:1n9, 18:3n6, 20:3n6, 22:1n9, 23:0 and C:N ($p < 0.001$, one-way ANOVA) whereas other biomarkers showed significant decreases at $p < 0.01$ or $p < 0.05$ levels (one-way ANOVA; Table 3). All $p < 0.001$ biomarker declines in the host fraction with increasing heterotrophy were autotrophic markers (Figure 13), except for 18:1n9 (interestingly, a similar decline in 18:1n9 was seen in *Turbinaria reniformis* fed natural zooplankton; Treignier et al., 2008). When considering all autotrophic biomarkers found in the host fraction, some were positively or negatively correlated with heterotrophy, suggesting divergent metabolic patterns. A possible interpretation of this pattern is that those biomarkers that were higher in the autotrophic source and were positively correlated with heterotrophy (16:0, 18:4n3, 22:4n6, 22:5n3; Table 3, Figure 15) could be due to feeding increasing the symbiont density (Figure 11) and photosynthesis of the symbionts (Grottoli, 2002), thus increasing symbiont biomarker influence. These FA could likely be a part of a "shorter turnover pool" of autotrophic biomarkers that are relayed to the coral host from the endosymbiont and respond quickly to changes in coral mixotrophy. For those FA that were higher in the autotrophic source but decreased with increasing heterotrophy (14:0, 16:1n7, 18:3n6, 20:3n6, 22:1n9, 22:6n3), this pattern suggests a "dilution effect" in that these fatty acids may be a part of a longer turnover pool of molecules that the host received from the symbiont but is not readily mobilized and thus got diluted by the unique fingerprint of biomarkers of the nauplii. Interestingly, the

carbon to nitrogen ratio (C:N) showed a strong and significant response to heterotrophy ($p < 0.001$, ANOVA) and may serve as a useful tool to accompany fatty acid and isotopic data.

Biomarker	HOST						SYMBIONT			
	control	**F_2x**	**F_6x**	**B_F_6x**	Feed effect	Bleach effect	control	F_2x	F_6x	Feed effect
C12:0	0.1 ±0.1	0.2 ±0.1	0.3 ±0.3	0.3 ±0.2			0.3 ±0.3	0.2 ±0.2	0.2 ±0.1	
C14:0	1.4 ±0.2	1.3 ±0.2	1.3 ±0.2	0.5 ±0.2	*	***	5.4 ±1.2	4.5 ±0.9	4.2 ±0.7	***
C14:1	0.1 ±0	0.1 ±0	0.1 ±0	0 ±0		***	0.5 ±0.1	0.6 ±0.1	0.7 ±0.1	***
C16:0	22.5 ±2	22.5 ±2.2	24 ±2	22.7 ±3	**		23.1 ±2	21.8 ±1.7	21.6 ±2.9	*
C16:1n9	0 ±0	0 ±0	0 ±0	0.1 ±0.2			0.9 ±0.5	1 ±0.4	1.4 ±0.6	**
C16:1n7	3.4 ±0.5	3.1 ±0.4	3.2 ±0.4	0.9 ±0.6	*	***	7.4 ±1.7	6.1 ±1.1	5.8 ±1	***
C16:2	0.1 ±0	0.1 ±0	0.1 ±0	0.1 ±0.1	*	*	0.6 ±0.2	0.4 ±0.2	0.5 ±0.2	
C18:0	13.3 ±1.9	13.6 ±1.5	15.4 ±1.7	31.1 ±6.5	***	***	6.4 ±1.5	6.3 ±1.2	6 ±1.2	
C18:1n9	10.5 ±1.6	9.7 ±1.6	8.4 ±2	4.6 ±1.4	***	***	7.2 ±2	6.1 ±1.5	5.5 ±2.3	**
C18:1n7	3.1 ±0.5	3.3 ±0.5	3.1 ±0.5	2.7 ±0.5		**	1.2 ±0.4	1.5 ±0.4	1.4 ±0.3	*
C18:2n6	0.8 ±0.1	0.9 ±0.1	1 ±0.1	1.5 ±0.4	***	***	1.6 ±0.2	1.4 ±0.2	1.4 ±0.2	***
C18:3n6	1.4 ±0.4	1.1 ±0.3	1 ±0.3	0.6 ±0.3	***	***	5.5 ±1.2	3.8 ±0.9	3.4 ±0.9	***
C18:3n3	0.1 ±0.1	0.6 ±0.1	0.5 ±0.1	0.9 ±0.5	***	***	0.1 ±0.1	0.5 ±0.1	0.4 ±0.1	***
C18:4n3	1.8 ±0.8	1.7 ±0.9	2 ±1.1	0.3 ±0.2		***	14.3 ±3.1	18.9 ±4.3	22.1 ±5.9	***
C20:0	0.7 ±0.1	0.6 ±0.1	0.7 ±0.1	1.1 ±0.3		***	0.3 ±0.1	0.3 ±0.1	0.3 ±0.1	
C20:1n9	3.2 ±0.8	3 ±0.8	2.5 ±0.8	1.6 ±0.5	**	***	1.8 ±1.4	1.6 ±1.4	1.6 ±1.7	
C20:2	0.7 ±0.1	0.8 ±0.3	0.7 ±0.1	1.1 ±0.2		***	0.3 ±0.1	0.4 ±0.3	0.3 ±0.1	
C20:3n6	4.5 ±1	3.6 ±0.9	2.7 ±0.6	0.8 ±0.5	***	***	1.5 ±0.6	1.3 ±0.4	1 ±0.5	**
C20:4n6	8.6 ±1.5	9.5 ±1.4	8.9 ±1.4	12.1 ±2.4		***	4.8 ±1.5	4.7 ±1.4	3.9 ±0.9	**
C20:4n3	2.2 ±0.6	1.9 ±0.4	1.7 ±0.4	0.3 ±0.2	**	***	0.7 ±0.3	0.7 ±0.3	0.6 ±0.3	
C20:5n3	2.1 ±0.4	2.7 ±0.4	3.4 ±0.7	3.1 ±1	***		2.6 ±0.9	2.7 ±0.7	2.9 ±0.8	
C22:0	0.3 ±0.1	0.3 ±0.1	0.3 ±0.1	0.7 ±0.2		***	0.1 ±0.1	0.2 ±0.1	0.2 ±0	***
C22:1n9	0.7 ±0.1	0.7 ±0.2	0.6 ±0.1	0.6 ±0.2	***		0.4 ±0.2	0.5 ±0.2	0.5 ±0.2	
C23:0	0.7 ±0.2	0.7 ±0.2	0.6 ±0.1	0.3 ±0.1	***	***	0.2 ±0.1	0.2 ±0.1	0.2 ±0.1	
C22:4n6	6.2 ±1	6.7 ±1.1	7.1 ±1.1	9.2 ±1.9	**	***	3.3 ±1	3.2 ±1	3 ±0.6	
C22:5n3	1.2 ±0.2	1.3 ±0.2	1.4 ±0.2	1.1 ±0.3	***	***	0.6 ±0.2	0.7 ±0.2	0.7 ±0.2	
C22:6n3	10.3 ±1.7	9.9 ±1.7	8.9 ±1.7	1.8 ±1.3	**	***	8.9 ±1.9	10.3 ±2	10.4 ±2.1	**
^{15}N (‰)	-0.35 ±0.36	1.73 ±0.77	3.39 ±0.63	3.32 ±0.76	***		-1.49 ±0.41	0.61 ±0.6	1.95 ±0.56	***

^{13}C (‰)	-17.04 ±0.98	-17.51 ±1.27	-17.46 ±0.8	-17.45 ±1.15			-15.98 ±0.8	-16.05 ±0.75	-16.22 ±0.98	
C:N	5.06 ±0.16	4.89 ±0.16	4.76 ±0.22	4.41 ±0.15	***	***	5.79 ±0.36	5.48 ±0.29	5.16 ±0.37	***

Table 3: Biomarker summary table including fatty acid relative abundance (% total FA), isotopic (‰ vs. N^2 for ^{15}N and VPDB for ^{13}C) and elemental (C:N) data with associated averages and standard deviations for each treatment condition and for each fraction of the coral holobiont (host + symbiont, bleached corals had no symbionts for analysis). Statistical tests (one-way ANOVA) were conducted to assess biomarker change due to feeding or bleaching. Feeding effect on biomarker was assessed by comparing control, F_2x and F_6x treatments and bleaching effect was assessed by comparing F_6x and B_F_6x conditions (host only). Significance levels are denoted by stars with the following pattern: [* ($p < 0.05$), ** ($p < 0.01$), ***($p<0.001$)].

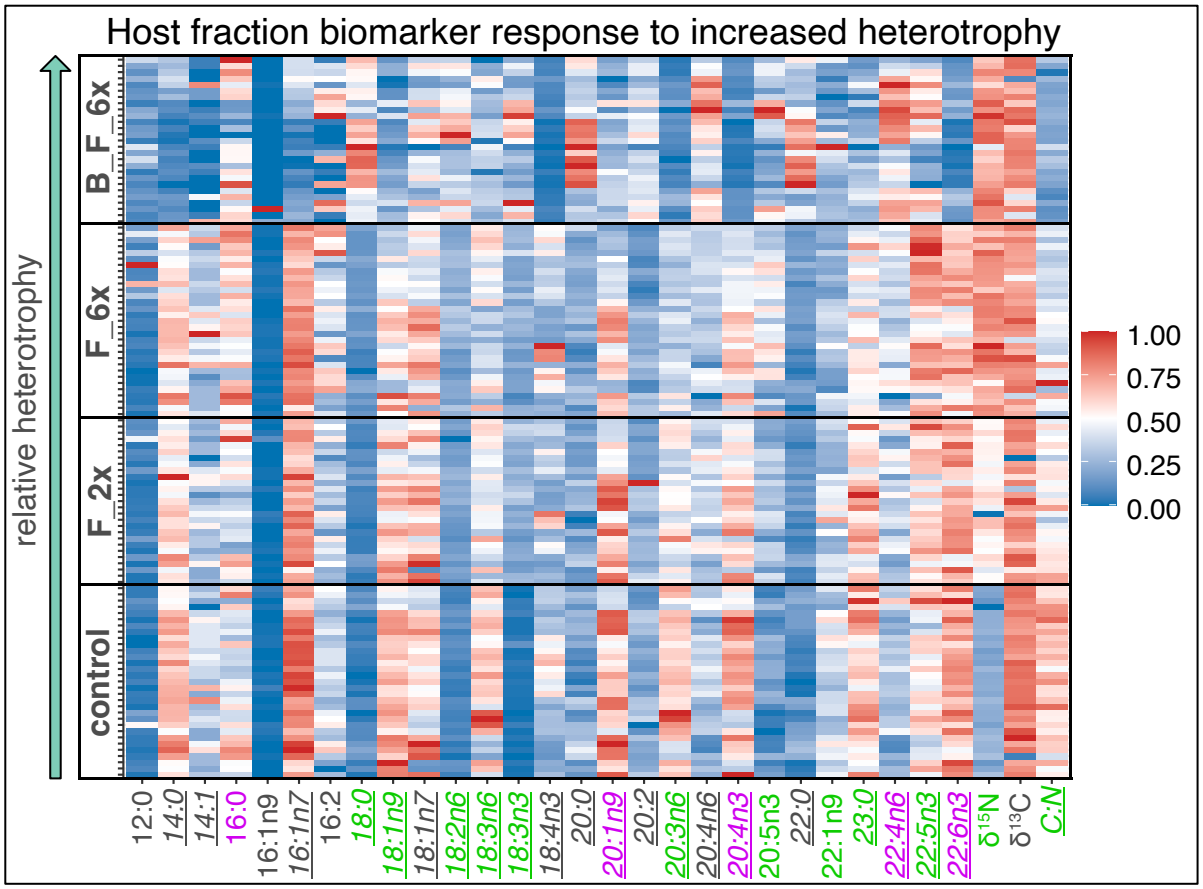

Figure 15. Heatmap of relative biomarker response in host tissue (min/max normalized) of all coral fragments during the experiment with increasing relative heterotrophy (% biomass acquired through feeding) on the y-axis and biomarkers on the x-axis. Biomarkers in purple represent a statistically significant feeding effect at the $p < 0.01$ level (one-way ANOVA), while biomarkers in green represent a statistically significant feeding effect at the $p < 0.001$ (one-way ANOVA) level showing that these biomarkers are highly responsive to changes in coral heterotrophy of nauplii. Biomarkers that are underlined and italicized represent significant bleaching effect ($p < 0.001$; one-way ANOVA). Note variation within treatments.

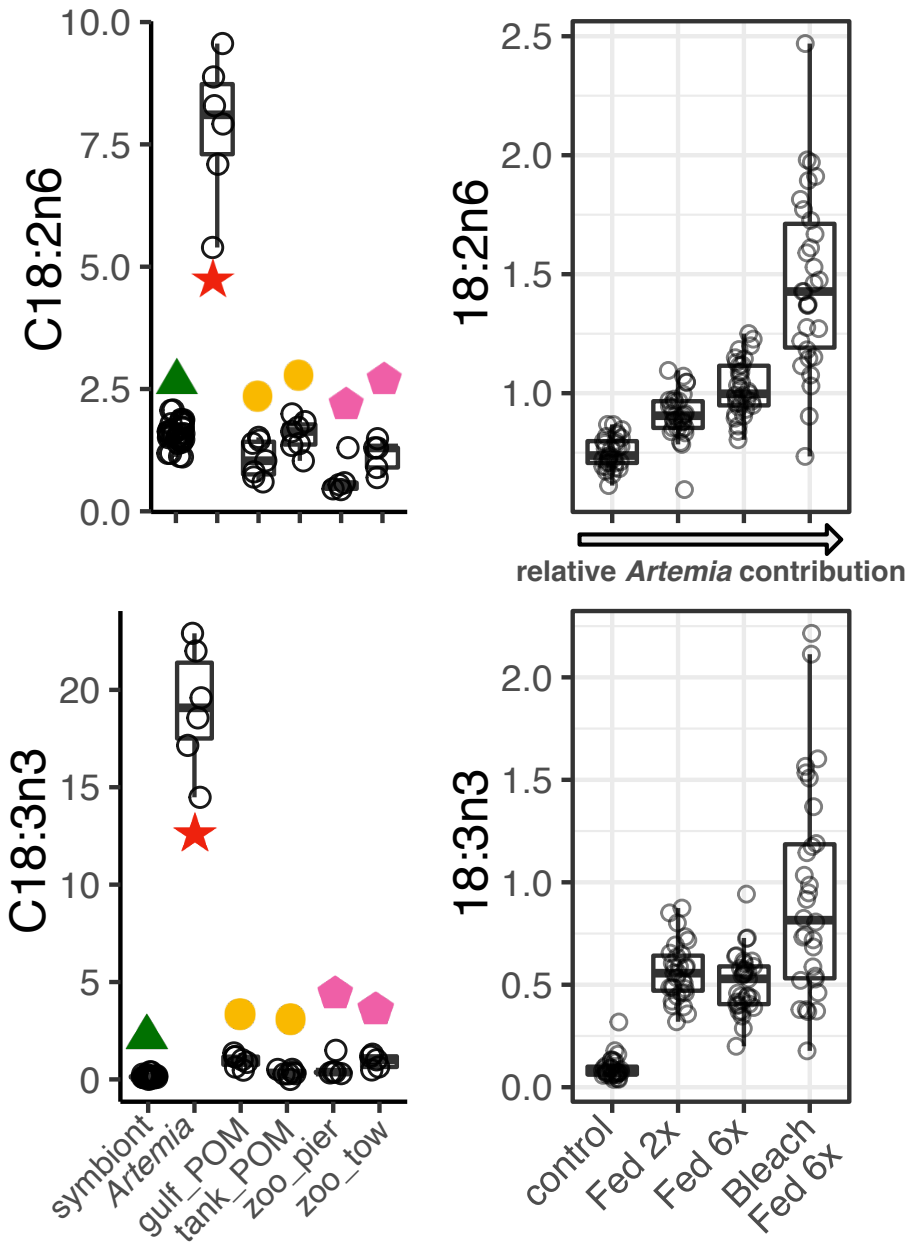

Figure 16. Increased feeding of *Artemia* nauplii which is high in essential fatty acids 18:2n6 and 18:3n3 shows a subsequent increase in the relative abundance of these two fatty acids in coral host tissue. Bleached and fed corals represent a ~full heterotrophic endmember, suggesting maximal values. The right plot shows nitrogen from feeding cooccurs with essential fatty acids in repeatable patterns.

In the symbiont fraction, four biomarkers that were significantly higher in the nauplii increased with increasing heterotrophy (18:3n3, $\delta^{15}N$, 22:0, $p < 0.001$; 18:1n7, $p < 0.05$; one-way ANOVA; Table 3) which is representative of translocation of these biomarkers from host

to symbiont. The essential fatty acid 18:3n3 which cannot be made by the host *de novo*, (Dunn et al., 2012), heterotrophically acquired in by the host in this study (Figure 16, Table 3), was likely transferred to the symbiont from the host, perhaps for the construction of other n-3 PUFA like the symbiont marker 18:4n3 (Figure 17). Indeed, it has been shown that 18:3n3 is often close to or undetectable in starved corals (Table 3, Bachok et al., 2006; Radice et al., 2019), while in heterotrophic corals it becomes detectable and exhibits identical isotopic ratios to the food source (Al-Moghrabi et al., 1995; Tolosa et al., 2011), suggesting that this FA may be sourced entirely from heterotrophy. However, it has also been shown that some species of *Acropora* exhibit remarkably high 18:3n3 values as the most predominant PUFA, suggesting chemotaxonomic differences between *Stylophora* and *Acropora* (Kim, Baker, et al., 2021). The low relative abundance of 18:3n3 in *S. pistillata* even in high feeding treatment corals (< 2 % of total FA) is indicative that this is a vital metabolic precursor molecule that is rapidly modified into other FA once it is consumed, such as 22:6n3 or 20:5n3, which collectively represent ~ 10% of total FA. This work stands in line with the literature by showing significant increase in both host and symbiont fractions of 18:3n3 with increased feeding and a near zero value in unfed corals (Table 3). This data further shows that this essential FA is a highly limiting resource for some coral and may be sourced almost exclusively from heterotrophy for some coral species.

Overall, there were fewer significant changes of biomarkers in the symbiont fraction and less strong correlations with increasing heterotrophy compared to the host fraction (Table 3, Figure 15), suggesting that there is either more *de novo* synthesis of FA in the symbiont and/or that the host may be gate-keeping heterotrophically acquired FA that are vital for metabolism, this is in line with the literature reports that the host can exert nutritional control

over the symbionts and does not transfer every metabolite (Xiang et al., 2020). Interestingly, some biomarkers in the symbiont fraction significantly decreased with increasing heterotrophy like 18:1n9 and 18:2n6 ($p < 0.01$, $p < 0.001$, respectively, one-way ANOVA) even though they were heterotrophic markers (Figure 13), although the reasons for this pattern are unclear.

In the symbiont fraction, some autotrophic biomarkers significantly increased in relative abundance (14:1, 18:4n3, $p < 0.001$; 22:6n3, $p < 0.01$; one-way ANOVA, Table 3) while others significantly decreased (14:0, 16:1n7, 18:3n6, C:N, $p < 0.001$; 20:3n6, $p < 0.01$; 16:0, $p < 0.05$; one-way ANOVA; Table 3). Considering the significant increase in the essential FA 18:3n3 in host and symbiont tissues which is a building block for other n-3 PUFA (Dunn et al., 2012; Imbs, Yakovleva, et al., 2010), this may explain the increase in 18:4n3 and 22:6n3 in the symbiont fraction, although the increase of 14:1 with heterotrophy is less clear. The decline in C:N ratio in the symbiont fraction with increasing heterotrophy can be explained by the high nitrogen content of nauplii compared to unfed coral symbionts, such that symbionts in more heterotrophic corals are benefitting from more available nitrogen translocated from the host through feeding on nauplii, as is evidenced by ^{15}N isotope data (Table 3, Figure 17, Figure 19). The reasons for the decline in autotrophic biomarker FA in the symbiont fraction from increasing heterotrophy are not clear, but may be partially explained that these FA (interestingly, two of which are n-6 PUFA) are part of a slower turnover pool or are less physiologically essential, such that they are "diluted" in the relative abundance calculation by the other "fast turnover" FA like 18:4n3 and 22:6n3 that increased with increasing heterotrophy. Overall, fewer heterotrophic biomarkers were effectively recorded into the symbiont fraction but the decrease in relative abundance of slower turnover

autotrophic biomarkers may provide useful information on short versus long time scale feeding behavior of coral on the reef.

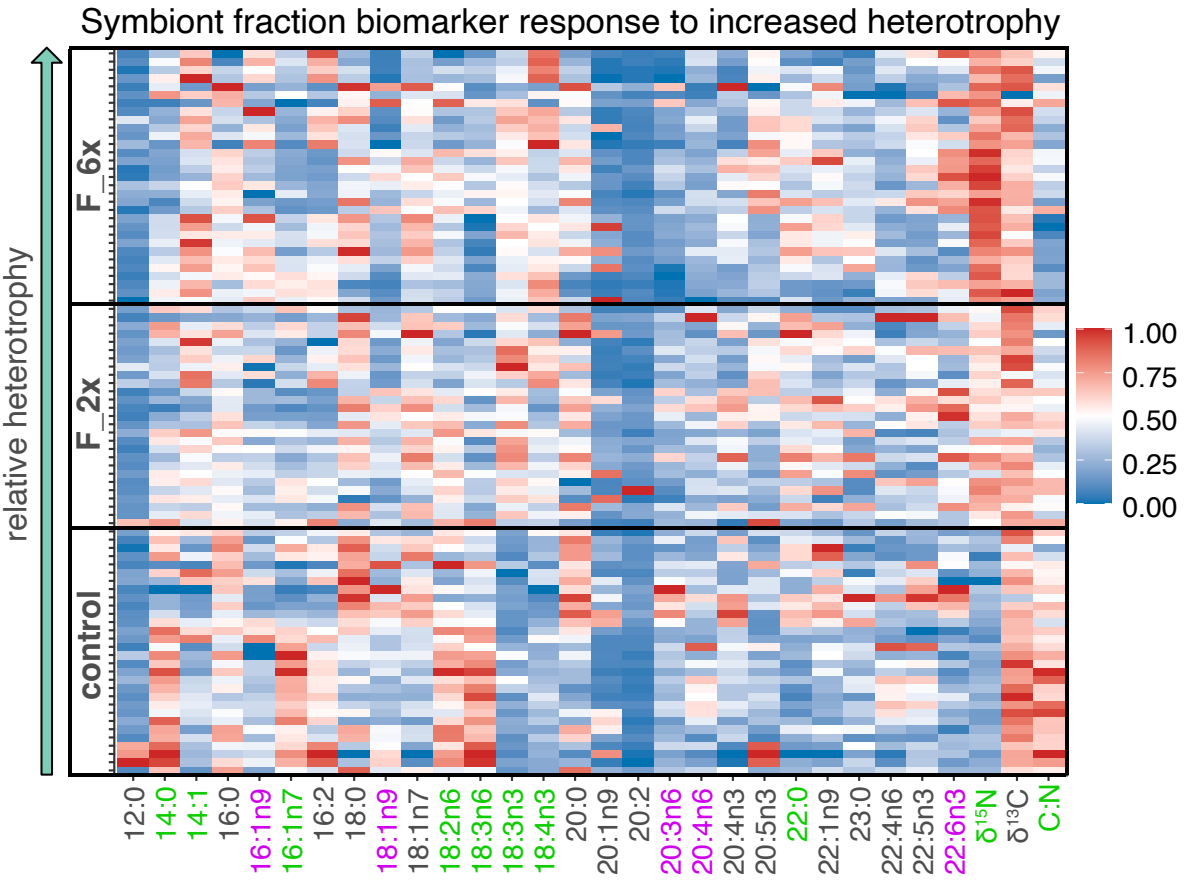

Figure 17. Heatmap of relative biomarker response in symbiont tissue (min/max normalized) of all coral fragments during the experiment with increasing relative heterotrophy (% biomass acquired through feeding) on the y-axis and biomarkers on the x-axis. Biomarkers in purple represent a statistically significant feeding effect at the $p < 0.01$ level (one-way ANOVA), while biomarkers in green represent a statistically significant feeding effect at the $p < 0.001$ (one-way ANOVA) level showing that these biomarkers are highly responsive to changes in coral heterotrophy of nauplii. Note variation within treatments.

Bleached corals exhibited significant declines in many FA (14:0, 16:1n7, 18:1n9, 18:3n6, 18:4n3, 20:1n9, 20:3n6, 20:4n3, 23:0, 22:5n3, 22:6n3; Table 3, Figure 15), suggesting that these FA are at least partially from symbiotic origin. Particularly, 16:1n7, 18:1n9, 18:4n3, 20:4n3, 20:3n6 and 22:6n3 show a dramatic decrease in relative abundance that suggests that

these FA come are translocated from the symbiont to the host in significant quantities, all these FA are in fact symbiont (autotrophic) biomarkers (Figure 13) during the experiment. Several FA also showed significant increases in bleached + fed corals like 18:0, 18:2n6, 18:3n3, 20:0, 20:2, 20:4n6, 22:0, 22:4n6 (Table 3), suggesting that these FA are strong indicators of heterotrophy for this experiment or that the host made these FA *de novo*. Due to the typical loss of PUFA from coral bleaching (Bachok et al., 2006, Table 3, Figure 15), the increase of relative abundance of saturated hydrocarbons may in fact be from loss of PUFA offsetting the balance of relative abundance calculations, although, 18:0 and 22:0 are both heterotrophic biomarkers (Figure 13). The FA 20:4n6 and 22:4n6 have been detected in both aposymbiotic and symbiotic anemones (Dunn et al., 2012) which indicates that the coral host is likely able to produce these FA given appropriate precursor molecules for anabolic construction. Due to the high relative abundance of essential FA 18:2n6 and 18:3n3 (FA that the host cannot make *de novo*) in nauplii and bleached + fed corals (Table 3, Figure 15 and 16) these FA appear to be directly deposited into coral host tissue from heterotrophy as metabolic precursors for construction of other n-3 and n-6 PUFA.

Overall, nearly all nauplii biomarkers increased within the host fraction with increasing heterotrophy, showing reliable recording of FA and elemental biomarkers in host tissues. Fewer heterotrophic biomarkers significantly increasing in the symbiont fraction with increased feeding, which may reflect a selective translocation from host to symbiont of heterotrophically acquired nutrients. Autotrophic biomarkers either significant increased or decreased in the host fraction with increased feeding. Positive correlation of symbiont biomarkers with feeding in the host fraction may be reflective of fast turnover FA translocated from the symbiont to the host and increase due to the increased symbiont density and

photosynthesis associated with increased heterotrophy (Grottoli, 2002). A decrease in symbiont biomarkers associated with increased heterotrophy in the host fraction may be reflective of a slower turnover pool of FA that was "diluted" by the FA acquired through feeding. In the symbiont fraction, select nauplii biomarkers positively correlated with feeding, suggesting translocation from host to symbiont while autotrophic markers either increased or decreased with feeding in the symbiont fraction, further suggesting a metabolic divergence of fast and slow turnover FA pools. Bleached + fed corals showed dramatic increases in some biomarkers suggesting that these are either sourced from heterotrophy and/or made *de novo*, while dramatic declines in biomarker with bleaching was interpreted to mean that these FA come primarily from the symbiont, with further evidence that these FA were all markers of the autotrophic source during experimentation (Figure 13). This technique (coupling of FA with isotopic and elemental biomarkers) would likely capture much smaller changes in heterotrophy than were detected in this experiment. Considering that 973 nauplii cm^{-2} consumed over a 3-week experiment for the F_2x condition, this still elicited notable changes in several biomarkers in the host fraction, this experimentally confirms the use of fatty acids as mixotrophic biomarkers, especially when considered in combination with isotopic and elemental ratio tracers as a tool for understanding coral mixotrophy.

Fatty Acid	HOST					SYMBIONT			
µg/ g dry tissue	B_F_6x	control	F_2x	F_6x	feeding effect	control	F_2x	F_6x	feeding effect
C12:0	0.01 ±0.01	0.01 ±0.01	0.01 ±0.01	0.02 ±0.02		0.19 ±0.19	0.16 ±0.11	0.12 ±0.07	
C14:0	0.01 ±0.01	0.12 ±0.09	0.12 ±0.06	0.12 ±0.07		3.64 ±0.82	3.01 ±0.66	2.77 ±0.72	***
C14:1	0 ±0	0 ±0.01	0.01 ±0.01	0 ±0		0.34 ±0.07	0.43 ±0.09	0.44 ±0.1	***
C16:0	0.54 ±0.26	1.87 ±1.15	2.03 ±0.85	2.09 ±1.08		15.89 ±2.59	15.15 ±3.71	14.89 ±4.12	
C16:1n9	0 ±0	0 ±0	0 ±0	0 ±0		0.56 ±0.29	0.63 ±0.28	0.87 ±0.39	**
C16.1n7	0.02 ±0.02	0.29 ±0.21	0.28 ±0.13	0.29 ±0.19		5.04 ±1.31	4.15 ±0.95	3.95 ±0.93	**
C16:2	0 ±0	0.01 ±0.01	0.01 ±0	0.01 ±0.01		0.36 ±0.15	0.31 ±0.14	0.33 ±0.17	
C18:0	0.7 ±0.25	1.09 ±0.65	1.2 ±0.5	1.32 ±0.61		4.38 ±1.13	4.38 ±1.03	4 ±0.94	
C18:1n9	0.12 ±0.11	0.91 ±0.65	0.92 ±0.5	0.77 ±0.53		5.11 ±2.21	4.37 ±1.98	3.99 ±2.4	
C18:1n7	0.07 ±0.05	0.27 ±0.21	0.31 ±0.17	0.29 ±0.21		0.85 ±0.29	1.03 ±0.29	0.94 ±0.26	
C18:2n6	0.04 ±0.03	0.06 ±0.04	0.08 ±0.04	0.09 ±0.05		1.11 ±0.25	1.01 ±0.28	0.95 ±0.31	
C18:3n6	0.01 ±0.01	0.11 ±0.08	0.1 ±0.04	0.08 ±0.04		3.76 ±1.05	2.76 ±1.01	2.49 ±0.96	***
C18:3n3	0.03 ±0.03	0.01 ±0.01	0.05 ±0.03	0.04 ±0.02	***	0.11 ±0.07	0.33 ±0.1	0.26 ±0.06	***
C18:4n3	0.01 ±0.01	0.15 ±0.1	0.15 ±0.07	0.2 ±0.19		9.59 ±1.85	13.14 ±2.69	14.74 ±4.44	***
C20:0	0.03 ±0.01	0.06 ±0.04	0.06 ±0.03	0.06 ±0.03		0.19 ±0.07	0.2 ±0.08	0.17 ±0.06	
C20:1n9	0.04 ±0.04	0.28 ±0.24	0.29 ±0.2	0.24 ±0.19		0.8 ±0.46	0.78 ±0.38	0.63 ±0.35	
C20:2	0.03 ±0.02	0.06 ±0.05	0.07 ±0.04	0.06 ±0.04		0.21 ±0.08	0.29 ±0.26	0.2 ±0.07	
C20:3n6	0.02 ±0.02	0.38 ±0.24	0.35 ±0.17	0.25 ±0.17	*	1.05 ±0.58	0.96 ±0.46	0.73 ±0.46	
C20:4n6	0.31 ±0.21	0.72 ±0.4	0.86 ±0.39	0.82 ±0.57		3.35 ±1.31	3.37 ±1.11	2.57 ±0.6	*
C20:4n3	0.01 ±0.01	0.2 ±0.18	0.19 ±0.12	0.17 ±0.13		0.47 ±0.19	0.51 ±0.26	0.43 ±0.21	
C20:5n3	0.08 ±0.07	0.18 ±0.11	0.25 ±0.13	0.31 ±0.23	*	1.81 ±0.71	2.01 ±0.72	2.07 ±0.69	
C22:0	0.02 ±0.01	0.02 ±0.02	0.02 ±0.01	0.02 ±0.01		0.08 ±0.03	0.12 ±0.03	0.1 ±0.03	***
C22:1n9	0.01 ±0.01	0.06 ±0.04	0.07 ±0.03	0.05 ±0.03		0.31 ±0.14	0.32 ±0.13	0.31 ±0.13	
C23:0	0.01 ±0.01	0.06 ±0.04	0.07 ±0.04	0.05 ±0.04		0.14 ±0.09	0.16 ±0.1	0.12 ±0.07	
C22:4n6	0.23 ±0.16	0.52 ±0.28	0.61 ±0.28	0.64 ±0.43		2.3 ±0.9	2.24 ±0.74	2.01 ±0.59	
C22:5n3	0.03 ±0.02	0.1 ±0.05	0.12 ±0.05	0.13 ±0.09		0.46 ±0.2	0.47 ±0.17	0.46 ±0.16	
C22:6n3	0.05 ±0.06	0.87 ±0.5	0.94 ±0.44	0.85 ±0.64		6.32 ±2.34	7.44 ±3.01	7.51 ±2.65	
total_FA	2.42 ±1.32	8.41 ±5.24	9.17 ±4.11	8.98 ±5.39		68.42 ±10.81	69.73 ±14.66	68.04 ±13.5	

Table 4: Biomarker summary table including fatty acid mass normalized abundance (% total FA with associated averages and standard deviations for each treatment condition and for each fraction of the coral holobiont (host + symbiont, bleached corals had no symbionts for analysis). Statistical tests (one-way ANOVA) were conducted to assess biomarker change due to feeding or bleaching. Feeding effect on biomarker was assessed by comparing control, F_2x and F_6x treatments. Significance levels are denoted by stars with the following[* ($p < 0.05$), ** ($p < 0.01$), ***($p<0.001$)].

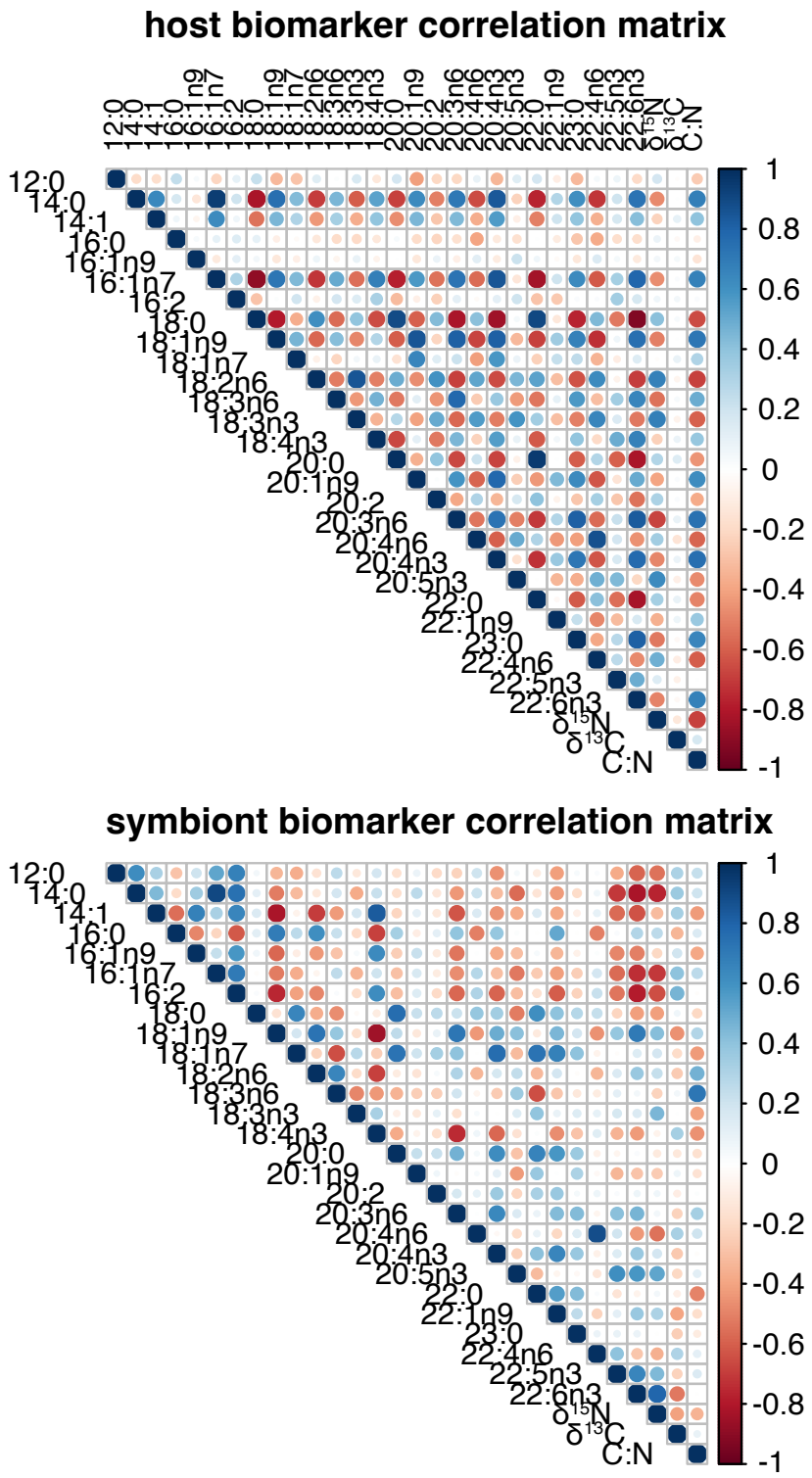

Figure 18. Global correlation matrix of entire feeding experiment of FA biomarkers (% total) and elemental biomarkers for the host and symbiont fraction for entire feeding experiment. Correlation values (R) are colored by a gradient, with positive correlations in blue, and negative correlations in red, darkness of color indicates strength of correlation, with transparent color indicating ~ no correlation between the two fatty acids.

2.4.4. Nitrogen and essential fats from heterotrophy integrate into host biomass while heterotrophic carbon is respired

The biomarkers with the strongest positive correlations with heterotrophy from this experiment were the essential fatty acids 18:2n6, 18:3n3 as well as the heterotrophic source tracer 20:5n3, and $\delta^{15}N$ and the C:N ratio (Table 3), all of which showed directional trends towards the heterotrophic source with increased heterotrophy (Figure 19a-c, Figure 16) showing that these biomarkers are well recorded into coral tissues. The symbiont fraction of control corals (autotrophic source) exhibited a $\delta^{15}N$ = -1.4 ±0.36 ‰, while the heterotrophic source signature (nauplii) had an isotopic ratio of a 9.57 ±1.13 ‰, revealing an 11 ‰ difference between the two experimental nutritional sources (Figure 19a). If we assume a trophic enrichment factor of 0 ‰ (Reynaud et al., 2009) because of high nitrogen retention in symbiotic corals (Tanaka et al., 2006) and thus very little loss of catabolized ^{14}N, then B_F_6x and F_6x coral hosts turned over 33.5 ± 7.5 % and 38.1 ± 7.3 %, respectively, of their total nitrogen with heterotrophically acquired nitrogen from nauplii in the host fraction. Given these same assumptions, F_6x symbionts turned over ~ 31 % of the nitrogen pool with heterotrophic nitrogen. F_2x corals turned over 22.4 ± 5.0 % of nitrogen with heterotrophically acquired nitrogen for the host fraction, while F_2x symbionts turned over ~ 19% as well. Additionally, there was no significant effect of feeding on the difference between host and symbiont nitrogen isotope ratios $\delta^{15}N_{host}$ - $\delta^{15}N_{symbiont}$ ($p = 0.991$, ANOVA) although the host fraction did always exhibit a ~ 2 ‰ larger $\delta^{15}N$ than the symbiont fraction which is common to find in symbiotic corals (Price et al., 2021; Reynaud et al., 2009). These data align with the well-established pattern that heterotrophically acquired nitrogen is shared generously with the symbionts (Houlbrèque & Ferrier-Pagès, 2009). As an extension of this phenomenon, the carbon to nitrogen ratio (C:N), which was significantly lower in nauplii than control

symbionts also served as a useful indicator of heterotrophy in both the host and symbiont fraction (Figure 19c), with significant negative correlation with $\delta^{15}N$ and 18:2n6 (Figure 19d). Additionally, bleached and fed corals exhibiting nearly identical C:N value as the heterotrophic (4.41 ±0.15 for B_F_6x and 4.48 ± 0.13 for nauplii), showing a convergence of this biomarker with its source contribution. Interestingly, zooplankton from the Gulf of Aqaba had statistically similar C:N values as nauplii (4.41 ±0.15 vs. 4.61 ±0.33; p = 0.5, one-way ANOVA) with fairly large spread among control corals (5.06 ±0.16 for host and 5.79 ±0.36 for symbiont) suggesting that C:N may be a useful biomarker in tracing nutritional contributions into coral tissue.

Carbon isotope ratios showed a slight decline towards the heterotrophic source ratio of $\delta^{13}C$ = -20.5 ±1 ‰ (Figure 19b) but with non-significant differences for feeding effect and bleaching effect (Table 3) and much larger variation than nitrogen isotope data (Table 3, Figure 19b). Given that the autotrophic source carbon isotope ratio is -16.07 ±0.86 ‰ and the heterotrophic source ratio is -20.5 ±1 ‰, this results in a difference of ~ 4.4 ‰ between nutritional sources. Assuming a trophic enrichment factor of 0 ‰ this would result in a turnover of ~ 9.5 % of host carbon with heterotrophically acquired carbon for F_6x and B_F_6x corals. The symbiont fraction of F_6x turned over less carbon than the host with only ~ 5.4 % of its carbon biomass replaced with heterotrophically acquired carbon. For the F_2x treatment, there was a similar ~ 9.5 % of host carbon replaced with heterotrophically acquired carbon and a ~ 1.5 % replacement of symbiont carbon with heterotrophic carbon. These data show that the deposition of heterotrophically acquired elemental carbon (which includes carbohydrates, lipids, proteins, and nucleic acids) into coral biomass is less than that nitrogen (proteins, nucleic acids) and heterotrophic source fatty acids (a subset of the lipid pool).

Considering the C:N ratio of ~ 4.5 for the heterotrophic source (9 atoms of carbon for every 2 atoms of nitrogen), this results in a preferential integration of nitrogen into biomass by a factor of ~ 16 for F_6x and B_F_6x host (i.e. ~ 16 atoms of heterotrophic nitrogen are recorded into host biomass for every 1 atom of heterotrophic carbon), a factor of ~ 26 for F_6x symbionts, a factor of ~ 9 for F_2x host and a factor of ~ 60 for F_2x symbionts. Interestingly, this shows that when corals are fed less (the F_2x treatment) they might translocate less nitrogen to their symbionts. Altogether, this shows that most heterotrophic carbon is preferentially respired or exuded as mucus (not recorded into biomass) compared to heterotrophic nitrogen which has been observed in the field for several coral species (Conti-Jerpe et al., 2020; Price et al., 2021). The use of bulk tissue carbon isotope ratios in assessing heterotrophy of reef-building corals may be vastly underestimating the importance of coral feeding outlined here, which is to capture and store limiting nutrients like elemental nitrogen (Figure 19a; Houlbrèque & Ferrier-Pagès, 2009) and specific essential carbon *molecules* required for metabolism like essential fats (Figure 16; Tolosa et al., 2011) and amino acids (Fox et al., 2019; Martinez et al., 2022).

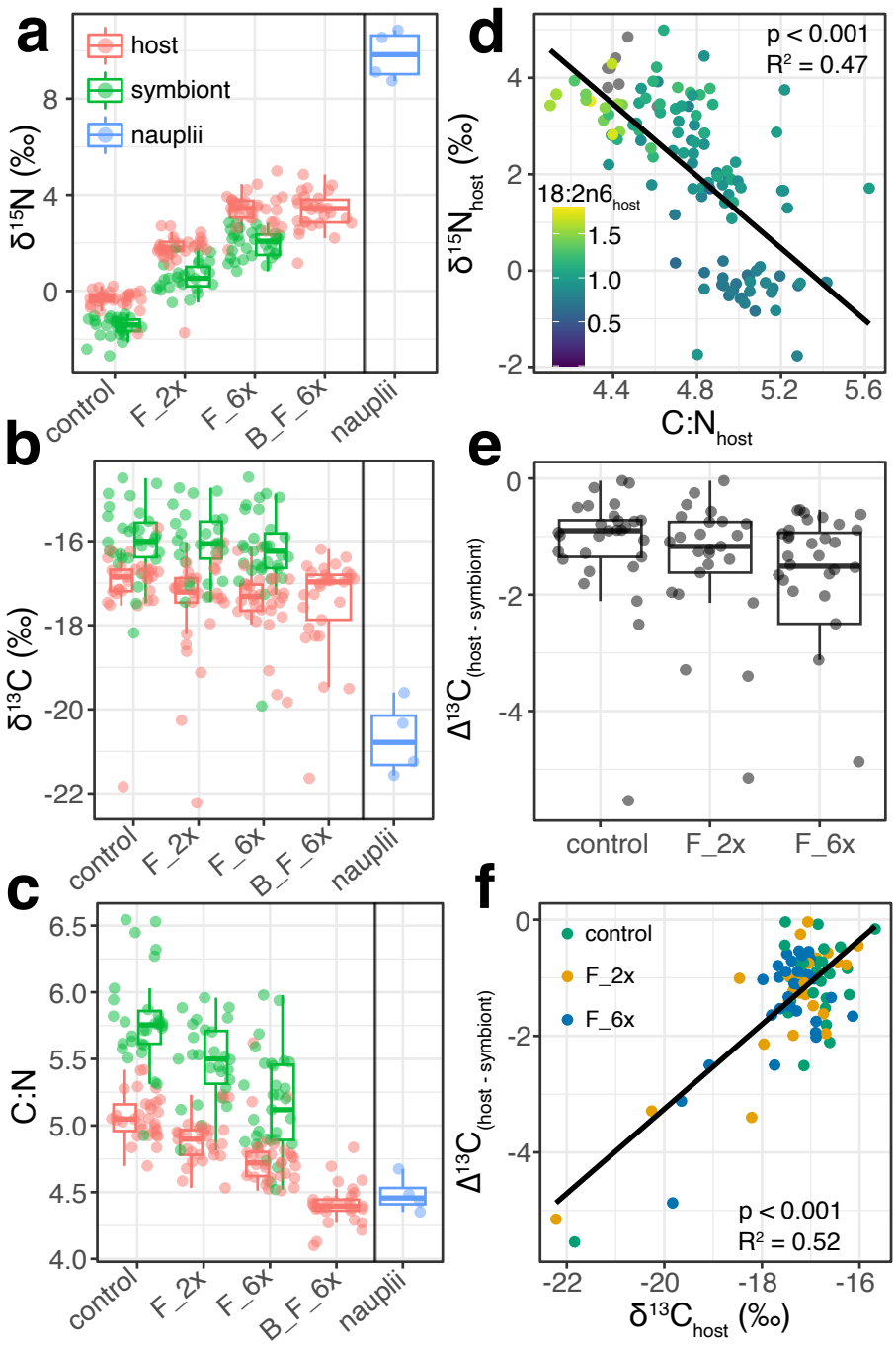

Figure 19. Isotopic and elemental multiplot. **A**, **B** show nitrogen and carbon isotope ratio and boxplots; **C** shows carbon to nitrogen ratio boxplot, nauplii are plotted on the far right as the main heterotrophic source, with treatments groups ordered from left to right as increasing relative heterotrophy. **D** shows nitrogen isotopes plotted with carbon to nitrogen ratio, colored by relative abundance (% total) of essential fatty acid 18:2n6. **E** shows a boxplot of carbon isotope ratio difference between host and symbiont (a classic proxy for coral heterotrophy (Muscatine et al., 1989) by treatment group. **F** shows carbon isotope ratio difference between host and symbiont plotted against host carbon isotope ratio of the host fraction, colored by treatment group.

To further explore this trend, the difference in carbon isotope ratio of host and symbiont ($\Delta^{13}C = \delta^{13}C_{host} - \delta^{13}C_{symbiont}$) which has been used as a classic proxy for coral heterotrophy (Grottoli et al., 2006; Muscatine et al., 1989), was calculated and plotted per treatment (Figure 19e). The effect of feeding on $\Delta^{13}C$ value did show an decrease in mean value per treatment with increasing % heterotrophy but the effect was non-significant ($p = 0.473$, $F = 0.756$, $df = 88$, ANOVA) showing that this classically used proxy did not effectively capture changes in coral heterotrophy even with a 4.4 ‰ difference between autotrophic and heterotrophic source groups that ~ matches the difference between corals and zooplankton in the Gulf of Aqaba (Figure 20). Additionally, $\Delta^{13}C$ did not strongly correlate ($R^2 < 0.16$) with any other measured parameters other than $\delta^{13}C_{host}$ ($R^2 = 0.52$), showing that a few fragments with very low $\delta^{13}C_{host}$ values (< - 2 ‰) were driving most of this trend (Figure 19f). Changes in heterotrophy were tracked better by many other biomarkers, such as $\delta^{15}N$, C:N and many essential and non-essential fatty acids (Table 3). This has been seen in the literature that $\Delta^{13}C$ is sometimes less reliable than nitrogen isotopes (Conti-Jerpe et al., 2020; Hoogenboom et al., 2015; Price et al., 2021). The strong correlation of $\Delta^{13}C$ with $\delta^{13}C_{host}$ (Figure 19f) shows that corals with large differences between host and symbiont are driven by the host feeding on nauplii (~ 4.4 ‰ more negative $\delta^{13}C$ ratio relative to autotrophic source) and not sharing carbon resources with the symbionts and instead recording it into biomass on the time scales of this experiment (~ 1 month). Figure 19f shows that while $\Delta^{13}C$ does track heterotrophy for a couple fragments, it might be better suited as a proxy for how much translocation of heterotrophic carbon there is from host to symbiont (Price et al., 2021). This long-used proxy captures heterotrophy in only a small fraction of colonies, 13 % of fragments in this experiment. Given its long usage, recent studies in the literature, and the results in this

experiment, this proxy for coral heterotrophy may be very misleading and has likely contributed to our underestimation of the importance of heterotrophy for reef-building corals. There appears to be a fundamental decoupling between elemental nitrogen and elemental carbon for most corals in which nitrogen and essential fats and amino acids (Fox et al., 2019) are reliably recorded into host tissue, but elemental carbon is mostly respired or exuded as mucous. Indeed, it appears heterotrophy of reef-building corals is suited mainly to supplement the holobiont with essential elements (nitrogen, phosphorus, etc.) and essential molecules that cannot be made *de novo* in significant quantities, with minimal contribution towards elemental carbon.

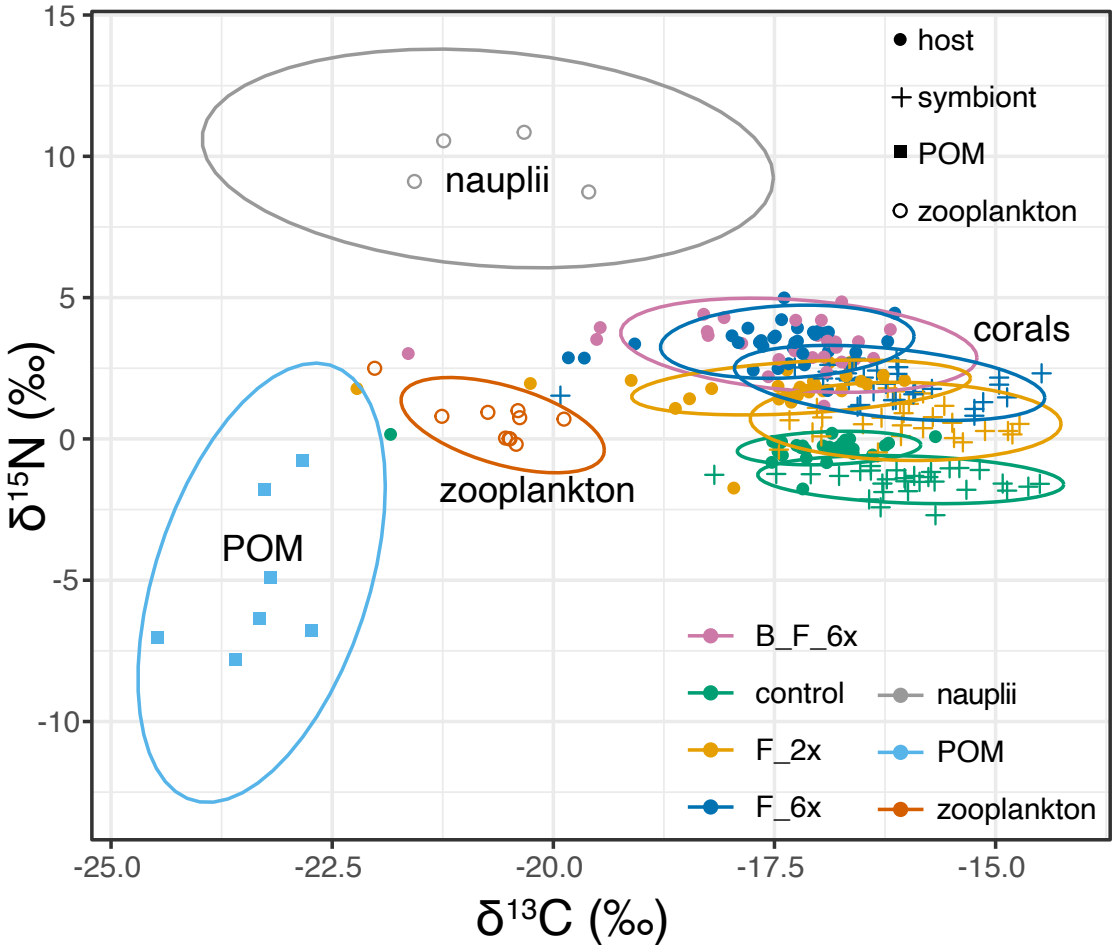

Figure 20. Isotope biplot of all experimental (control symbionts, nauplii) and *in situ* nutritional sources (POM, zooplankton) and corals (host and symbiont), 95% confidence ellipses are colored by tissue type and labeled for clarity.

2.4.5 Nitrogen and heterotrophic fatty acids correlate non-linearly

The turnover of the host nitrogen pool due to heterotrophy and heterotrophic fatty acid markers within the host showed a strong non-linear trend for all coral fragments (Figure 21b-d). Percent of host nitrogen turned over with heterotrophic nitrogen was calculated by assuming no trophic enrichment (Reynaud et al., 2009) and subtracting mean control $\delta^{15}N$ values (unfed) from each colony from the $\delta^{15}N$ values of fed fragments from the same colony, then dividing this number by the total difference between nauplii and average control coral $\delta^{15}N$ (~ 11 ‰). The maximum host nitrogen turnover was 52.6 %, with both mean F_6x and B_F_6x treatments revealing N turnover with heterotrophic nitrogen at 38.1 ± 7.3 % and 33.5 ± 7.5 %, respectively, while F_2x showed an average 22.4 ± 5.0 % N turnover and control corals showed 0 ± 1.7 %.

When plotted with cumulative nauplii capture, N turnover data follow a near linear trend with $R^2 = 0.84$, but with a logarithmic model fitting better ($R^2 = 0.94$) suggesting that corals may have been declining heterotrophic nitrogen incorporation into biomass due to high food availability and/ or high feeding rates (Figure 9 and 10). When plotting N turnover data with heterotrophic source markers 18:2n6, 18:3n3 and 20:5n3, data follow a stronger non-linear trend that appears to have a maximum N turnover at ~ 45-50 % with increasing values of % total FA (Figure 21b, c and d). While fitting of linear and logarithmic models to these data revealed logarithmic models showing larger R^2 values for all three FA, the data appear to exhibit a "saturation effect" for nitrogen in which even with more heterotrophic fatty acid incorporation, nitrogen turnover did not exceed ~ 45-50 %. As such, from a mechanistic point of view, a hyperbolic Michaelis-Menten was chosen to better capture the nitrogen "saturation" effect that is seen in these data (Figure 21).

All data except for cumulative nauplii capture data were fitted to a modified Michaelis-Menten curve in which there was an additional term ('c' in Figure 19) that allowed the curve to cross at a non-zero point along the x-axis, because these FA were already found at measurable amounts in the unfed corals. In this experiment and in Red Sea *S. pistillata* it appears 18:3n3 is the strongest heterotrophic marker since unfed corals exhibit extremely low values of this essential FA (as has been seen in the literature for some corals; Tolosa et al., 2011) and shows a strong incorporation signal into the host tissues. This model fit revealed statistically significant estimates for all model coefficients ($p < 0.001$; Figure 19c), with the 'a' term estimated at 49.4 % N turnover, and the 'b' term estimated at 0.29 % of 18:3n3. The 'a' term in this model is analogous to V_{max} (maximal enzyme reaction velocity) from the Michaelis-Menten enzyme kinetics equation in which the curve asymptotes and the 'b' term represents the K_m term (distance value on x-axis from where the curve crosses x-axis to where the curve reaches one-half of V_{max}). It appears that most of the high FA abundance values that are driving this non-linearity (Figure 21c) are due to bleached and fed corals (B_F_6x). This trend, driven largely by these corals, leads to the hypothesis that in this experiment, some bleached corals are continuing to incorporate essential FA 18:3n3 into tissues while slowing down heterotrophic N incorporation.

For the FA 18:2n6 and 20:5n3, both heterotrophic markers in this experiment, the same trend is observed although with larger horizontal data spread (more variation in FA) and less significant model coefficient estimates for 20:5n3 (Figure 21d). This appears to be driven by the horizontal spread of the control coral data (variation in FA relative abundance), with 18:2n6 exhibiting larger variance than 18:3n3 and 20:5n3 exhibiting a larger variation than 18:2n6 (Table 3, Figure 19b, c and d). The larger variation in control coral FA values seems

to indicate that these FA, and particularly 20:5n3, may be sourced from both autotrophic and heterotrophic sources or that they turn over slower than the duration of coral starvation (4-weeks) and have been retained from feeding on the reef. The fatty acid 20:5n3 has been known to be both a marker of symbiont autotrophy and zooplankton (Kim, Baker, et al., 2021; Kim, Lee, et al., 2021), and while it records well into host tissues, shows much larger variation than essential FA 18:3n3 and 18:2n6, which is suggestive of two sources.

The mean soft tissue nitrogen density (µg cm^{-2}) for each fragment was calculated using measured total fragment host soft tissue mass and dividing by surface area; this was then multiplied by % N from elemental analysis data. Additionally, the total heterotrophic nitrogen consumed during the experiment (µg cm^{-2}) was calculated using an average nauplii mass of 3.2 µg nauplii $^{-1}$ (Peykaran et al., 2011) and average % N of nauplii from elemental analysis (~8.64 %, n = 5). The ratio of soft tissue nitrogen mass density to total nitrogen consumed per cm^{-2} was then multiplied by percent nitrogen turnover to give the proportion of heterotrophically acquired nitrogen that was incorporated into host tissues. It is important to note that every fed treatment consumed enough nauplii to completely recycle host nitrogen, so it was plausible for every fed treatment to completely turn over its nitrogen pool (Table 5).

F_2x and F_6x corals both incorporated ~16% of heterotrophically acquired nitrogen into host tissues, while the rest was presumably transferred to endosymbionts (Figure 19a) or respired, this shows that for non-bleached corals, N incorporation rates remains unchanged even with dramatic increases in feeding, showing perhaps an upper limit of heterotrophic nitrogen incorporation into host tissues in this experiment. Interestingly, B_F_6x corals incorporated only ~10% of heterotrophically acquired nitrogen in soft tissues which may partially explain the “saturation” trends seen in Figure 19. Given that these corals consumed

less cumulative nauplii than F_6x corals (Figure 9) and have minimal endosymbionts, yet exhibited nearly identical nitrogen isotope values (Table 3), this is suggestive that a larger portion of the heterotrophic nitrogen acquired by bleached corals was respired which likely enriched the $\delta^{15}N$ values of these corals due to catabolic release of ^{14}N (Fry, 2006). Additionally, since % heterotrophically acquired N incorporation was calculated using % N turnover, in which it is assumed no trophic enrichment, it is likely that bleached and fed corals incorporated actually showed < 10% incorporation of heterotrophic nitrogen and likely have lower % N turnover rates than those calculated in Figure 21. A larger trophic enrichment of nitrogen for bleached corals makes sense because bleached corals have very few symbionts (an order of magnitude lower than non-bleached corals in this experiment, Table 2, Figure 11B) and this significantly impairs the ability to recycle and retain essential nutrients like nitrogen. Because of this, an increased proportion of heterotrophic nitrogen respired would lead to respiration of the lighter isotope, thus retaining the heavy ^{15}N isotope and artificially "inflating" the ^{15}N signal when compared to non-bleached corals.

Overall, these data show that that corals may reach a limit of heterotrophic N incorporation, particularly for bleached corals due to more respiration (and subsequent loss) of this heterotrophic nitrogen that cannot be recycled back to the host via symbionts. Since heterotrophic fatty acid biomarkers (especially 18:2n6 and 18:3n3) still increased even with ~ equivalent % N turnover this indicates that these fatty acids are recorded and retained in host tissues even when nitrogen incorporation reaches its maxima. This may be extremely useful in assessing mixotrophy on time scales smaller than estimated N turnover rates for corals (> 1 year) and may be particularly useful for assessing heterotrophic sources of bleached or previously bleached corals in the field.

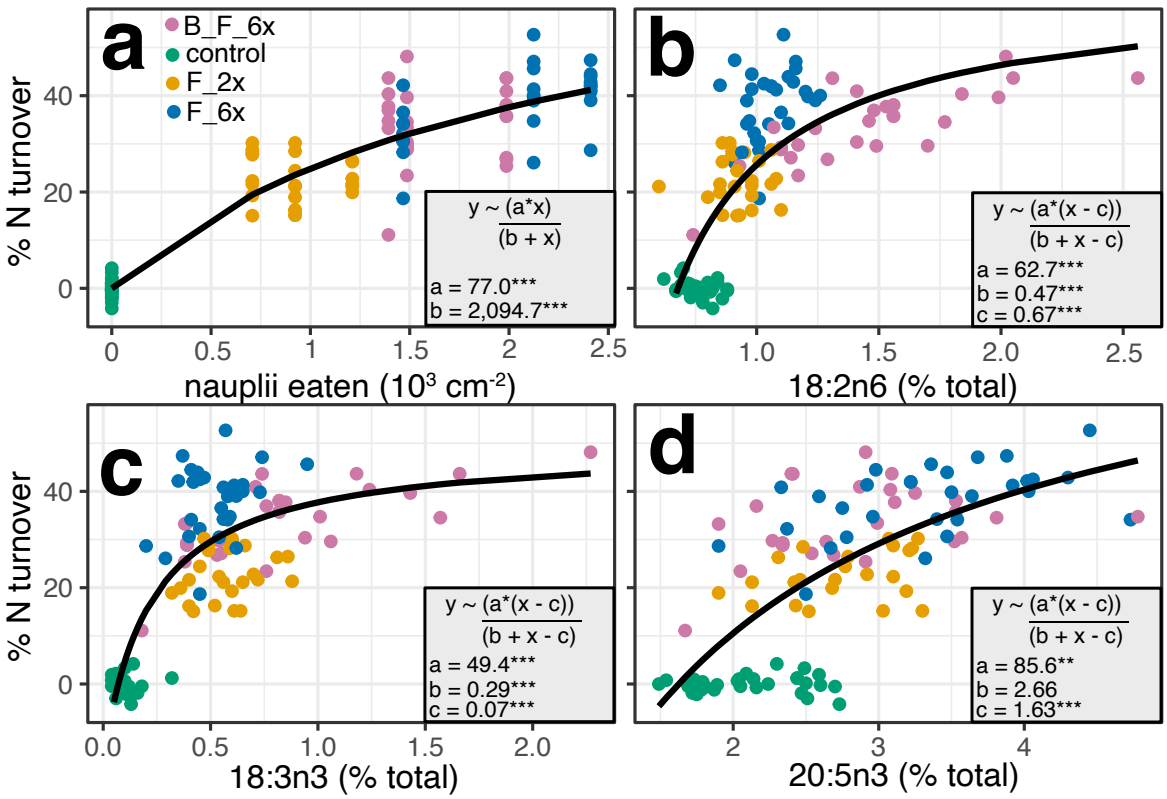

Figure 21. Multiplot of host nitrogen turnover with heterotrophically acquired nitrogen and various host tissue parameters. Figure a was fitted to a Michaelis-Menten hyperbolic equation with a full zero intercept while figures b, c, and d were fitted to a modified Michaelis-Menten equation in which the fitted line does not go through the origin, with the offset on the x-axis represented by parameter 'c'. Fitted parameter estimates are listed on each plot with associated significance level of each fitted parameter ($p < 0.05$ = *; $p < 0.01$; = **; $p < 0.001$ = ***).

parameter	control	F_2x	F_6x	B_F_6x
% N host tissue	1.62	1.74	2.18	1.58
mg host tissue cm^{-2}	10.34	11.2	12.14	8.78
µg host N cm^{-2}	156.88	185.63	232.87	132.71
cumulative nauplii eaten cm^{-2}	NA	918.04	1996.81	1609.64
µg N consumed cm^{-2}	NA	253.82	552.08	445.03
% host N turnover	~ 0	22.45	38.09	33.59
N turnover potential	NA	1.37	2.37	3.35
% heterotrophic N integrated	NA	16.42	16.07	<10.02

Table 5. Treatment averaged soft tissue nitrogen data with associated nitrogen mass consumption data. 'N turnover potential' represents the number of times the coral host could have completely turned over its nitrogen pool with heterotrophic nitrogen.

2.4.6 Contextualizing experimental results with environmental sampling

As stated previously, the food source fed to corals during the experiment (*Artemia* nauplii) is not a natural food source of corals in nature, but the results of this study can be used to better understand the biomarker changes one might see in nature depending on the biomarker profiles of various nutritional source groups (symbionts, POM and zooplankton, Figure 22). For reef-building corals, the translocation of fatty acids between host and symbiont complicates the delineation of source contributions for coral nutrition and virtually eliminates the possibility of using single fatty acids as trophic biomarkers (Dalsgaard et al., 2003; Mocking et al., 2012; Monroig et al., 2013). Thus, small changes in several biomarkers towards a source group identified by a multivariate reduction analysis (principal component analysis, non-metric multidimensional scaling or linear discriminant analysis) is likely better suited in qualitatively (sometimes quantitatively) detecting shifts in coral heterotrophy (Fox et al., 2019; Radice, Brett, et al., 2019) rather than one or a few biomarkers. Implicit in this, given the large chemotaxonomic variation in coral fatty acid profiles (Imbs et al., 2007; Kim, Baker, et al., 2021) and planktonic variability in reef environments (Hamner et al., 2007), singular biomarkers or indices (ratios) of corals in nature without measurements of source groups in the same reef environment should be interpreted with extreme caution. Here I present a framework to approach and interpreted fatty acid + isotopic biomarker data from the reef environment.

A particularly helpful approach used in this study that may help provide context to coral heterotrophy for future studies is keeping several coral fragments in closed or semi-enclosed aquaria without feeding for several weeks or months (or until the full symbiont community is turned over). In this way coral symbionts will be closer to representative of a

"fully autotrophic" source with no heterotrophic biomarkers that could be translocated from the host to symbiont, thus "diluting" the autotrophic source signature. In theory, the endosymbiont biomarker profiles of similar coral species and symbiont clades that are unfed for > 1 month should converge towards a fully representative autotrophic source group that can then be used to interpret the mixing of biomarkers into coral host tissues of coral colonies on the reef. In this study, corals were starved for ~ 4 weeks in semi-enclosed aquaria (130 μm filtered water from the Gulf of Aqaba), with carbon turnover estimates for holobionts estimated at ~37 days (Tanaka et al., 2018), this suggests that most of the carbon was turned over without heterotrophic feeding (although it is likely that some POM was consumed on that made it through the 130 μm filter). Thus, moving forward, the endosymbionts of unfed control corals will act as a representative "fully autotrophic" source group while zooplankton and particulate organic matter collected from the Gulf of Aqaba represent two distinct heterotrophic source groups that corals in the Gulf of Aqaba would consume (Figure 22). The biomarker response in corals from increased feeding on *Artemia* nauplii and the overlap in biomarkers of this source with Gulf of Aqaba food sources and nauplii will be analyzed and discussed to enhance understanding of a theoretical biomarker response to heterotrophy on the reef.

A principal component analysis of *in situ* nutritional sources shows that zooplankton, POM and symbionts of unfed corals separate completely with 95% confidence ellipses (Figure 22). Horizontal separation along the PC1 axis show that autotrophic and heterotrophic sources (POM + zooplankton) separate by several biomarkers, with 18:3n3, 20:0, 18:0, and 18:1n7 showing strong and significant heterotrophic source separation (Table 6, Figure 22) and 18:4n3, 22:4n6, 20:1n9, 18:2n6, $\delta^{13}C$, 20:3n6, and 22:1n9 showing strong separation for the

autotrophic source along the PC1 axis (Table 6, Figure 22). Statistical analysis of biomarkers for the three source groups (POM, zooplankton, symbionts from starved corals) showed significant differences between source groups with a $p < 0.001$ statistical difference between sources for 26 out of 30 biomarkers (Table 5). The PC2 axis revealed separation between POM and zooplankton source groups such that more positive values appear to exhibit higher trophic level markers (zooplankton), with biomarkers like 20:5n3, 22:6n3 and $\delta^{15}N$ aiding separation for positive PC2 values. Negative PC2 values were more associated with POM and were distinguished by characteristic biomarker C:N with some increased separation by both 14:0 and 16:1n7, both of which are found in smaller microbial phytoplankton and bacteria (Dalsgaard et al., 2003). Given these data, dimensional reduction analysis of the three potential source groups for coral host nutrition appear to have separation for both autotrophy/ heterotrophy (PC1) and trophic level (PC2). This result may in large part be possible by the addition of elemental biomarkers $\delta^{15}N$ and C:N to FA biomarkers, which can help indicate the trophic level at which corals are feeding. This shows the importance of adding elemental and isotopic markers to FA analysis to enhance source group separation and elucidation of trophic levels.

Comparison of biomarkers that separated source groups of *in situ* reef sources and those that separated experimental source groups (Figure 13) indicates several overlapping biomarkers that aid in autotrophic and heterotrophic source separation and significantly change with increasing heterotrophy. These biomarkers include 18:3n3 and 18:0 (heterotrophic markers) that would theoretically increase in the host fraction with increasing heterotrophy on the reef, while 22:0 and 18:1n7 would theoretically increase in the symbiont fraction with increasing heterotrophy. Interestingly, 18:1n7 is typically thought of as an

autotrophic marker (Graeve et al., 1997) and has been used in indices for photosynthetic vs. animal derived input into coral tissues (Radice, Brett, et al., 2019) but data from the Gulf of Aqaba shows that this FA is an indicator of heterotrophy in this reef environment (Figure 20). This could be because 16:1n7, which is a precursor to 18:1n7 via elongation, contributes to the negative direction of the PC2 axis (low trophic level POM), is a strong biomarker for diatoms and bacteria (Dalsgaard et al., 2003) and POM (De Goeij et al., 2008; Duan et al., 1997) and is present in significantly higher quantities than the symbionts (Table 6). Interestingly, several studies have shown that coral heterotrophy relies on diatom supported food webs (Radice, Brett, et al., 2019; Stahl, 2021) more than previously expected and this may be a useful biomarker alongside other biomarkers for tracing that support. Overlapping autotrophic biomarkers from *in situ* sources and experimental sources that exhibit significant changes with heterotrophy include 20:3n6, 22:1n9 and 22:4n6 in the host fraction and 14:1, 18:4n3, 20:3n6 for the symbiont fraction.

For trophic level biomarkers (PC2 axis, Figure 20), 20:5n3 and $\delta^{15}N$ are two of the three contributors towards zooplankton separation from POM and these biomarkers also significantly change with increased feeding during the experiment, with $\delta^{15}N$ significantly increasing in both host and symbiont fraction and 20:5n3 only increasing in the host fraction (Table 3). While $\delta^{15}N$ is a somewhat obvious trophic level indicator due to isotopic enrichment factors of ~ 3 ‰ per trophic level (Post, 2002), 20:5n3 is less obvious. It has been shown that 20:5n3 is often used as a marker for symbiont autotrophy contributions to cnidarian hosts (Revel et al., 2016) although recent work has shown that 20:5n3 and 22:6n3 (both of which aid in separation of zooplankton, Figure 22) were both enriched in zooplankton from Hong Kong waters (Kim, Lee, et al., 2021), which is exactly in line with these results.

The C:N ratio was the only biomarker that indicated strong separation of lower planktonic trophic levels (POM) and significantly changed in the feeding experiment (Table 3). 14:0 and 16:1n7 showed less strong correlation with the PC2 axis but helped separate POM from zooplankton, which is in accordance that both of these FA have been used as bacterial and phytoplankton biomarkers (Dalsgaard et al., 2003; Thurber, 2007). The use of C:N ratio may be fundamental to understanding trophic level of corals (Figure 19c), given that zooplankton have a significantly lower C:N ratio than coral symbionts (Table 6). However, the use of C:N amongst other biomarkers must be exercised with caution as it has been shown that the C:N ratio can vary with symbiont clade type (Ezzat et al., 2017) such that comparisons of heterotrophy of different species, or the same species across a range of depths in which major symbiont types change must be exercised with caution. Still, the use of C:N within same coral species, same clade types, may be a highly useful indicator of trophic level of corals.

Overall, these results indicate that there are several biomarkers in the experiment and within Gulf of Aqaba food sources that overlap and respond to coral heterotrophy. While much of the data stands in line with literature FA data, there are a couple fatty acids that exhibit inverse trends to their expected source groups (such as 18:1n7) within the Gulf of Aqaba and highlight the importance of measuring biomarkers of source groups when interpreting coral biomarker data from the field. These results show that there are many biomarkers that respond well to heterotrophy of *S. pistillata* within the experiment that also significantly separate source groups in the Gulf of Aqaba, indicating useful mixotrophic and trophic level biomarkers for the most studied coral species in the Red Sea.

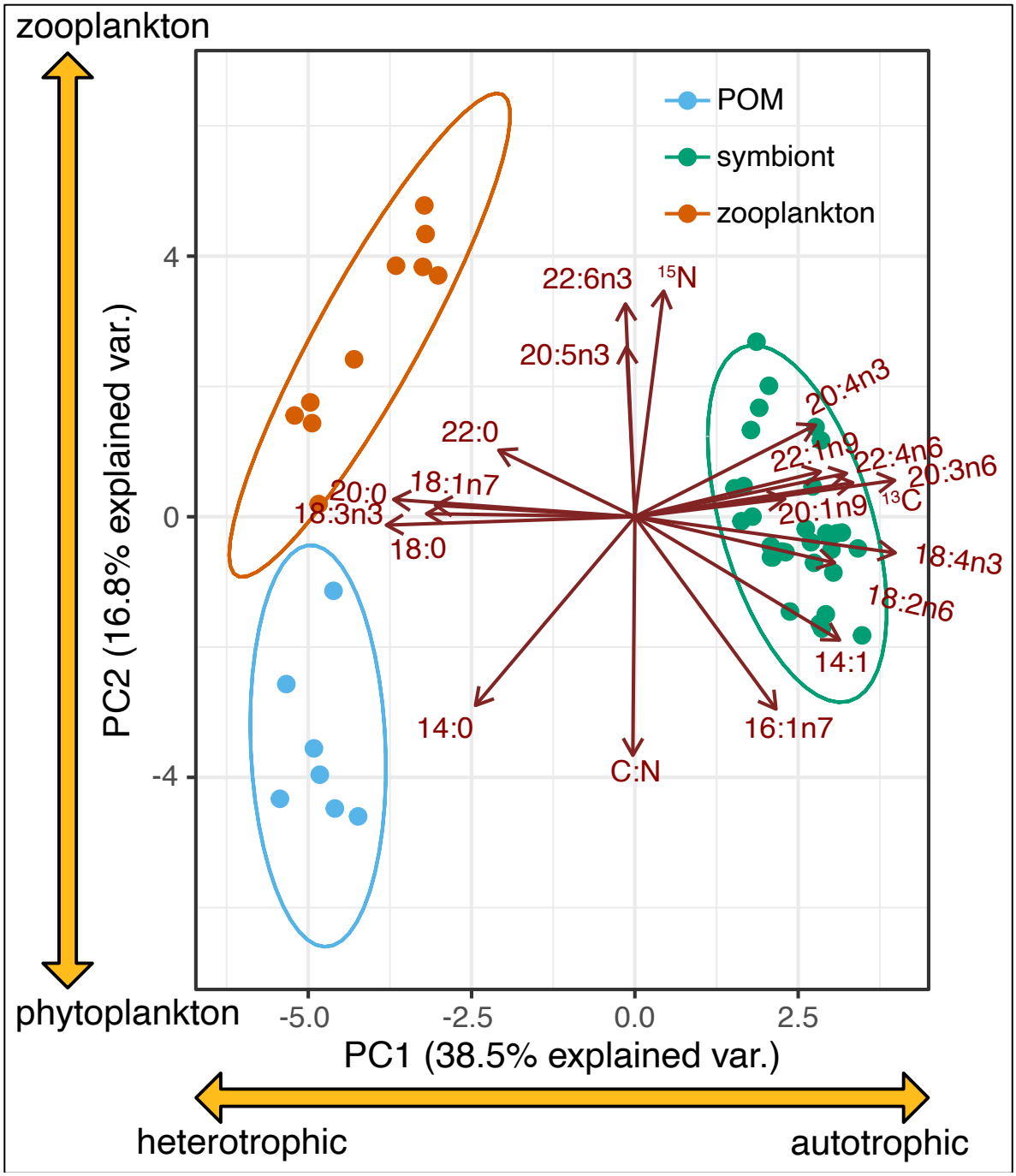

Figure 22: Principal component analysis of *in situ* nutritional sources that a coral in nature would experience. Groups are separated by source type, with control coral symbionts (corals unfed for 3 weeks), zooplankton (collected from both the pier and mid-gulf) and particulate organic matter (collected above nursery where corals were collected). Arrows show PCA weightings of select biomarkers. Axis 1 mainly separates autotrophic and heterotrophic sources while axis 2 mainly separates along plankton trophic level (phytoplankton give negative PC2 value, while zooplankton give a positive PC2 value).

biomarker	symbiont	POM	zooplankton	significance
C12:0	0.28 ±0.27	0.15 ±0.12	0.14 ±0.12	
C14:0	5.4 ±1.16	11.43 ±2.01	6.17 ±2.65	***
C14:1	0.51 ±0.14	0.31 ±0.1	0.02 ±0.02	***
C16:0	23.07 ±2	46.33 ±2.44	31.98 ±9.39	***
C16:1n9	0.94 ±0.49	0.9 ±0.34	0.31 ±0.12	***
C16:1n7	7.41 ±7	7.47 ±1.12	3.07 ±0.54	***
C16:2	0.56 ±0.22	0.21 ±0.13	0.39 ±0.18	***
C18:0	6.37 ±1.45	16.01 ±3.29	14.7 ±4.74	***
C18:1n9	7.22 ±1.96	7.06 ±2.6	6.8 ±1.34	
C18:1n7	1.24 ±0.4	2.69 ±1.18	2.24 ±0.69	***
C18:2n6	1.6 ±0.25	1.07 ±0.38	0.9 ±0.41	***
C18:3n6	5.48 ±1.17	0.07 ±0.08	0.26 ±0.4	***
C18:3n3	0.14 ±0.08	0.95 ±0.31	0.75 ±0.45	***
C18:4n3	14.27 ±3.1	0.78 ±0.3	0.86 ±0.68	***
C20:0	0.29 ±0.1	0.64 ±0.11	0.63 ±0.18	***
C20:1n9	1.81 ±1.35	0.17 ±0.24	0.48 ±0.18	***
C20:2	0.3 ±0.08	0.25 ±0.39	0.19 ±0.09	
C20:3n6	1.51 ±0.56	0.08 ±0.18	0.14 ±0.13	***
C20:4n6	4.77 ±1.5	0.08 ±0.09	4.91 ±9.2	*
C20:4n3	0.69 ±0.28	0.11 ±0.16	0.28 ±0.21	***
C20:5n3	2.59 ±0.86	0.69 ±0.41	5.11 ±4.36	***
C22:0	0.12 ±0.05	0.31 ±0.16	0.36 ±0.34	***
C22:1n9	0.43 ±0.19	0.06 ±0.06	0.1 ±0.05	***
C23:0	0.2 ±0.12	0.11 ±0.09	0.46 ±0.22	***
C22:4n6	3.27 ±1.03	0.06 ±0.09	0.86 ±1.87	***
C22:5n3	0.65 ±0.2	0.41 ±0.2	0.35 ±0.23	***
C22:6n3	8.88 ±1.9	1.43 ±0.99	17.54 ±12.62	***
^{15}N (‰)	-1.49 ±0.41	-5.06 ±2.74	0.65 ±0.79	***
^{13}C (‰)	-15.98 ±0.8	-23.35 ±0.58	-20.66 ±0.59	***
C:N	5.79 ±0.36	7.31 ±0.67	4.61 ±0.33	***

Table 6. In situ source data summary table including fatty acid, isotopic and elemental data of potential autotrophic (symbiont) and heterotrophic sources of nutrition (particulate organic matter collected from the Gulf of Aqaba and zooplankton collected from the IUI pier and open water Gulf) with mean and standard deviation described. These sources represent the typical sources that corals would be eating in the Gulf of Aqaba, with significance results from one-way ANOVA between all source groups listed [* ($p < 0.05$), ** ($p < 0.01$), ***($p<0.001$)].

2.5 Conclusion

Overall, the data show reliable recording of fatty acid and nitrogen biomarkers from a heterotrophic source group into coral tissues in predictable patterns. Nearly all heterotrophic source biomarkers significantly scaled with feeding in the host, showing that the use of FA and isotopic biomarkers together provide strong response to feeding, with only a small subset of these increasing in the symbiont fraction, which may indicate metabolic gatekeeping by the host. Some autotrophic markers increased with feeding in the host and symbiont fraction due to increased symbiont density, chlorophyll and likely photosynthesis (Grottoli, 2002) associated with feeding, representing a "fast turnover" pool of FA, while some decreased with feeding, representative of a dilution of "slower turnover" FA with the fast turnover autotrophic biomarkers and heterotrophic biomarkers. It was also found that carbon isotopes did not reliably scale with heterotrophy, while nitrogen and heterotrophic source FA did such that ~ 10-60 nitrogen atoms derived from feeding were recorded for every 1 atom of carbon derived from feeding, the variation in integrated heterotrophic nitrogen was dependent on the tissue type (host or symbiont) and feeding regime. It is hypothesized that since corals are typically not carbon limited, much of this heterotrophically acquired carbon is likely respired or exuded as high C:N mucous. Thus, the long-used proxy for coral heterotrophy ($\mathbf{\Delta}^{13}C = \delta^{13}C_{host} - \delta^{13}C_{symbiont}$) is likely not adequately capturing the vital contributions of heterotrophy to reef-building corals. It was found that only ~10 % of corals in this study scaled $\mathbf{\Delta}^{13}C$ with heterotrophy and may be more accurately measuring biomass growth (heterotrophic carbon retention) and the degree of resource sharing with the symbiont. From this data it appears the vital function of feeding for reef-building corals is mainly to acquire nitrogen and essential biomolecules like fats (Figure 16) and amino acids (Fox et al., 2019), not elemental carbon.

The non-linear correlations of nitrogen turnover and essential heterotrophic fatty acid markers show that bleached corals continue to deposit and record the fatty acid signature of the heterotrophic source even when nitrogen incorporation may have reached its limit. This means that fatty acids, especially for bleached corals, may provide the most reliable short-term estimations of diet such as seasonal shifts due to local oceanography to study reef-ocean connectivity. Lastly, the overlap of responsive heterotrophic source biomarkers in this experiment and Gulf of Aqaba sources (zooplankton and POM) are discussed to create understanding of how biomarker shifts of corals on the reef may be interpreted and which biomarkers may be reliable recorders of mixotrophy while others appear to be reliably record trophic level (22:6n3, 22:5n3, $\delta^{15}N$ and C:N). The best circumstances for reliable interpretation of shifts in select biomarkers is also discussed.

These data show the role of heterotrophy for reef-building corals and that it may be vastly more important than previously thought. The flexibility for corals to feed when food is available and the overlooked reliance on feeding for nitrogen and essential biomolecules firmly ties reef-building corals into the food webs and biogeochemical cycles of coastal reef environments such that physical oceanographic forcing which modulates planktonic concentrations on overlying reef waters may govern coral survivorship in a warming global ocean.

Chapter 3

Heterotrophy of particulate organic matter subsidies contributes to divergent bleaching responses of *Acropora hyacinthus* in Mo'orea

3.1 Abstract

Heterotrophy on plankton and particulate organic matter (POM) by tropical scleractinian corals is known to help corals resist and recover from thermally induced bleaching. However, the relative importance of heterotrophy of the same species of coral in different reef environments in context of oceanographic forcing is limited. In 2019 the island of Mo'orea experienced a widespread marine heat wave with mass coral mortality. Due to limited internal wave forcing, extreme temperatures were nearly constant down to 30 m on the reef slope. During this mass bleaching event it was observed that *Acropora hyacinthus* colonies on the shallow forereef (5 m) near the reef crest were resistant to bleaching, while colonies on the deeper forereef (14 m) bleached and subsequently recovered (by colored bleaching score), despite similar thermal stress. The role of heterotrophy in this divergent bleaching response was investigated using fatty acid, isotopic and elemental biomarkers. Data reveal through several lines of evidence including feeding proxies, isotopic niche overlap and putative POM fatty acid biomarkers that bleaching resistant colonies near the reef slope were likely consuming more POM than their bleached and recovered counterparts. Additionally, it was found that although visually recovered, the host of recovered colonies was still compromised and exhibited proportionally less mono- and polyunsaturated fatty acids than resistant colonies. These result stands in line with previous studies, showing the long-term costs of bleaching and that benthic communities at the reef crest are a net sink for oceanic POM due to wave forcing, further showing the vital role of oceanographic forcing and particulate subsidies in structuring coral bleaching response.

3.2 Introduction

3.2.1 Barrier Reefs and Oceanography of Mo'orea, French Polynesia

The island of Mo'orea located in the central South Pacific (17°30'S, 149°50'W) is a 1.5-2-million-year-old (Neall & Trewick, 2008) volcanic island surrounded by barrier reefs ~ 0.5 – 1.5 km from shore. Mo'orea's barrier reefs creates distinct reef habitats that are shaped be oceanographic forcing, water transport and retention processes (Leichter et al., 2013; Figure 23). The forereef composes the 'outward' side of this barrier reef which steeply slopes down to ~ 500 m within 1 km offshore of the reef crest (James et al., 2020; Nelson et al., 2011) and faces oceanic waters (Figure 23). The shallowest part of the forereef creates the reef 'crest' in which wave breaking results in unidirectional water flow of oceanic waters over the reef crest and onto the back reef (Hench et al., 2008). The backreef of Mo'orea is the land-ward side of the reef crest (Figure 23) and is typically a shallow water (< 3 m) lagoon partially protected from oceanographic processes, with wave forcing over the reef crest as a significant driver of water movement on this reef habitat (Leichter et al., 2013; Monismith et al., 2013). The back reef is characterized by relatively slower flow rates and longer water retention times than the forereef habitat (hours to tens of hours, dependent on wave forcing; Hench et al., 2008). The fringing reef flanks the lands edge within the reef lagoon (Figure 23) and is most influenced by land-based processes such as terrestrial runoff (Adam et al., 2021; Donovan et al., 2020). The barrier reefs around Mo'orea are broken by several deep passes such that wave-driven water flow over the reef crest and onto the back reef is balanced by transport out of these passes (Hench et al., 2008). There are several factors that modulate water flow rates over the reef crest but are primarily driven by wave forcing from significant swell events (swell period > 16 s) and trade-wind driven short period swell (swell period < 9 s) dependent on

season and side of the island. The northern side of Mo'orea where this study was conducted experiences long-period high energy waves during austral summer (December - February) and more short period trade-wind driven swell from the north-east in the austral winter (May – September) that drive wave breaking and water movement over the reef crest.

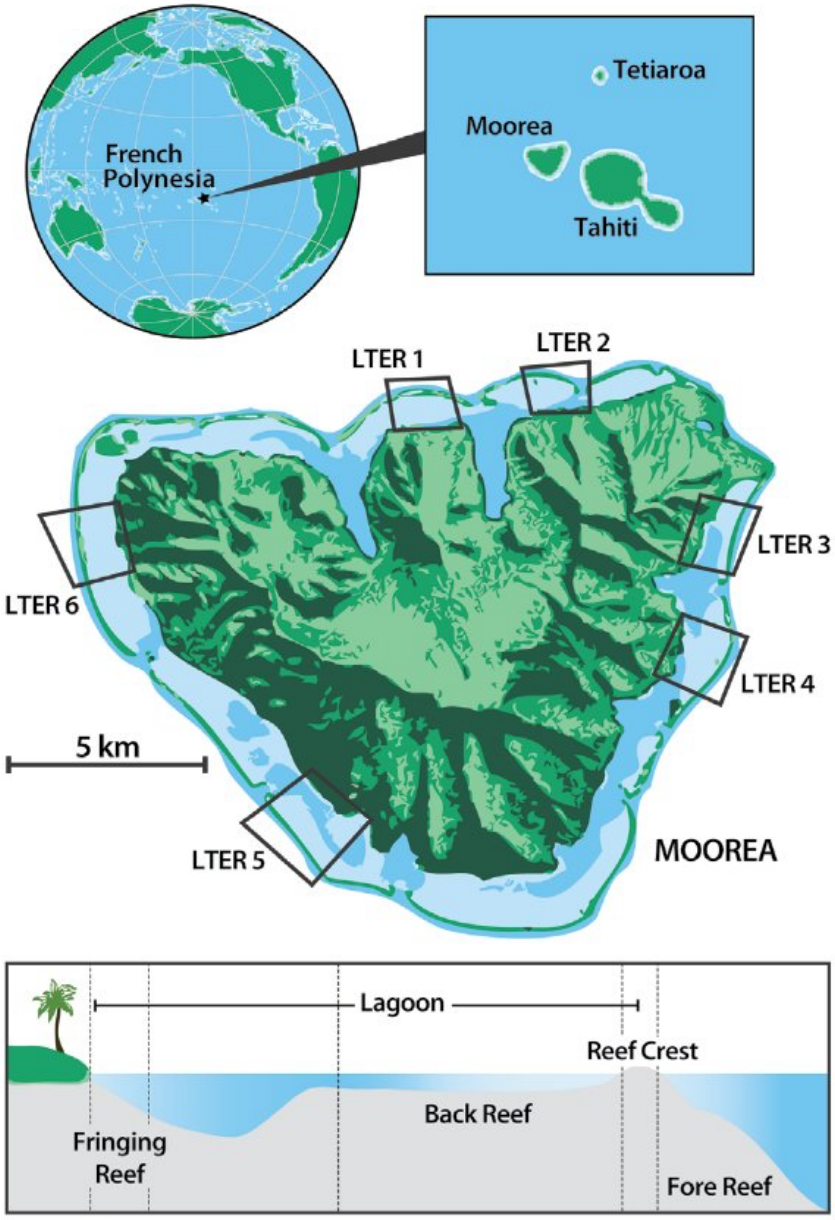

Figure 23. Schematic figure of Mo'orea from Leichter et al., 2013. Top panel shows a map of Mo'orea in the central South Pacific showing Mo'orea Coral Reef Long Term Ecological Research (MCR-LTER) on the middle panel, with sites around the island. The bottom panel shows a schematic view of the different reef environments: fore reef, reef crest, back reef, lagoon and fringing reef.

The forereef and backreef habitats show distinctive chemical and biological characteristics when compared to oceanic waters (> 5 km offshore; James et al., 2020). Reef associated waters consistently present higher POC, PON, chlorophyll *a* and DOC concentrations than oceanic waters (Alldredge & Carlson, 2011; Leichter et al., 2013) and chlorophyll *a* concentrations have been shown to slowly attenuate until ~10 km offshore (James et al., 2020), suggesting an island mass effect (Doty & Oguri, 1956) in which the island of Mo'orea strongly influences the biogeochemistry of nearby waters (James et al., 2020; Johannes et al., 1972; Odum & Odum, 1955). Indeed, coral reef organisms interact with and influence the biogeochemical characteristics of the overlying waters (Nelson et al., 2011; Patten et al., 2011; Wyatt et al., 2013). Wyatt et al., 2013 show with multiple lines of evidence that the reef crest of a model barrier reef (unidirectional flow over crest onto backreef) is a net sink of oceanic POM (phyto- and zooplankton; 4 to 30 mmol N m^{-2} d^{-1} and 6 to 130 mmol C m^{-2} d^{-1}) with this same reef showing sharp declines of oceanic picophytoplankton (*Prochlorococcus*, *Synechococcus*, and picoeukaryotes) as water flowed over the reef crest (Patten et al., 2011), showing the reliance of benthic reef communities on oceanic POM subsidies. This observation is further supported via theoretical modeling and field observations of coral bleaching events in Japan, which show that at higher flow rates the diffusive boundary layer around coral colonies is smaller and allows for quicker uptake or release (mass transfer) of dissolved components such as dissolved nutrients, gasses, and metabolites (Nakamura & Van Woesik, 2001). There is a growing body of evidence showing a high reliance of reef communities on dissolved and particulate oceanic subsidies (Fox et al., *in review*; Radice, Hoegh-Guldberg, et al., 2019; Skinner et al., 2021; Wyatt et al., 2010)

particularly at the reef crest where water flow rates are high and water depth is shallow, such that benthic communities can more easily access oceanic subsidies.

The island of Mo'orea presents a representative case study for other Pacific Islands with barrier reefs or atolls in which the movement of oceanic water and thus dissolved and particulate components influence the benthic reef communities of fore- and backreef environments. Given that Mo'orea has been a Long-Term Ecological Research (LTER) site for close to 20 years, the abundance of oceanographic and ecological data from prolonged surveys and studies can provide context to how similar organisms in different reef environments around the island are responding to ocean warming, oceanographic forcing, and ocean weather (i.e. internal waves; Wyatt et al., 2023)

3.2.2 The 2019 bleaching event and *Acropora hyacinthus* bleaching patterns

The island of Mo'orea experienced a prolonged marine heatwave (MHW) from December 2018 until ~ May 2019 which resulted in island-wide mass coral bleaching and mortality (Speare et al., 2022). The north shore of Mo'orea has experienced 16 local-scale (0.1° x 0.1°) MHW with differing severities and characteristics since 1985 (Wyatt et al., 2023). The 2016 and 2019 bleaching events in Mo'orea provide an interesting point of contrast because both events showed similar temperature metrics and bleaching predictions but exhibited contrasting ecological responses (Burgess et al., 2021; Hédouin et al., 2020), with the 2019 bleaching event being more severe. Wyatt et al. (2023) show that variations in mesoscale (10s to 100s of km) eddy fields around Mo'orea drove variations in internal waves around the island. During the 2019 bleaching event, they show that internal wave cooling on the forereef was reduced while in 2016 it was enhanced, resulting in negligible bleaching stress below ~20 m during the 2016 event (Wyatt et al., 2023). Without internal wave cooling,

the 2019 bleaching event showed a persistent subsurface marine heat wave down to ~ 40 m, with depth integrated heat accumulation estimates ~ 5- to 150-fold greater than 2016 (Wyatt et al., 2023). This means that thermal stress was near constant down to depths of ~ 30-40 m on the forereefs of Mo'orea.

While island-wide coral bleaching and mortality was observed along the 10 m isobath of the fore-reef habitats of Mo'orea during the 2019 bleaching event (Speare et al., 2022), marked colony level differences were observed in *Acropora hyacinthus* on the forereef near LTER site 2 just north-east of Cooks Bay (Figure 23). At this site, some individuals of *Acropora hyacinthus* remained unbleached throughout the 2019 MHW ("resistant" colonies) while other individuals bleached but later recovered after the thermal stress subsided ("recovered" colonies) (Leinbach et al., 2021). *Acropora* is a key reef-building coral in the Indo-Pacific and is known to be highly sensitive to climate change (Baird & Marshall, 2002; Vernon, 2000), thus this divergent bleaching pattern presents a unique investigative opportunity to disentangle why this phenomenon was observed. Leinbach et al. documented the differences between symbiotic microalgae of resistant and recovered colonies, noting that resistant colonies typically were dominated by the genus *Symbiodinium* (formerly referred to as clade A) symbionts during and after bleaching, while recovered colonies mainly harbored the genus *Cladocopium* (formerly referred to as clade C), with no evidence of symbiont shuffling after bleaching (shifts in dominant Symbiodiniaceae type over time). Another covariate with bleaching response observed was depth, such that nearly all resistant colonies were found at < 5 m depth on the shallow forereef (adjacent to the reef crest), while recovered colonies were found at 14 m depth, deeper on the forereef. The authors also show that of the shallow forereef colonies that did bleach, these corals had a mixture of *Symbiodinium* and

Durisdinium (formerly referred to as clade D) or *Cladocopium* symbionts, whereas the shallow forereef colonies that did not bleach harbored ~100% *Symbiodinium*, showing that symbiont clade type and proportions are large determinants of bleaching response of the same coral species and the same reef environment (Leinbach et al., 2022). In contrast, Bowden-Kerby & Carne (2012) showed the vital role of the coral host in thermal tolerance in a restoration project in Belize in which several *Acropora* genotypes hosting *Symbiodinium* symbionts in the same reef environment bleached while others did not, which suggests that the host is also playing a vital role in bleaching resilience. This is further supported by experimental work showing high genetic variability within the host of *Acropora* results in thermal tolerance variability (Yetsko et al., 2020). Overall, this paints a picture that both *Acropora* host and symbiont as well as environment play fundamental roles in coral thermal tolerance and bleaching response.

The notable differences in oceanographic forcing of the deep and shallow forereef (reef crest) rests on theoretical and empirical data such that the high flow rates on the reef crest may aid corals in accessing dissolved nutrients (Nakamura & Van Woesik, 2001) and that benthic communities at the reef crest may be consuming more particulate oceanic subsidies (Patten et al., 2011; Wyatt et al., 2010, 2013) than colonies on the deep forereef. Since it is known that heterotrophy confers resistance to thermally induced bleaching (Conti-Jerpe et al., 2020) this leads to the question: did bleaching resistant colonies of *Acropora hyacinthus* on the shallow forereef consume more oceanic subsidies than their deeper fore reef counter parts? To answer this question, I will present work in collaboration with the authors of Leinbach et al., 2022 that sampled colonies during the 2019 bleaching event.

3.2.3 *Acropora* physiology, trophic ecology, and photo symbiont diversity

Acroporid corals are common and often major reef-building corals found in in the Indo-Pacific (Veron, 2000), Caribbean (Baums et al., 2006) and the Red Sea (Ziegler et al., 2016). *Acroporids* are known to be highly sensitive to rising global ocean temperatures (Baird & Marshall, 2002), high genetic (Richards & van Oppen, 2012) and endosymbiont diversity (Crabbe & Carlin, 2009; Leinbach et al., 2022) of this genus results in varied thermal tolerance and bleaching responses at the species and even colony level (Bowden-Kerby & Carne, 2012; Leinbach et al., 2022; Yetsko et al., 2020). It has been shown that *Acropora* recover quickly from bleaching and can increase thermal tolerance with up to 50% mortality reductions after successive bleaching events (Maynard et al., 2008), which suggests that this genus of coral may be suited to survive warming ocean temperatures.

Acropora corals are known to harbor multiple genera of photo symbionts (Crabbe & Carlin, 2009; Van Oppen et al., 2001). It is generally understood that *Durisdinium* symbionts are more thermally tolerant than other symbionts, offering up to 1.5 °C increased thermal tolerance when compared to *Cladocopium* (Berkelmans & Van Oppen, 2006). This thermal tolerance comes at a cost though, with *Durisdinium* symbionts photosynthesizing less than *Cladocopium*, resulting in up to 40% slower growth of the coral holobiont (A. Jones & Berkelmans, 2010). Stat & Gates reviewed the global distribution of *Durisdinium* symbionts and concluded that these were generalist opportunistic endosymbionts that outcompete and replace optimal symbionts (*Cladocopium* mainly) in health-comprised corals and even propose monitoring *Durisdinium* symbionts as indicators of habitat degradation. Symbiont shuffling from *Cladocopium* to *Durisdinium* has been noted in *Acropora* corals (A. M. Jones et al., 2008) although was not observed in Mo'orea following the 2019 bleaching event (Leinbach et al., 2022). *Symbiodinium* symbionts are also found in *Acropora*, with Stat et al.

(2008) concluding that these symbionts may represent parasitic rather than a mutualistic endosymbiosis. *Symbiodinium* symbionts have been shown to transfer less photosynthate to the coral host and are shown to be basal to the other symbiont types (Stat et al., 2008), suggesting that these symbionts were the first group to form a symbiosis with invertebrates. Often, *Symbiodinium* symbionts are found in high light environments whereas *Cladocopium* symbionts which exhibit higher photosynthetic efficiency are found in deeper waters (Coope et al., 2011; Eckert et al., 2020; Wall et al., 2020; Ezzat et al., 2017). As such, *Symbiodinium* symbionts offer UV protective mechanisms and produce less hydrogen peroxide than *Cladocopium*, a product known to induce coral bleaching (Suggett et al., 2008; T. Banaszak, et al., 2000). Interestingly, although *Symbiodinium* symbionts are thought to be more metabolically 'selfish' than *Cladocopium* symbionts (Stat et al., 2008) and can sometimes show less thermal tolerance (Mieog et al., 2009), many of them are found in more thermally tolerant *Acropora* and *Porites* (Camp et al., 2020; Grottoli et al., 2014; Schwiesow et al., 2021). This shows that *Durisdinium* is not the only determining factor in coral thermal tolerance and that *Symbiodinium* symbionts can also be associated with high thermal tolerance (Leinbach et al., 2022). Colony level variability of thermal tolerance of *Acropora* harboring *Symbiodinium* symbionts in the same reef environment (Bowden-Kerby & Carne, 2012) also shows that the host plays a large role in thermal tolerance, perhaps due to control of the symbiont population and/or from heterotrophic feeding.

The family *Acropora* are generally thought of as more autotrophic corals due to tight overlap of isotopic niche between host and symbiont (ellipse overlap of ^{13}C and ^{15}N of both fractions) (Conti-Jerpe et al., 2020) but as was shown in chapter 2 (Figure 19) this is often a colony-specific response of resource sharing, rather than heterotrophy itself. It has been shown

that *Acropora* grow best on a phytoplankton diet rather than zooplankton and tend to prefer natural diets which would undermine the efficacy of feeding experiments using *Artemia* nauplii (Conlan et al., 2019). *Acropora* corals show reliable increases in select heterotrophic FA biomarkers such as 18:2n6, 18:1n9, 18:3n3 and 22:4n6 with feeding on phytoplankton (Conlan et al., 2019) showing that corals are benefiting from phytoplankton subsidies and altering FA proportions with feeding. The preference of *Acropora* corals for consuming phytoplankton rather than zooplankton and the often-small differences between isotope ratios of host and symbiont fraction which may not capture heterotrophy (Figure 19), suggests that the literature may be underestimating the reliance of *Acropora* on heterotrophic subsidies. The strong variability of thermal tolerances (Bowden-Kerby & Carne, 2012; Yetsko et al., 2020) and growth (Baird & Marshall, 2002) due to host genotype, not symbiont type, hints that the host is playing a vital role in trophic and metabolic processes of the holobiont. In this work I use the same combination of fatty acids, isotopic and elemental biomarkers used in Chapter 2 to elucidate if there were differences in relative contributions of heterotrophy associated with divergent bleaching responses of *Acropora hyacinthus* seen on the north shore of Mo'orea during the 2019 bleaching event. Namely, I aim to address if resistant colonies consumed more particulate organic matter (POM) subsidies than colonies that bleached and recovered.

3.2.4 Addressing Fatty acid oxidation during sample storage

Due to limitations from the COVID-19 pandemic, coral samples which were intended for compound-specific isotope analysis of amino acids (CSIA-AA, Fox et al., 2019) were analyzed for fatty acid (FA) proportions instead. After coral collection, host and symbiont separation, corals were dried in a 60 °C oven overnight and then stored in a -80 °C freezer for ~ 1.5 years. For isotopic analysis, this approach is commonly used, however for fatty acid

analysis this approach is typically avoided because increased temperatures and exposure to oxygen greatly increases the probability of acyl bond hydrolysis and oxidation of double bonds of fatty acids. The combination of hydrolysis and double bond oxidation can lead to lipid degradation that alters fatty acid profiles (Rudy et al., 2016). In live tissues, the oxidation of double bonds on fatty acids is typically controlled by antioxidants, but this function can decrease significantly after death (Petillo et al., 1998). Additionally, lipids are typically hydrolyzed by lipases (broken from acyl bonds into free fatty acids) in live or dead tissues so long as water is present for correct protein folding and function of the lipases. As such, researchers often try to limit water exposure by freezing samples or freeze-drying tissues immediately or soon after collection to avoid hydrolysis (Ingemansson et al., 1995) and store samples with antioxidants (Budge et al., 2006; Hixson et al., 2013) or under nitrogen gas to avoid double bond oxidation.

Since all samples were exposed to oxygen at high temperatures during oven drying it is likely polyunsaturated fatty acids were oxidized (Fu et al., 2016) and/ or hydrolyzed. Because of this, it is important to note that using the proportions of FA measured here should not be compared across studies. However, since it is known that lipid oxidation and hydrolysis rates during storage are species-, tissue- and temperature-dependent (Ingemansson et al., 1995; Nazemroaya et al., 2011; Rudy et al., 2016) and all samples were of the same species and received the same handling, treatment, and storage it is reasonable to make comparisons within this study and between the same tissue type (host to host, or symbiont to symbiont, POM to POM). Thus, a comparative approach used for this study between tissue types is valid and can still allow for assessment of relative differences in heterotrophy on POM seen in the FA and isotope data.

3.3 Methods

3.3.1 Sampling site and details

Samples were collected during a field campaign during the 2019 bleaching event in Mo'orea by the authors of Leinbach et al., 2021, 2022; there is greater detail found in those publications. However, replication of sampling details from these publications will be provided here for ease of reading.

In May 2019, during the height of the bleaching event, SCUBA divers surveyed one site on the north shore of Mo'orea (17.4731° S, 149.8176°W (forereef) and 14.4751° S, 149.8170° W (backreef)) to identify bleached and healthy *Acropora hyacinthus* coral colonies in three reef habitats: backreef (~ 3 m depth), shallow forereef (~ 5 m depth), and deep forereef (~ 14 m depth). For context, the forereef site maintained ~ 47% live coral cover (mean of six outer reef sites at 10 m depth) as of January 2019 (Edmunds, 2020). Colonies from the shallow and deep forereef habitats were tagged for future sampling. On the deep forereef in May 2019, no *A. hyacinthus* colonies without some degree of bleaching could be found (Leinbach et al., 2021). By August 2019, all the previously tagged bleached colonies in the deep forereef had died. Despite this high mortality, August surveys on the deep forereef (~ 14 m depth), which occurred after the period of accumulated thermal stress, identified previously bleached, untagged colonies that were observed to be visibly recovering from bleaching (Figure 24b and d; Leinbach et al., 2022). These new colonies were photographed, tagged, and sampled. Due to the high prevalence of bleaching at this site in May (53.2% severely bleached and 46.8% partially bleached; Leinbach et al., 2021), it is maintained that these previously untagged colonies were bleached during the bleaching event (Leinbach et al., 2021). In October 2019, 30 and 28 previously tagged colonies at ~ 5 and 14 m, respectively, were found, photographed,

and sampled via SCUBA for physiological metrics and/or reproductive histology (Leinbach et al., 2021). For all corals sampled, bleaching severity and colony area were determined using standardized photographs. Each colony was assigned a score from 1 to 5 according to the bleaching severity the colony experienced, with a 1 indicating stark white bleaching and a 5 indicating no visible bleaching (Figure 24b). Colony area was estimated by tracing the outline of each colony and calculating the planar surface area using ImageJ (Schneider et al., 2012).

Particulate organic matter was sampled by filtering 4 L of seawater from the collection site (deep forereef, shallow forereef, or backreef ("lagoon")) over pre-combusted 0.7 µm Whatman glass fiber filters. Zooplankton was sampled using a 30 cm 200 µm pore-size net for a 150 m tow at the approximate depth of coral sampling (14 m for deep forereef, ~ 5 m for shallow fore reef, ~ 3 m for backreef). Any chunks of macroalgae or sediment were removed prior to filtering over a pre-combusted glass fiber filter.

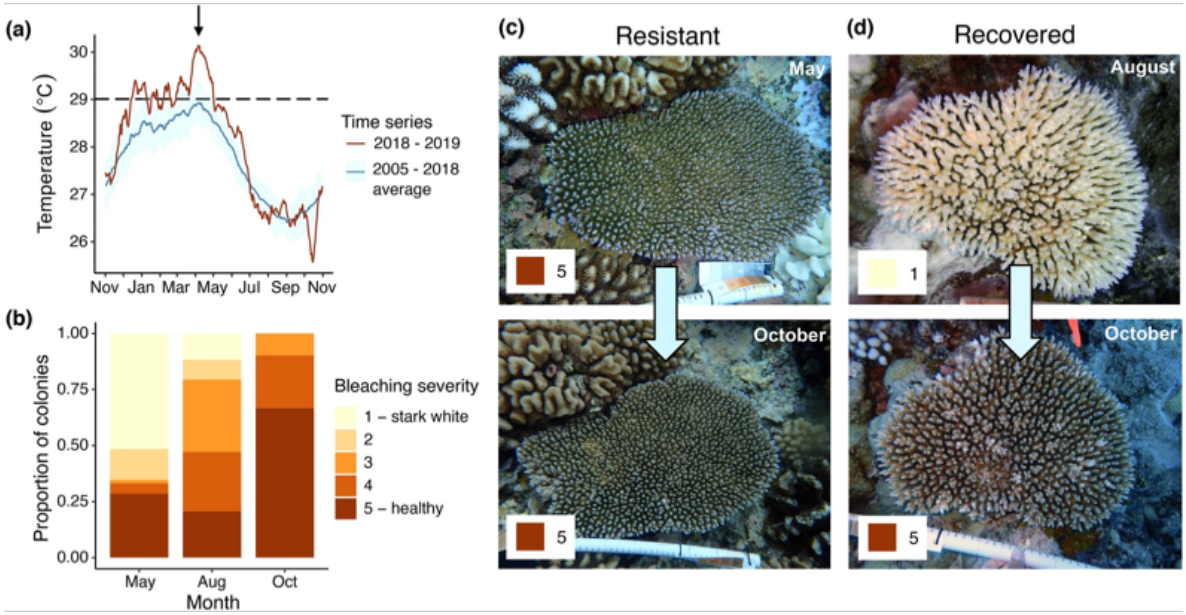

Figure 24. Sampling Scheme and bleaching response from Leinbach et al., 2021. A shows the 2019 thermal anomaly relative to a long term average. B shows the proportion of colonies with various bleaching scores. C shows a photo sequence of resistant colonies from May – October. D shows a photo sequence of recovered colonies from August - October.

3.3.2 Sample processing

Coral fragments of approximately 2 cm were collected from each colony. Fragmented samples were then frozen at - 40°C to facilitate later removal of tissue. Using filtered seawater coral fragments were airbrushed to remove coral tissue and algal cells (blastate) from the calcium carbonate skeleton. The blastate was then homogenized using an electric homogenizer and added to a 15-mL tube. The volume of the homogenized blastate was noted, and 200 ul of the sample was collected and fixed using Z-fix for algal symbiont counts.

The remaining volume of homogenized blastate was then centrifuged (2,000 x g for 2 minutes) to separate animal tissue from endosymbiont cells, where animal tissue remains in the supernatant while the endosymbiont pellets out. The animal fraction was pipetted out into a separate 15-mL tube. With the supernatant removed from the tube, the endosymbiont pellet was then resuspended in 2 mL of FSW and centrifuged an additional time to separate out any remaining animal tissue. The supernatant from this centrifugation was subsequently removed and combined to the 15-mL tube containing animal tissue from the original separation event. The animal fraction was centrifuged an additional time to pellet any endosymbiont cells remaining in solution. The supernatant collected from this additional centrifugation was considered our “pure” animal fraction to be used for later analysis. The endosymbiont fraction was cleaned six times to ensure the removal of animal tissue from the pellet. Cleaning of the algal pellet involved repeating the following steps: resuspension in 5 mL of FSW, centrifugation, and removal of the supernatant. All supernatants from this cleaning process were discarded. After cleaning was complete, the algal pellet was resuspended one final time in 5 mL of FSW and put through filter for stable isotope analysis (see below).

Following separation of animal tissue and endosymbiont cells, each fraction (and zooplankton and POM samples) was filtered through a 25mm GF/F filter. Samples were then rinsed with 1mL of 1N HCl to remove any residual calcium carbonate from the coral skeleton, then rinsed once more with 1mL of deionized water. Filters were placed in a drying oven overnight set at 60 °C and kept dry until transportation to UC Santa Barbra. Upon arrival at UC Santa Barbara, samples were immediately placed into a -80 °C freezer until analysis.

3.3.3 Fatty Acid and Stable Isotope analyses

Coral host, symbiont, POM and zooplankton samples were analyzed for fatty acid relative abundance and stable isotope ratios of carbon and nitrogen according to Chapter 2.

3.3.4 Statistical analyses

Statistical analyses were conducted in R (version 4.2.1) and R studio (version 2022.12.0+353). ANOVA tests were run using the ‘aov()’ function.

3.4 Results and Discussion

3.4.1 Coarse biomarker differences between divergent bleaching response

Colonies of *Acropora hyacinthus* on the forereef showed significant differences in several biomarkers with respect to bleaching response (resistant or recovered) in both tissue fractions ($p < 0.05$; host = 11; symbiont = 9; Table 7). In general, the host of resistant colonies exhibited significantly more ($p < 0.001$; ANOVA) mono- and polyunsaturated fatty acids (MUFA + PUFA) (15.8 ± 5.7 %) than recovered colonies (9.1 ± 1.2 %) and with larger variation, while the host of recovered colonies consequently had larger proportions of saturated fatty acids (SAFA; resistant = 90.9 ± 1.2 %, recovered = 84.2 ± 5.7 %; $p < 0.001$, ANOVA, Figure 25). In the symbiont fraction, a similar trend is seen although with smaller differences, with the symbionts of resistant colonies showing higher MUFA + PUFA (15.2 ± 4.0 %) than recovered colonies (13.0 ± 6.6 %) ($p < 0.001$, ANOVA, Figure 25). The same trend for saturated fatty acids seen in the host is also seen in the symbionts (recovered = 87.0 ± 6.6 %, resistant = 84.8 ± 4.0 %; $p < 0.001$, ANOVA; Figure 25). Interestingly, an inverse relationship in data variability is found in the symbiont fraction such that there is larger variation in major FA classes (MUFA + PUFA) in symbionts of recovered colonies relative to symbionts of resistant colonies (Figure 25), while in the host fraction this trend is inverted and there is more MUFA + PUFA variation found in the host of resistant colonies than recovered colonies (Figure 25, Table 7). More FA variability in the symbionts of recovered colonies could be explained at least partially by recent (< 2 months, Figure 24) horizontal transmission of symbionts from the environment during bleaching recovery (Buddemeier & Fautin, 1993) or variability in repopulation dynamics of the small photo symbiont community after bleaching. For the host, increased MUFA + PUFA variability in resistant colonies

relative to recovered colonies (and their own symbionts) may be due to colony-level differences in nutritional sourcing that would cause a divergence in FA profiles from their symbionts such as differences in trophic strategy (see section 2.4.3) which has been seen readily in nature (Fox et al., 2019). Since all resistant colonies were found near the reef crest which is known to be a net sink of oceanic POM (Wyatt et al., 2013), colony-level variability in consumption of these particulate subsidies would cause more FA variation in the host of resistant colonies relative to the host of deeper colonies on the reef slope (recovered colonies) and to their own symbionts, as was seen here (Figure 25).

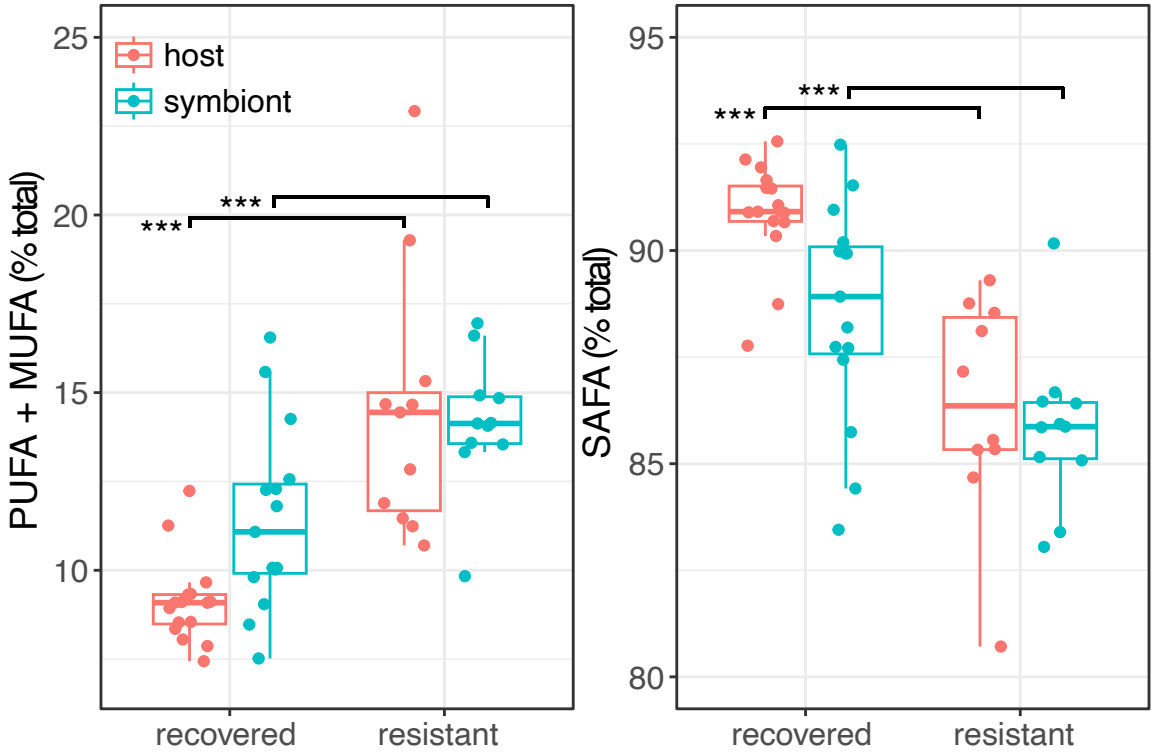

Figure 25. Left panel shows boxplot of sum of mono- and polyunsaturated fatty acids (MUFA + PUFA) separated by bleaching response and tissue type (host or symbiont). Right panel shows boxplot of saturated fatty acid (SAFA). Brackets show significance level test between same tissue type with bleaching response as the independent variable [* ($p < 0.05$), ** ($p < 0.01$), ***($p<0.001$)].

The shift in the FA profile balance seen in recovered colonies towards SAFA has been seen during thermal stress of *Acropora digitifera* in which it is hypothesized that MUFA and

PUFA may act as the last line of defense for oxidative stress (Safuan et al., 2021). Considering that bleached corals were visibly "recovered" from bleaching during sampling and exhibited statistically similar symbiont densities (Leinbach et al., 2021) these data confirm the physiological and molecular effects of bleaching last beyond visual recovery not only for protein and carbohydrates (Leinbach et al., 2021) but also for fatty acids (Figure 25). Interestingly, the mean difference of PUFA + MUFA between host and symbiont fractions ($host_{MUFA+PUFA}$ - $symbiont_{MUFA+PUFA}$) of the two bleaching responses was considerably larger and negative for recovered colonies (-3.8 %) than for resistant colonies (0.6 %) (Figure 25). This suggests that in resistant colonies, fatty acids are readily being shared between host and symbiont ($host_{MUFA+PUFA}$ - $symbiont_{MUFA+PUFA}$ ~ 0) while in recovered colonies the host still had not acquired sufficient MUFA + PUFA from their symbionts to converge the relative abundance of these coarse biomarkers. The trend seen for resistant colonies stands in contrast to some literature that *Symbiodinium* symbionts are more parasitic than mutualistic (Stat et al., 2008), with evidence here showing convergence of coarse FA biomarkers of *Symbiodinium* symbionts (resistant colonies) with the host relative to *Cladocopium* symbionts (recovered colonies, Figure 25), although bleaching effect must be considered.

Even though symbiont densities were statistically similar for recovered and resistant colonies (Leinbach et al., 2021), the recent reestablishment of the symbiont community in recovered colonies before sampling with *Cladocopium* symbionts (fully bleached 2 months before sampling, Figure 24) reveals that this symbiont which is known for its high photosynthetic efficiency (A. Jones & Berkelmans, 2010; Stat et al., 2008) had not yet translocated enough FA to the host for recovery of the host lipid pool from bleaching (Figure 25). Overall, the significant decrease in MUFA + PUFA in the host of recovered colonies

despite larger proportions found in their symbionts exemplifies the metabolically compromised state that recovered colonies were even after visual recovery from bleaching.

3.4.2 Isotopic and elemental ratios of divergent bleaching response

The divergent bleaching response of *Acropora hyacinthus* revealed distinct patterns in isotopic and elemental ratios. $\delta^{13}C$ was significantly lower for both the host and symbiont fraction in recovered colonies ($p < 0.001$, ANOVA, Table 7, Figure 26) while the C:N ratio was significantly higher in recovered colonies ($p < 0.01$ for host, $p < 0.001$ for symbiont, ANOVA, Table 7, Figure 26). $\delta^{15}N$ was slightly higher (+ 0.4 ‰) in the host of resistant colonies than recovered colonies, although this was non-significant due to high variability in the resistant colonies (Figure 26d). $\delta^{15}N$ in the symbionts was lower in resistant colonies than recovered colonies (- 0.7‰) which was also non-significant due to high variability in both bleaching response types (Table 7).

The strong carbon isotope difference between bleaching response types (~ 3‰ lower in recovered colonies of both host and symbiont, Figure 26a) is very likely due to irradiance and depth being large covariates in bleaching response, with recovered colonies at 14 m depth and resistant colonies at ~ 5 m depth. This isotopic effect has been readily observed in coral isotope studies along depth gradients (Alamaru et al., 2009; Muscatine et al., 1989; Wall et al., 2020) and is nearly identical to the observations from Wall et al., 2020 despite different photo symbiont communities, showing that this trend is irradiance driven. The physiochemical explanation underlying this response was formulated by Muscatine et al. and is known as the "depletion-diffusion hypothesis". This explanation primarily notes that under high irradiance and high rates of photosynthesis the fixation of internal CO_2 by Rubisco (Ribulose biphosphate carboxylase) is faster than what can be refilled by seawater bicarbonate, thus the

internal CO_2 pool becomes enriched in ^{13}C (and $\delta^{13}C$) and this is seen in the photosynthetic products relative to corals under low light conditions where carbon fixation rates do not outpace bicarbonate diffusion into the organism.

The C:N ratio of the host of recovered colonies exhibited remarkably high values relative to their symbionts and with large variation (Figure 26c, Table 7). This is likely due to catabolism of protein reserves from bleaching (Figure 11d) that had not yet been replenished (Leinbach et al., 2021). The larger difference in the C:N ratio ($\mathbf{\Delta}$C:N = $C:N_{host} - C:N_{symbiont}$) of recovered colonies ($\mathbf{\Delta}$C:N = 4.9) relative to resistant colonies ($\mathbf{\Delta}$C:N = 2.7) suggests that the symbionts of recovered colonies were either passing off less organic nitrogen products to the host and/ or that there was not enough time after bleaching and the sampling time point (~ 2 months) for full translocation and replenishment of the host nitrogen pool. The lower C:N ratio of resistant colony symbionts relative to recovered colony symbionts observed here (Figure 26c) has been observed between *Symbiodinium* (resistant colonies) and *Cladocopium* symbionts (recovered colonies); with *Symbiodinium* symbionts typically showing lower C:N ratios relative to *Cladocopium* symbionts due to faster inorganic nitrogen assimilation rates (Ezzat et al., 2017). This is the exact pattern that is seen here (Figure 26c). This effect may have been further amplified by relatively higher flow rates found at the shallower forereef (reef crest) relative to the deeper forereef which makes the diffusive boundary layer smaller, resulting in faster diffusion of dissolved inorganic nitrogen across the boundary layer to the coral holobiont (Nakamura & Van Woesik, 2001) that would ultimately decrease C:N ratios.

The difference in carbon isotope ratios ($\mathbf{\Delta}^{13}C = \delta^{13}C_{host} - \delta^{13}C_{symbiont}$), which has classically been used as a proxy for coral heterotrophy (Grottoli et al., 2006; Muscatine et al., 1989) was lower in resistant colonies than recovered colonies (Figure 26b), although non-

significantly. While larger (more negative) $\Delta^{13}C$ values do capture relatively more heterotrophy (Fox et al., 2018), the lack thereof does not exclude heterotrophy as an explanation since heterotrophically acquired nitrogen (Price et al., 2021), essential fats (Figure 16, 19 and 21) and amino acids (Ferrier-Pagès et al., 2021; Fox et al., 2019) are preferentially retained in host tissues over elemental carbon, most of which is likely catabolized or exuded as mucous, as was demonstrated in Chapter 2 (Figure 19). Still, the relatively lower $\Delta^{13}C$ values of resistant colonies (Figure 26b) points towards relatively more heterotrophy in resistant colonies, but not as the only line of evidence. An isotope biplot of carbon and nitrogen grouped by tissue type and bleaching response shows that the host recovered colonies exhibited more isotopic niche overlap (Newsome et al., 2007) with their symbionts than did resistant colonies (Figure 26d) which is an indicator of increased reliance on heterotrophy for resistant colonies (Conti-Jerpe et al., 2020).

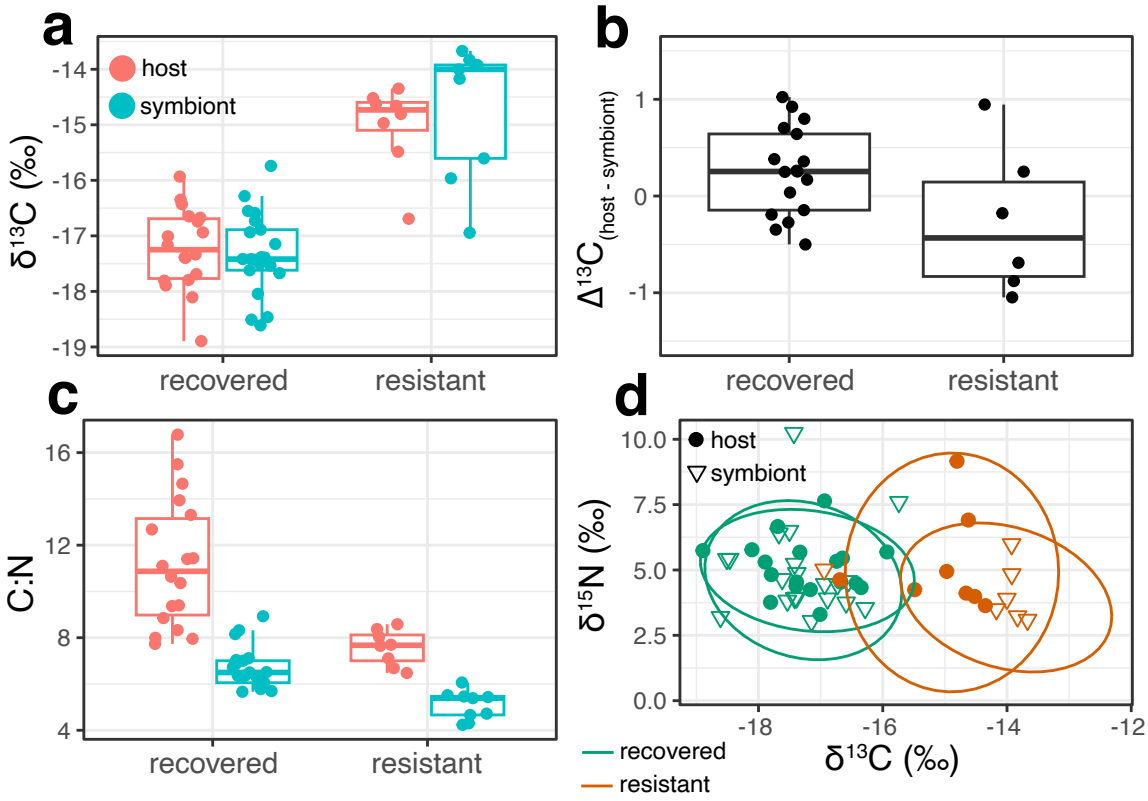

Figure 26. Isotopic and elemental ratios of divergent bleaching response of *Acropora hyacinthus*. Panel A shows $\delta^{13}C$ of both host and symbiont fraction grouped by bleaching response. B shows $\Delta^{13}C = \delta^{13}C_{host} - \delta^{13}C_{symbiont}$ grouped by bleaching response. Panel C shows carbon to nitrogen ratio of host and symbiont fraction grouped by bleaching response. D shows isotope biplot of corals with 95% confidence ellipses, colored by bleaching response, with point shape representing tissue fraction.

3.4.3 Biomarker differences suggest heterotrophy on POM for resistant colonies

The differences between biomarkers in the same tissue type (host or symbiont) of resistant and recovered colonies was calculated to compare divergent bleaching response of *Acropora hyacinthus* (Table 7, Figure 27). The difference in individual biomarkers of the symbiont fraction ($resistant_{symbiont} - recovered_{symbiont}$), which yielded a positive or negative value (green or orange), was typically mirrored in the host fraction (Figure 27). This signifies translocation of most FA within the symbiosis and convergence of most of the FA profile between the host and symbiont, which has been observed in *Acropora* corals (Kim, Baker, et al., 2021). However, there were select biomarkers that exhibited an inverse trend in which biomarker difference was negative in the symbiont (lower in resistant colony symbionts) but positive in the host fraction (higher in resistant colony host; Figure 27). While many of these biomarkers exhibited only a small and non-significant inverse trend, several exhibited significant trends in the host fraction ($p < 0.05$, ANOVA) such as 14:1, 16:1n7 and 18:2n6. These FA were found in significantly larger proportions in the host fraction of resistant colonies than recovered colonies but were found in smaller proportions in the symbiont fraction of resistant colonies than recovered colonies (Table 7, Figure 27), which suggests alternate or supplemental sourcing of these FA for the host of resistant colonies.

Analysis of POM collected at the study site reveals that two of these FA, 18:2n6 and 16:1n7, were found in larger proportions than the host or symbiont of any corals sampled (except for one symbiont sample higher in 16:1n7, Figure 28a and b) and are thus

characteristic biomarkers for heterotrophy of POM at this site. This is in line with literature that these two FA are typically found in high proportions in oceanic POM and marine phytoplankton (Dalsgaard et al., 2003; Wyatt et al., 2013). In particular, the essential FA 18:2n6, which is known to be sourced through heterotrophy for corals as a building block for other n-6 PUFA (Imbs, Yakovleva, et al., 2010) has been shown to decline rapidly in POM as oceanic water flows over the reef crest (Wyatt et al., 2013) and benthic communities consume the POM (Wyatt et al., 2010, 2013). This is consistent with the observations that resistant corals adjacent to the reef crest have relatively higher 18:2n6 than deep fore reef colonies (recovered colonies) despite their symbionts having less 18:2n6 (Figure 27 and 28a, Table 7). Additionally, 18:2n6 is shown to reliably track coral heterotrophy in host tissues but not symbiont tissues (Figure 16, Table 3), which is the pattern seen here for resistant colonies (Figure 27 and 28a).

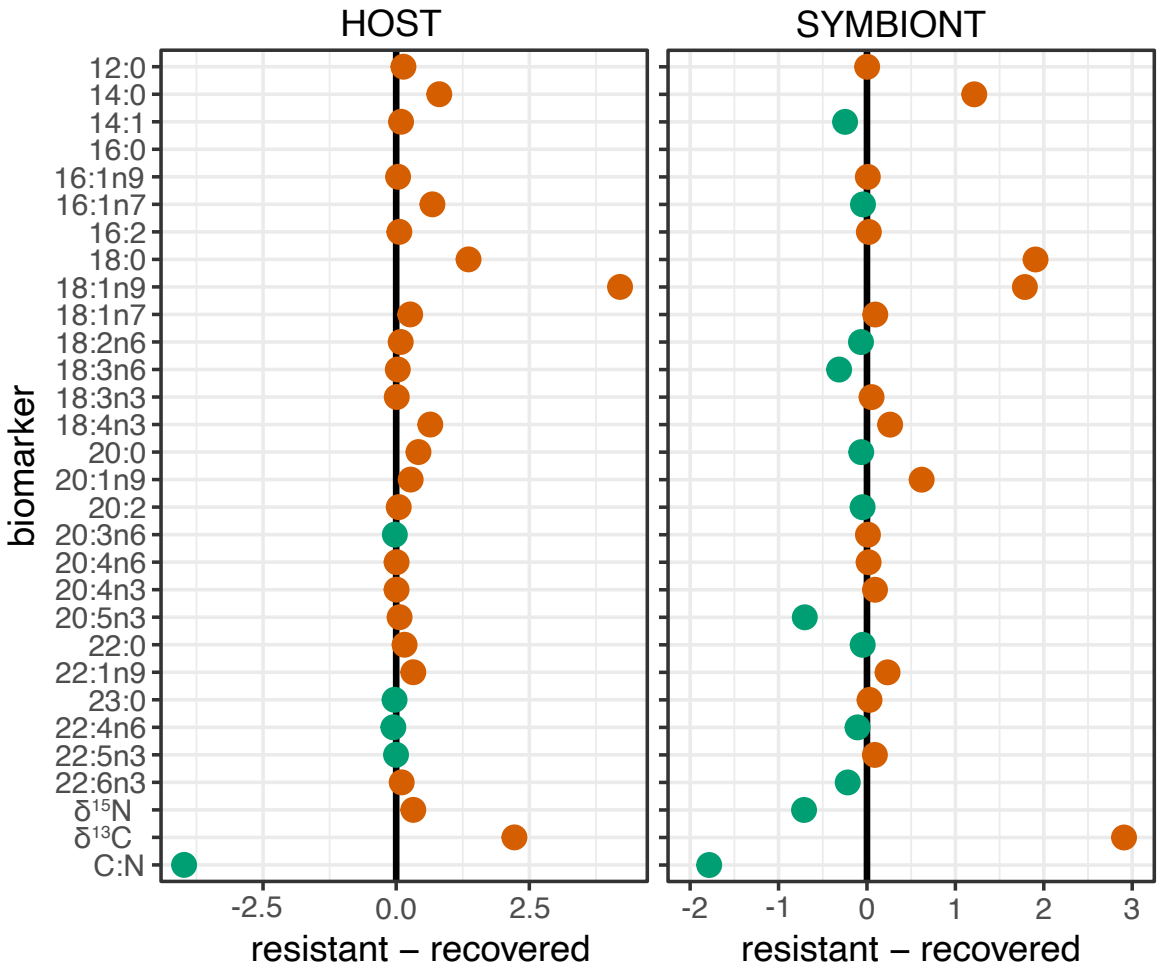

Figure 27. Difference between biomarkers for resistant and recovered colonies for the host and symbiont fraction, positive values are colored orange, negative values are colored green. Difference between fatty acid values is in % total, difference between isotopic values is in permill (‰), differences between elemental ratios is unitless.

The trend found in 18:2n6 was also found for 16:1n7, with POM exhibiting a larger proportion of this FA than all coral samples, except for one symbiont tissue sample (Figure 28b). While 16:1n7 is often found in large quantities in coral endosymbionts, it is also found in marine bacteria and phytoplankton and is known to increase in the tissues of consumers fed a diatom rich diet (Dalsgaard et al., 2003); this FA has also shown to be a tracer for low trophic level heterotrophy (i.e. consumption of smaller phytoplankton rather than zooplankton; Figure 22). Interestingly, $\delta^{15}N$ also exhibits a similar inverse trend as seen in these select FA, whereby average $\delta^{15}N$ was higher in the host of resistant colonies than recovered colonies, but lower

in the symbiont fraction of resistant colonies relative to recovered colonies (Figure 27, Table 7), although the effect was non-significant due to high variability. $\delta^{15}N$ is a reliable tracer of heterotrophy (Figure 19a; Conti-Jerpe et al., 2020; Price et al., 2021) and this pattern, although non-significant adds some support to the fatty acid biomarker patterns seen here.

To further distinguish relative contribution of POM subsidies to coral host tissues, the sum of distinct POM biomarkers (18:2n6 + 16:1n7) was calculated for the host and symbiont fraction of each coral. The difference of this POM metric between the host and symbiont fraction was then plotted and grouped by bleaching response type (Figure 28c) such that values ~ 0 are indicative of convergence of these biomarkers with the symbiont, values > 0 are indicative of heterotrophic sourcing of POM biomarkers and values < 0 are indicative of reduced translocation of these FA from symbiont to host and little heterotrophic reliance on POM. The data reveal that most resistant colonies (except for 4 colonies) had positive values of these biomarkers, indicating principal reliance on POM in this reef environment, whereas recovered colonies typically exhibited values at ~ 0 or < 0, indicating convergence of these FA with the symbiont profile or reduced translocation of these FA from their symbionts, respectively. There was a significant effect of bleaching response type on this POM feeding metric ($p < 0.01$; ANOVA), showing that resistant colonies were very likely feeding on more POM in the water column relative to bleached and recovered colonies.

Overall, the host of resistant colonies of *Acropora hyacinthus* exhibited larger proportions of POM biomarkers than the host of recovered colonies despite their symbionts having lower quantities of these FA than symbionts on the deep reef slope. This supports the hypothesis that colonies on the reef crest were consuming more POM than recovered colonies. This data further exemplifies the role that reef habitat and oceanic subsidies have in structuring

bleaching response. This same bleaching pattern has been observed on Mo'orea before, in which shallower corals on the reef slope bleached less than their deeper counterparts (Penin et al., 2007) despite increased irradiance stress. This data, in conjunction with Leinbach et al., 2022 show that the synergistic effects of reef habitat, heterotrophy on particulate organic matter and symbiont clade type were likely factors in determining bleaching resistance of *Acropora hyacinthus* at the reef crest (Wyatt et al., 2023).

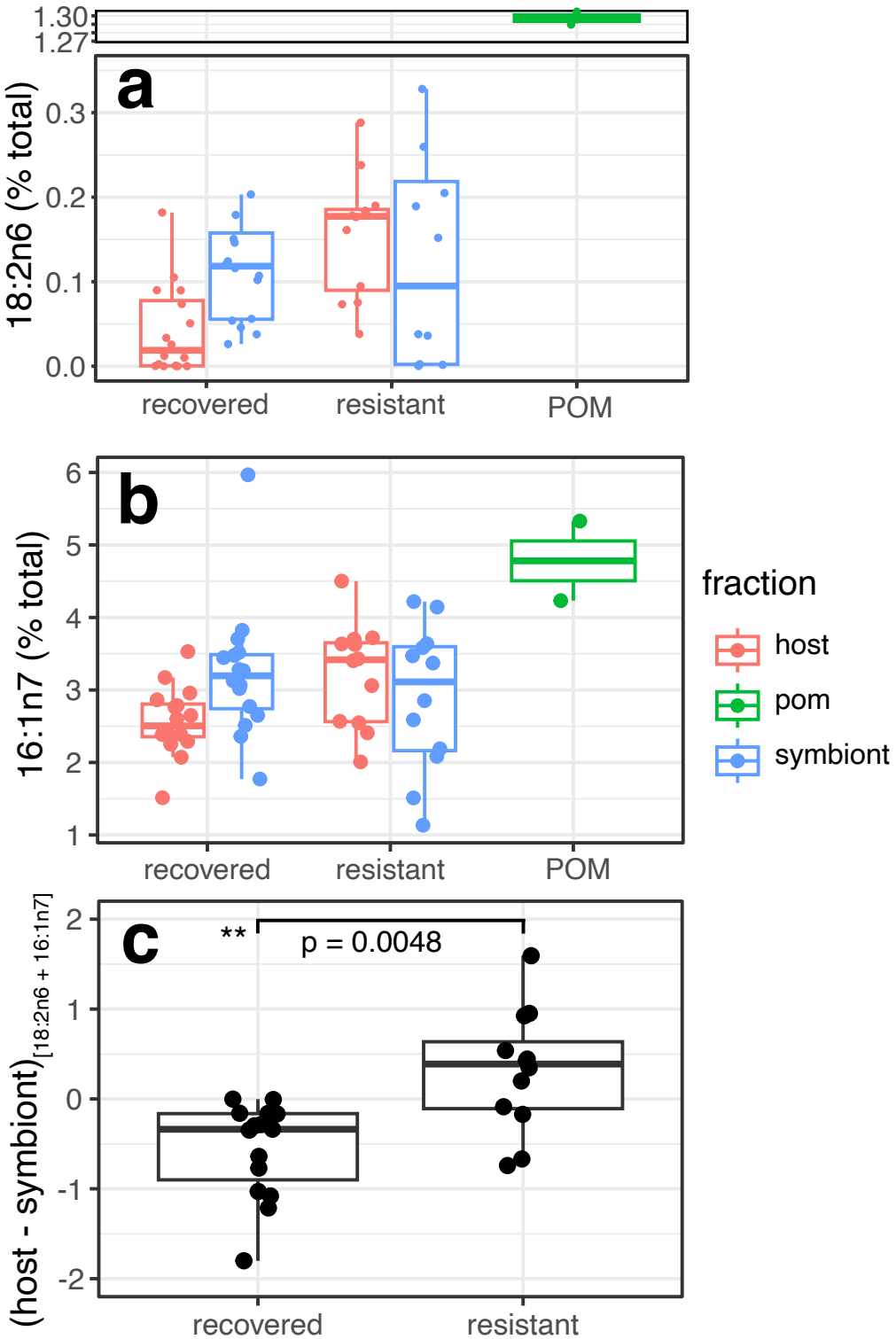

Figure 28. Multiplot of distinct POM biomarkers. Panel A shows relative proportion of essential FA 18:2n6 in resistant and recovered colonies separated by tissue type and particulate organic matter. Panel B shows relative proportion of 16:1n7. Panel C shows difference between host and symbiont tissues of the sum of these two POM biomarkers with a statistically significant difference.

	HOST	HOST		SYMBIONT	SYMBIONT	
biomarker	**recovered**	**resistant**	**p-value**	**recovered**	**resistant**	**p-value**
C12:0	0.07 ±0.05	0.21 ±0.13	**	0.16 ±0.1	0.16 0.19	
C14:0	6.41 ±0.91	7.22 ±2.4		8.09 ±0.68	9.3 ±2.12	*
C14:1	0.02 ±0.01	0.11 ±0.15	*	0.52 ±0.28	0.27 ±0.19	*
C16:0	69.5 ±3.41	59.81 ±7.41	***	66.45 ±5.46	61.87 ±2.8	*
C16:1n9	0.03 ±0.02	0.06 ±0.06		0.14 ±0.45	0.15 ±0.1	
C16:1n7	2.58 ±0.51	3.26 ±0.82	*	3.23 ±0.91	3.19 ±0.69	
C16:2	0.01 ±0.01	0.07 ±0.05	***	0.05 ±0.05	0.07 ±0.06	
C18:0	12.27 ±2.66	13.63 ±4.75		10.2 ±2	12.11 ±2.85	
C18:1n9	3.32 ±0.69	7.52 ±4.74	**	4.02 ±1.75	5.8 ±0.45	*
C18:1n7	0.23 ±0.05	0.5 ±0.36	*	0.16 ±0.08	0.25 ±0.12	*
C18:2n6	0.05 ±0.05	0.13 ±0.07	**	0.17 ±0.19	0.1 ±0.11	
C18:3n6	0.11 ±0.2	0.14 ±0.18		0.46 ±0.8	0.14 ±0.21	
C18:3n3	0.03 ±0.03	0.04 ±0.05		0.01 ±0.02	0.07 ±0.1	
C18:4n3	0.29 ±0.2	0.93 ±1.41		0.85 ±1.67	1.11 ±1.01	
C20:0	2.07 ±0.39	2.49 ±0.73		1.61 ±0.33	1.55 ±0.42	
C20:1n9	1.68 ±0.35	1.95 ±0.46		0.92 ±0.25	1.53 ±0.16	***
C20:2	0.05 ±0.07	0.09 ±0.1		0.06 ±0.1	0.01 ±0.02	
C20:3n6	0.07 ±0.06	0.05 ±0.04		0.08 ±0.08	0.09 ±0.08	
C20:4n6	0.06 ±0.05	0.07 ±0.1		0.05 ±0.05	0.07 ±0.05	
C20:4n3	0.06 ±0.04	0.07 ±0.09		0.05 ±0.05	0.14 ±0.16	*
C20:5n3	0.07 ±0.13	0.14 ±0.14		0.89 ±1.97	0.18 ±0.15	
C22:0	0.43 ±0.19	0.59 ±0.22		0.47 ±0.19	0.42 ±0.26	
C22:1n9	0.29 ±0.14	0.61 ±0.39	*	0.56 ±0.24	0.79 ±0.4	
C23:0	0.08 ±0.04	0.04 ±0.03		0.07 ±0.1	0.09 ±0.16	
C22:4n6	0.1 ±0.1	0.05 ±0.04		0.17 ±0.48	0.06 ±0.03	
C22:5n3	0.05 ±0.04	0.04 ±0.04		0.12 ±0.08	0.21 ±0.22	
C22:6n3	0.07 ±0.07	0.17 ±0.24		0.46 ±1.07	0.24 ±0.23	
^{15}N (‰)	4.88 ±0.94	5.2 ±1.89		4.93 ±1.85	4.22 ±1.08	
^{13}C (‰)	-17.23 0.78	-15.01 0.76	***	-17.26 0.73	-14.35 1.15	***
C:N	11.56 ±2.96	7.58 ±0.77	**	6.68 ±0.77	4.89 ±0.55	***

Table 7. Data summary table for divergent bleaching responses of *Acropora hyancithus* in Mo'orea, French Polynesia. Data including fatty acid, isotopic and elemental ratios of the host and symbiont fraction with significance results from one-way ANOVA between bleaching response of same tissue type [* ($p < 0.05$), ** ($p < 0.01$), ***($p<0.001$)].

3.5 Conclusion

The bleaching response patterns of *Acropora hyacinthus* observed on the northern forereef of Mo'orea reveal that colonies on the shallow forereef near the reef crest were likely consuming more POM than colonies that bleached and recovered on the deep forereef. Several lines of evidence converge on this interpretation including high variation in MUFA + PUFA in the host of resistant colonies (Figure 25), larger and more negative $\Delta^{13}C$ values in resistant colonies (Figure 26b), less isotopic niche overlap of the host and symbiont of resistant colonies (Figure 26d) than recovered colonies, and larger proportions of putative POM fatty acid biomarkers 18:2n6 and 16:1n7 in the host of resistant colonies relative to recovered colonies. This interpretation stands in line with evidence that that benthic communities on the reef crest are a net sink of oceanic POM (Patten et al., 2011; Wyatt et al., 2010, 2013) and that increased reliance on heterotrophy is associated with bleaching resistance (Conti-Jerpe et al., 2020). These data show the vital importance of reef environment, oceanographic forcing and planktonic and particulate organic matter subsidies in structuring bleaching response of corals in a warming ocean and ultimately show that the reef crest may serve as a potent zone for reseeding coral populations after marine heat waves.

References

Adam, T. C., Burkepile, D. E., Holbrook, S. J., Carpenter, R. C., Claudet, J., Loiseau, C., Thiault, L., Brooks, A. J., Washburn, L., & Schmitt, R. J. (2021). Landscape-scale patterns of nutrient enrichment in a coral reef ecosystem: implications for coral to algae phase shifts. *Ecological Applications*, *31*(1), 1–16. https://doi.org/10.1002/eap.2227

Al-Moghrabi, S., Allemand, D., Couret, J. M., & Jaubert, J. (1995a). Fatty acids of the scleractinian coral Galaxea fascicularis: effect of light and feeding. *Journal of Comparative Physiology B*, *165*(3), 183–192. https://doi.org/10.1007/BF00260809

Al-Moghrabi, S., Allemand, D., Couret, J. M., & Jaubert, J. (1995b). Fatty acids of the scleractinian coral Galaxea fascicularis: effect of light and feeding. *Journal of Comparative Physiology B*, *165*(3), 183–192. https://doi.org/10.1007/BF00260809

Alamaru, A., Loya, Y., Brokovich, E., Yam, R., & Shemesh, A. (2009). Carbon and nitrogen utilization in two species of Red Sea corals along a depth gradient: Insights from stable isotope analysis of total organic material and lipids. *Geochimica et Cosmochimica Acta*, *73*(18), 5333–5342. https://doi.org/10.1016/j.gca.2009.06.018

Alfaro, A. C., Thomas, F., Sergent, L., & Duxbury, M. (2006). Identification of trophic interactions within an estuarine food web (northern New Zealand) using fatty acid biomarkers and stable isotopes. *Estuarine, Coastal and Shelf Science*, *70*(1–2), 271–286. https://doi.org/10.1016/j.ecss.2006.06.017

Alldredge, A. L., & Carlson, C. A. (2011). *MCR LTER: Coral Reef: Water Column: Nearshore Water Profiles, CTD, Primary Production, and Chemistry*. http://metacat.lternet.edu/knb/metacat/ knb-lter-mcr.10.30/lter.

Anthony, K. R. N., Hoogenboom, M. O., Maynard, J. A., Grottoli, A. G., & Middlebrook, R. (2009). Energetics approach to predicting mortality risk from environmental stress: A case study of coral bleaching. *Functional Ecology*, *23*(3), 539–550. https://doi.org/10.1111/j.1365-2435.2008.01531.x

Armoza-Zvuloni, R., Schneider, A., Sher, D., & Shaked, Y. (2016). Rapid Hydrogen Peroxide release from the coral Stylophora pistillata during feeding and in response to chemical and physical stimuli. *Scientific Reports*, *6*(February 2015), 1–10. https://doi.org/10.1038/srep21000

Arrington, E. C. (2021). *Genomic Insights into the Marine Microbial Response to Oil Spills: Biogeographic Priming, Cryptic Hydrocarbon Cycling, and Substrate Specialization*.

Bachar, A., Achituv, Y., Pasternak, Z., & Dubinsky, Z. (2007). Autotrophy versus heterotrophy: The origin of carbon determines its fate in a symbiotic sea anemone. *Journal of Experimental Marine Biology and Ecology*, *349*(2), 295–298. https://doi.org/10.1016/j.jembe.2007.05.030

Bachok, Z., Mfilinge, P., & Tsuchiya, M. (2006). Characterization of fatty acid composition in healthy and bleached corals from Okinawa, Japan. *Coral Reefs*, *25*(4), 545–554. https://doi.org/10.1007/s00338-006-0130-9

Baird, A. H., & Marshall, P. A. (2002). Mortality, growth and reproduction in scleractinian corals following bleaching on the Great Barrier Reef. *Marine Ecology Progress Series*, *237*(July), 133–141. https://doi.org/10.3354/meps237133

Barnett, T. P., Pierce, D. W., AchutaRao, K. M., Gleckler, P. J., Santer, B. D., Gregory, J. M., & Washington, W. M. (2005). Ocean science: Penetration of human-induced warming into the world's oceans. *Science*, *309*(5732), 284–287.

https://doi.org/10.1126/science.1112418
Baumann, J., Grottoli, A. G., Hughes, A. D., & Matsui, Y. (2014). Photoautotrophic and heterotrophic carbon in bleached and non-bleached coral lipid acquisition and storage. *Journal of Experimental Marine Biology and Ecology*, *461*, 469–478. https://doi.org/10.1016/j.jembe.2014.09.017
Baums, I. B., Miller, M. W., & Hellberg, M. E. (2006). Geographic variation in clonal structure in a reef-building Caribbean coral, Acropora palmata. *Ecological Monographs*, *76*(4), 503–519. https://doi.org/10.1890/0012-9615(2006)076[0503:GVICSI]2.0.CO;2
Bellworthy, J., & Fine, M. (2018). The Red Sea Simulator: A high-precision climate change mesocosm with automated monitoring for the long-term study of coral reef organisms. *Limnology and Oceanography: Methods*, *16*(6), 367–375. https://doi.org/10.1002/lom3.10250
Berkelmans, R., & Van Oppen, M. J. H. (2006). The role of zooxanthellae in the thermal tolerance of corals: A "nugget of hope" for coral reefs in an era of climate change. *Proceedings of the Royal Society B: Biological Sciences*, *273*(1599), 2305–2312. https://doi.org/10.1098/rspb.2006.3567
Bowden-Kerby, A., & Carne, L. (2012). Thermal Tolerance as a factor in Caribbean Acropora Restoration. *Proceedings of the 12th International Coral Reef Symposium*, *2006*(July), 9–13.
Bradford, M. (1976). A Rapid and Sensitive Method for the Quantification of Microgram Quantities of Protein Utilizing the Principle of Protein-Dye Binding. *Analytical Biochemistry*, *72*(1–2), 248–254. https://doi.org/10.1016/j.cj.2017.04.003
Buddemeier, R. W., & Fautin, D. G. (1993). Coral Bleaching as an Adaptive Mechanism. *BioScience*, *43*(5), 320–326. https://doi.org/10.2307/1312064
Budge, S. M., Iverson, S. J., & Koopman, H. N. (2006). Studying trophic ecology in marine ecosystems using fatty acids: A primer on analysis and interpretation. *Marine Mammal Science*, *22*(4), 759–801. https://doi.org/10.1111/j.1748-7692.2006.00079.x
Burgess, S. C., Johnston, E. C., Wyatt, A. S. J., Leichter, J. J., & Edmunds, P. J. (2021). Response diversity in corals: hidden differences in bleaching mortality among cryptic Pocillopora species. *Ecology*, *102*(6), 1–13. https://doi.org/10.1002/ecy.3324
Burriesci, M. S., Raab, T. K., & Pringle, J. R. (2012). Evidence that glucose is the major transferred metabolite in dinoflagellate-cnidarian symbiosis. *Journal of Experimental Biology*, *215*(19), 3467–3477. https://doi.org/10.1242/jeb.070946
Camp, E. F., Suggett, D. J., Pogoreutz, C., Nitschke, M. R., Houlbreque, F., Hume, B. C. C., Gardner, S. G., Zampighi, M., Rodolfo-Metalpa, R., & Voolstra, C. R. (2020). Corals exhibit distinct patterns of microbial reorganisation to thrive in an extreme inshore environment. *Coral Reefs*, *39*(3), 701–716. https://doi.org/10.1007/s00338-019-01889-3
Cavender-Bares, K. K., Karl, D. M., & Chisholm, S. W. (2001). Nutrient gradients in the western North Atlantic Ocean: Relationship to microbial community structure and comparison to patterns in the Pacific Ocean. *Deep-Sea Research Part I-Oceanographic Research Papers*, *48*(1), 2373–2395. //000170730800002
Chen, H. K., Wang, L. H., Chen, W. N. U., Mayfield, A. B., Levy, O., Lin, C. S., & Chen, C. S. (2017). Coral lipid bodies as the relay center interconnecting diel-dependent lipidomic changes in different cellular compartments. *Scientific Reports*, *7*(1), 1–13.

https://doi.org/10.1038/s41598-017-02722-z
Chisholm, S. W., Olson, R. J., Zettler, E. R., Goericket, R., Waterbury, J. B., & Welschmeyert, N. A. (1988). A novel free-living prochlorophyte abundant in the oceanic euphotic zone. *Nature*, *52*(2), 169–173. https://www.nature.com/articles/334340a0.pdf
Coates, R. C., Podell, S., Korobeynikov, A., Lapidus, A., & Pevzner, P. (2014). Characterization of Cyanobacterial Hydrocarbon Composition and Distribution of Biosynthetic Pathways. *PLoS ONE*, *9*(1), 85140. https://doi.org/10.1371/journal.pone.0085140
Conlan, J. A., Humphrey, C. A., Severati, A., Parrish, C. C., & Francis, D. S. (2019). Elucidating an optimal diet for captive Acropora corals. *Aquaculture*, *513*(April), 734420. https://doi.org/10.1016/j.aquaculture.2019.734420
Conti-Jerpe, I., Thompson, P., Wong, C. W., Oliveira, N., Duprey, N. N., Moynihan, M. A., & Baker, D. M. (2020). Trophic strategy and bleaching resistance in reef-building corals. *Science Advances*, *6*(15). https://doi.org/10.1126/sciadv.abd9453
Cox, E. F. (2007). Continuation of sexual reproduction in Montipora capitata following bleaching. *Coral Reefs*, *26*(3), 721–724. https://doi.org/10.1007/s00338-007-0251-9
Crabbe, M. J. C., & Carlin, J. P. (2009). Multiple Symbiodinium clades in Acropora species scleractinian corals from the Ningaloo reef, Australia. *International Journal of Integrative Biology*, *5*(2), 72–74.
Dalsgaard, J., St. John, M., Kattner, G., Müller-Navarra, D., & Hagen, W. (2003). Fatty acid trophic markers in the pelagic marine environment. *Advances in Marine Biology*, *46*, 225–340. https://doi.org/10.1016/S0065-2881(03)46005-7
De Goeij, J. M., Moodley, L., Houtekamer, M., Carballeira, N. M., & Van Duyl, F. C. (2008). Tracing 13C-enriched dissolved and particulate organic carbon in the bacteria-containing coral reef sponge Halisarca caerulea: Evidence for DOM feeding. *Limnology and Oceanography*, *53*(4), 1376–1386. https://doi.org/10.4319/lo.2008.53.4.1376
Donovan, M. K., Adam, T. C., Shantz, A. A., Speare, K. E., Munsterman, K. S., Rice, M. M., Schmitt, R. J., Holbrook, S. J., & Burkepile, D. E. (2020). Nitrogen pollution interacts with heat stress to increase coral bleaching across the seascape. *Proceedings of the National Academy of Sciences of the United States of America*, *117*(10), 5351–5357. https://doi.org/10.1073/pnas.1915395117
Doty, M. S., & Oguri, M. (1956). The island mass effect. *ICES Journal of Marine Science*, *22*(1), 33–37. https://doi.org/10.1093/icesjms/22.1.33
Duan, Y., Cui, M., Ma, L., Song, J., Zhou, S., & Luo, B. (1997). Organic geochemical studies of sinking particulate material in China sea area II. *Chinese Science Bulletin*, *42*(22), 1894–1898. https://doi.org/10.1007/BF02882785
Dubinsky, Z., Stambler, N., Ben-Zion, M., McCloskey, L. R., Muscatine, L., & Falkowski, P. G. (1990). The effect of external nutrient resources on the optical properties and photosynthetic efficiency of Stylophora pistillata. *Proceedings of the Royal Society B: Biological Sciences*, *239*(1295), 231–246. https://doi.org/10.1098/rspb.1990.0015
Dunn, S. R., Thomas, M. C., Nette, G. W., & Dove, S. G. (2012). A Lipidomic Approach to Understanding Free Fatty Acid Lipogenesis Derived from Dissolved Inorganic Carbon within Cnidarian-Dinoflagellate Symbiosis. *PLoS ONE*, *7*(10), 46801. https://doi.org/10.1371/journal.pone.0046801

Durand, M. D., & Olson, R. J. (1996). Contributions of phytoplankton light scattering and cell concentration changes to diel variations in beam attenuation in the equatorial pacific from flow cytometric measurements of pico-, ultra and nanoplankton. *Deep-Sea Research Part II: Topical Studies in Oceanography*, *43*(4–6), 891–906. https://doi.org/10.1016/0967-0645(96)00020-3

Edmunds, P. J. (2020). *Moorea Coral Reef LTER 2020 MCR LTER: Coral reef: Long- term population and community dynamics: Corals, ongoing since 2005*.

Ezzat, L., Fine, M., Maguer, J. F., Grover, R., & Ferrier-Pagès, C. (2017). Carbon and nitrogen acquisition in shallow and deep holobionts of the scleractinian coral S. pistillata. *Frontiers in Marine Science*, *4*(APR). https://doi.org/10.3389/fmars.2017.00102

Falkowski, P. G., Dubinsky, Z., Muscatine, L., & Porter, J. W. (1984). Light and the Bioenergetics of a Symbiotic Coral. *BioScience*, *34*(11), 705–709. https://doi.org/10.2307/1309663

Ferrier-Pagès, C., & Gattuso, J. P. (1998). Biomass, production and grazing rates of pico- and nanoplankton in coral reef waters (Miyako Island, Japan). *Microbial Ecology*, *35*(1), 46–57. https://doi.org/10.1007/s002489900059

Ferrier-Pagès, C., Martinez, S., Grover, R., Cybulski, J., Shemesh, E., & Tchernov, D. (2021). Tracing the trophic plasticity of the coral-dinoflagellate symbiosis using amino acid compound-specific stable isotope analysis. *Microorganisms*, *9*(1), 1–16. https://doi.org/10.3390/microorganisms9010182

Ferrier-Pagès, C., Witting, J., Tambutté, E., & Sebens, K. P. (2003). Effect of natural zooplankton feeding on the tissue and skeletal growth of the scleractinian coral Stylophora pistillata. *Coral Reefs*, *22*(3), 229–240. https://doi.org/10.1007/s00338-003-0312-7

Fey, P., Parravicini, V., Bănaru, D., Dierking, J., Galzin, R., Lebreton, B., Meziane, T., Polunin, N. V. C., Zubia, M., & Letourneur, Y. (2021). Multi-trophic markers illuminate the understanding of the functioning of a remote, low coral cover Marquesan coral reef food web. *Scientific Reports*, *11*(1), 1–14. https://doi.org/10.1038/s41598-021-00348-w

Field, C. B., Behrenfeld, M. J., Randerson, J. T., & Falkowski, P. (1998). Primary production of the biosphere: Integrating terrestrial and oceanic components. *Science*, *281*(5374), 237–240. https://doi.org/10.1126/science.281.5374.237

Flombaum, P., Gallegos, J. L., Gordillo, R. A., Rincón, J., Zabala, L. L., Jiao, N., Karl, D. M., Li, W. K. W., Lomas, M. W., Veneziano, D., Vera, C. S., Vrugt, J. A., & Martiny, A. C. (2013). Present and future global distributions of the marine Cyanobacteria Prochlorococcus and Synechococcus. *Proceedings of the National Academy of Sciences of the United States of America*, *110*(24), 9824–9829. https://doi.org/10.1073/pnas.1307701110

Folch, J., Lees, M., & Sloane Stanley, G. . (1957). A Simple Method for the Isolation and Purification of Total Lipides from Animal Tissues. *Journal of Biological Chemistry*, *55*(5), 999–1033.

Fox, M. D., Guillaume-Castel, R., Edwards, C. ., Glanz, J., Gove, J. ., Green, J. A. M., Juhlin, E., Smith, J. E., & Williams, G. J. (n.d.). Ocean currents magnify upwelling and deliver nutritional subsidies to reef-building corals during El Niño heatwaves. *Science Advances*.

Fox, M. D., Smith, E. A., Smith, J. E., & Newsome, S. D. (2019). Trophic plasticity in a common reef-building coral: Insights from d13C analysis of essential amino acids. *Functional Ecology*, *August*, 1–12. https://doi.org/10.1111/1365-2435.13441

Fox, M. D., Williams, G. J., Johnson, M. D., Radice, V. Z., Zgliczynski, B. J., Kelly, E. L. A., Rohwer, F. L., Sandin, S. A., & Smith, J. E. (2018). Gradients in Primary Production Predict Trophic Strategies of Mixotrophic Corals across Spatial Scales. *Current Biology*, *28*(21), 3355-3363.e4. https://doi.org/10.1016/j.cub.2018.08.057

Fry, B. (2006). Stable Isotope Ecology. In *Springer-Verlag New York, New York, NY Fry*. https://doi.org/10.1016/b978-0-12-409548-9.10915-7

Fu, M., Qu, Q., Yang, X., & Zhang, X. (2016). Effect of intermittent oven drying on lipid oxidation, fatty acids composition and antioxidant activities of walnut. *Lwt*, *65*, 1126–1132. https://doi.org/10.1016/j.lwt.2015.10.002

Galloway, A. W. E., & Budge, S. M. (2020). The critical importance of experimentation in biomarker-based trophic ecology. *Philosophical Transactions of the Royal Society B: Biological Sciences*, *375*(1804). https://doi.org/10.1098/rstb.2019.0638

Goreau, T. F., Goreau, N. I., & Yonge, C. M. (1971). Reef Corals: Autotrophs or Heterotrophs? *The Biological Bulletin*, *141*, 247–260.

Graeve, M., Kattner, G., & Piepenburg, D. (1997). Lipids in arctic benthos: Does the fatty acid and alcohol composition reflect feeding and trophic interactions? *Polar Biology*, *18*(1), 53–61. https://doi.org/10.1007/s003000050158

Grande, K. D., Williams, P. J. L. B., Marra, J., Purdie, D. A., Heinemann, K., Eppley, R. W., & Bender, M. L. (1989). Primary production in the North Pacific gyre: a comparison of rates determined by the 14 C, O 2 concentration and 18 O methods. *Deep Sea Research Part A, Oceanographic Research Papers*, *36*(11), 1621–1634. https://doi.org/10.1016/0198-0149(89)90063-0

Grottoli, A. G. (2002). Effect of light and brine shrimp on skeletal δ13C in the Hawaiian coral Porites compressa: A tank experiment. *Geochimica et Cosmochimica Acta*, *66*(11), 1955–1967. https://doi.org/10.1016/S0016-7037(01)00901-2

Grottoli, A. G., Rodrigues, L. J., & Palardy, J. E. (2006). Heterotrophic plasticity and resilience in bleached corals. *Nature*, *440*(7088), 1186–1189. https://doi.org/10.1038/nature04565

Grottoli, A. G., Warner, M. E., Levas, S. J., Aschaffenburg, M. D., Schoepf, V., Mcginley, M., Baumann, J., & Matsui, Y. (2014). The cumulative impact of annual coral bleaching can turn some coral species winners into losers. *Global Change Biology*, *20*(12), 3823–3833. https://doi.org/10.1111/gcb.12658

Gschwend, P., Zafiriou, O. C., & Gagosian, R. B. (1980). Volatile organic compounds in seawater from the Peru upwelling region. *Limnology and Oceanography*, *25*(6), 1044–1053. https://aslopubs.onlinelibrary.wiley.com/doi/pdf/10.4319/lo.1980.25.6.1044

Guenther, A. B., Jiang, X., Heald, C. L., Sakulyanontvittaya, T., Duhl, T., Emmons, L. K., & Wang, X. (2012). The model of emissions of gases and aerosols from nature version 2.1 (MEGAN2.1): An extended and updated framework for modeling biogenic emissions. *Geoscientific Model Development*, *5*(6), 1471–1492. https://doi.org/10.5194/gmd-5-1471-2012

Guerrero, A. I., & Rogers, T. L. (2020). Evaluating the performance of the Bayesian mixing tool MixSIAR with fatty acid data for quantitative estimation of diet. *Scientific Reports*, *10*(1), 1–14. https://doi.org/10.1038/s41598-020-77396-1

Gustafsson, M. S. M., Baird, M. E., & Ralph, P. J. (2013). The interchangeability of autotrophic and heterotrophic nitrogen sources in Scleractinian coral symbiotic relationships: A numerical study. *Ecological Modelling*, *250*, 183–194. https://doi.org/10.1016/j.ecolmodel.2012.11.003

Hamner, W. M., Colin, P. L., & Hamner, P. P. (2007). Export-import dynamics of zooplankton on a coral reef in Palau. *Marine Ecology Progress Series*, *334*, 83–92. https://doi.org/10.3354/meps334083

Han, J., McCarthy, E. D., Hoeven, W. V., Calvin, M., & Bradley, W. H. (1968). Organic Geochemical Studies II. A Preliminary Report On The Distribution of Aliphatic Hydrocarbons in Algae, in Bacteria, and in Recent Lake Sediment. *Proceedings of the National Academy of Sciences*, *59*(1), 29–33. https://doi.org/10.1073/pnas.59.1.29

Happel, A., Stratton, L., Kolb, C., Hays, C., Rinchard, J., & Czesny, S. (2016). Evaluating quantitative fatty acid signature analysis (QFASA) in fish using controlled feeding experiments. *Canadian Journal of Fisheries and Aquatic Sciences*, *73*(8), 1222–1229. https://doi.org/10.1139/cjfas-2015-0328

Hédouin, L., Rouzé, H., Berthe, C., Perez-Rosales, G., Martinez, E., Chancerelle, Y., Galand, P. E., Lerouvreur, F., Nugues, M. M., Pochon, X., Siu, G., Steneck, R., & Planes, S. (2020). Contrasting patterns of mortality in Polynesian coral reefs following the third global coral bleaching event in 2016. *Coral Reefs*, *39*(4), 939–952. https://doi.org/10.1007/s00338-020-01914-w

Hench, J. L., Leichter, J. J., & Monismith, S. G. (2008). Episodic circulation and exchange in a wave-driven coral reef and lagoon system. *Limnology and Oceanography*, *53*(6), 2681–2694. https://doi.org/10.4319/lo.2008.53.6.2681

Hixson, S. M., Parrish, C. C., & Anderson, D. M. (2013). Effect of replacement of fish oil with camelina (Camelina sativa) oil on growth, lipid class and fatty acid composition of farmed juvenile Atlantic cod (Gadus morhua). *Fish Physiology and Biochemistry*, *39*(6), 1441–1456. https://doi.org/10.1007/s10695-013-9798-2

Hoegh-Guldberg, O. (1999). Climate change, coral bleaching and the future of the world's coral reefs. *Marine and Freshwater Research*, *50*(8), 839–866. https://doi.org/10.1071/MF99078

Hoogenboom, M., Rottier, C., Sikorski, S., & Ferrier-Pagès, C. (2015). Among-species variation in the energy budgets of reef-building corals: Scaling from coral polyps to communities. *Journal of Experimental Biology*, *218*(24), 3866–3877. https://doi.org/10.1242/jeb.124396

Houlbrèque, F., & Ferrier-Pagès, C. (2009). Heterotrophy in tropical scleractinian corals. In *Biological Reviews* (Vol. 84, Issue 1, pp. 1–17). Wiley/Blackwell (10.1111). https://doi.org/10.1111/j.1469-185X.2008.00058.x

Houlbrèque, F., Tambutté, E., & Ferrier-Pagès, C. (2003). Effect of zooplankton availability on the rates of photosynthesis, and tissue and skeletal growth in the scleractinian coral Stylophora pistillata. *Journal of Experimental Marine Biology and Ecology*, *296*(2), 145–166. https://doi.org/10.1016/S0022-0981(03)00259-4

Hughes, A. D., & Grottoli, A. G. (2013). Heterotrophic compensation: A possible mechanism for resilience of coral reefs to global warming or a sign of prolonged stress? *PLoS ONE*, *8*(11), 1–10. https://doi.org/10.1371/journal.pone.0081172

Hughes, A. D., Grottoli, A. G., Pease, T. K., & Matsui, Y. (2010). Acquisition and assimilation of carbon in non-bleached and bleached corals. *Marine Ecology Progress*

Series, *420*(2), 91–101. https://doi.org/10.3354/meps08866
Hughes, T. P., Anderson, K. D., Connolly, S. R., Heron, S. F., Kerry, J. T., Lough, J. M., Baird, A. H., Baum, J. K., Berumen, M. L., Bridge, T. C., Claar, D. C., Eakin, C. M., Gilmour, J. P., Graham, N. A. J., Harrison, H., Hobbs, J. P. A., Hoey, A. S., Hoogenboom, M., Lowe, R. J., … Wilson, S. K. (2018). Spatial and temporal patterns of mass bleaching of corals in the Anthropocene. *Science*, *359*(6371), 80–83. https://doi.org/10.1126/science.aan8048
Imbs, A. B., Demidkova, D. A., Latypov, Y. Y., & Pham, L. Q. (2007). Application of fatty acids for chemotaxonomy of reef-building corals. *Lipids*, *42*(11), 1035–1046. https://doi.org/10.1007/s11745-007-3109-6
Imbs, A. B., Latyshev, N. A., Dautova, T. N., & Latypov, Y. Y. (2010). Distribution of lipids and fatty acids in corals by their taxonomic position and presence of zooxanthellae. *Marine Ecology Progress Series*, *409*(Meyers 1979), 65–75. https://doi.org/10.3354/meps08622
Imbs, A. B., Yakovleva, I. M., Latyshev, N. A., & Pham, L. Q. (2010). Biosynthesis of polyunsaturated fatty acids in zooxanthellae and polyps of corals. *Russian Journal of Marine Biology*, *36*(6), 452–457. https://doi.org/10.1134/S1063074010060076
Ingemansson, T., Kaufmann, P., & Ekstrand, B. (1995). Multivariate Evaluation of Lipid Hydrolysis and Oxidation Data from Light and Dark Muscle of Frozen Stored Rainbow Trout (Oncorhynchus mykiss). *Journal of Agricultural and Food Chemistry*, *43*(8), 2046–2052. https://doi.org/10.1021/jf00056a017
Iverson, S. J., Field, C., Bowen, W. D., & Blanchard, W. (2004). Quantitative fatty acid signature analysis: A new method of estimating predator diets. *Ecological Monographs*, *74*(2), 211–235. https://doi.org/10.1890/02-4105
James, A. K., Washburn, L., Gotschalk, C., Maritorena, S., Alldredge, A., Nelson, C. E., Hench, J. L., Leichter, J. J., Wyatt, A. S. J., & Carlson, C. A. (2020). An Island Mass Effect Resolved Near Mo'orea, French Polynesia. *Frontiers in Marine Science*, *7*(January), 1–13. https://doi.org/10.3389/fmars.2020.00016
Jeffrey, S. W., & Humphrey, G. F. (1975). New spectrophotometric equations for determining chlorophylls a, b, c1 and c2 in higher plants, algae and natural phytoplankton. *Biochemie Und Physiologie Der Pflanzen*. https://doi.org/10.1016/s0015-3796(17)30778-3
Johannes, A. R. E., Alberts, J., Elia, C. D., Kinzie, R. A., Pomeroy, L. R., Sottile, W., Wiebe, W., Marsh, J. A., Helfrich, P., Maragos, J., Meyer, J., Smith, S., Crabtree, D., Roth, A., Mccloskey, L. R., Betzer, S., Marshall, N., Pilson, M. E. Q., Telek, G., … Wells, J. M. (1972). The Metabolism of Some Coral Reef Communities: A Team Study of Nutrient and Energy Flux at Eniwetok Author(s): *BioScience*, *22*, 541–543.
Johnson, Z. I., Zinser, E. R., Coe, A., McNulty, N. P., Woodward, E. M. S., & Chisholm, S. W. (2006). Niche partitioning among Prochlorococcus ecotypes along ocean-scale environmental gradients. *Science*, *311*(5768), 1737–1740. https://doi.org/10.1126/science.1118052
Jokiel, P. L., Maragos, J. E., & Franzisket, L. (1978). Coral growth: buoyant weight technique. *Coral Reefs: Research Methods*, 529–541.
Jones, A., & Berkelmans, R. (2010). Potential costs of acclimatization to a warmer climate: Growth of a reef coral with heat tolerant vs. sensitive symbiont types. *PLoS ONE*, *5*(5). https://doi.org/10.1371/journal.pone.0010437

Jones, A. M., Berkelmans, R., Van Oppen, M. J. H., Mieog, J. C., & Sinclair, W. (2008). A community change in the algal endosymbionts of a scleractinian coral following a natural bleaching event: Field evidence of acclimatization. *Proceedings of the Royal Society B: Biological Sciences*, *275*(1641), 1359–1365. https://doi.org/10.1098/rspb.2008.0069

Karl, D. M., & Church, M. J. (2014). Microbial oceanography and the Hawaii Ocean Time-series programme. In *Nature Reviews Microbiology* (Vol. 12, Issue 10, pp. 699–713). https://doi.org/10.1038/nrmicro3333

Karl, D. M., & Church, M. J. (2017). Ecosystem Structure and Dynamics in the North Pacific Subtropical Gyre: New Views of an Old Ocean. *Ecosystems*, *20*(3), 433–457. https://doi.org/10.1007/s10021-017-0117-0

Kim, T., Baker, D. M., Ju, S. J., & Lee, J. C. Y. (2021). Fatty acid profiles of separated host–symbiont fractions from five symbiotic corals: applications of chemotaxonomic and trophic biomarkers. *Marine Biology*, *168*(11), 1–13. https://doi.org/10.1007/s00227-021-03979-9

Kim, T., Lee, J. C. Y., Kang, D.-H., Duprey, N. N., Leung, K. S., Archana, A., & Baker, D. M. (2021). Modification of fatty acid profile and biosynthetic pathway in symbiotic corals under eutrophication. *Science of The Total Environment*, *771*, 145336. https://doi.org/10.1016/j.scitotenv.2021.145336

Knoot, C. J., & Pakrasi, H. B. (2019). Diverse hydrocarbon biosynthetic enzymes can substitute for olefin synthase in the cyanobacterium Synechococcus sp. PCC 7002. *Scientific Reports*, *9*(1). https://doi.org/10.1038/s41598-018-38124-y

Krueger, T., Bodin, J., Horwitz, N., Loussert-Fonta, C., Sakr, A., Escrig, S., Fine, M., & Meibom, A. (2018). Temperature and feeding induce tissue level changes in autotrophic and heterotrophic nutrient allocation in the coral symbiosis – A NanoSIMS study. *Scientific Reports*, *8*(1), 12710. https://doi.org/10.1038/s41598-018-31094-1

Krueger, T., Horwitz, N., Bodin, J., Giovani, M.-E., Escrig, S., Meibom, A., & Fine, M. (2017). Common reef-building coral in the Northern Red Sea resistant to elevated temperature and acidification. *Royal Society Open Science*, *4*(5), 170038. https://doi.org/10.1098/rsos.170038

Lea-Smith, D. J., Biller, S. J., Davey, M. P., Cotton, C. A. R., Sepulveda, B. M. P., Turchyn, A. V, Scanlan, D. J., Smith, A. G., Chisholm, S. W., & Howe, C. J. (2015). Contribution of cyanobacterial alkane production to the ocean hydrocarbon cycle. *Proceedings of the National Academy of Sciences of the United States of America*, *112*(44), 13591–13596. https://doi.org/10.1073/pnas.1507274112

Lea-Smith, D. J., Ortiz-Suarez, M. L., Lenn, T., Nürnberg, D. J., Baers, L. L., Davey, M. P., Parolini, L., Huber, R. G., Cotton, C. A. R., Mastroianni, G., Bombelli, P., Ungerer, P., Stevens, T. J., Smith, A. G., Bond, P. J., Mullineaux, C. W., & Howe, C. J. (2016). Hydrocarbons are essential for optimal cell size, division, and growth of Cyanobacteria. *Plant Physiology*, *172*(3), 1928–1940. https://doi.org/10.1104/pp.16.01205

Leal, M. C., Ferrier-Pagès, C., Calado, R., Thompson, M. E., Frischer, M. E., & Nejstgaard, J. C. (2014). Coral feeding on microalgae assessed with molecular trophic markers. *Molecular Ecology*, *23*(15), 3870–3876. https://doi.org/10.1111/mec.12486

Leal, M. C., Hoadley, K., Pettay, D. T., Grajales, A., Calado, R., & Warner, M. E. (2015). Symbiont type influences trophic plasticity of a model cnidarian-dinoflagellate symbiosis. *Journal of Experimental Biology*, *218*(6), 858–863.

https://doi.org/10.1242/jeb.115519
Leichter, J. J., Alldredge, A., Bernardi, G., Brooks, A. J., Carlson, C. A., Carpenter, R. C., Edmunds, P. J., Fewings, M. R., Hanson, K. M., Hench, J. L., Holbrook, S. J., Nelson, C. E., Schmitt, R. J., Toonen, R. J., Washburn, L., & Wyatt, A. S. J. (2013). Biological and Physical Interactions on a Tropical Island Coral Reef. *Oceanography*, *26*(3), 51–63.
Leichter, J. J., & Genovese, S. J. (2006). Intermittent upwelling and subsidized growth of the scleractinian coral Madracis mirabilis on the deep fore-reef slope of Discovery Bay, Jamaica. *Marine Ecology Progress Series*, *316*(October), 95–103. https://doi.org/10.3354/meps316095
Leinbach, S. E., Speare, K. E., Rossin, A. M., Holstein, D. M., & Strader, M. E. (2021). Energetic and reproductive costs of coral recovery in divergent bleaching responses. *Scientific Reports 2021 11:1*, *11*(1), 1–10. https://doi.org/10.1038/s41598-021-02807-w
Leinbach, S. E., Speare, K. E., & Strader, M. E. (2022). Reef habitats structure symbiotic microalgal assemblages in corals and contribute to differential heat stress responses. *Coral Reefs*, *42*(1), 205–217. https://doi.org/10.1007/s00338-022-02316-w
Lesser, M. P. (2006). Oxidative stress in marine environments: Biochemistry and physiological ecology. *Annual Review of Physiology*, *68*(3), 253–278. https://doi.org/10.1146/annurev.physiol.68.040104.110001
Levitus, S., Antonov, J., & Boyer, T. (2005). Warming of the world ocean, 1955-2003. *Geophysical Research Letters*, *32*(2), 1–4. https://doi.org/10.1029/2004GL021592
Li, X., del Cardayre, S. B., Popova, E., Schirmer, A., & Rude, M. A. (2010). Microbial Biosynthesis of Alkanes. *Science*, *329*(5991), 559–562. https://doi.org/10.1126/science.1187936
Liu, H. B., Campbell, L., & Landry, M. R. (1995). Growth and mortality rates of Prochlorococcus and Synechococcus measured with a selective inhibitor technique. *Marine Ecology Progress Series*, *116*(1–3), 277–288. https://doi.org/10.3354/meps116277
Lomas, M. W., Steinberg, D. K., Dickey, T., Carlson, C. A., Nelson, N. B., Condon, R. H., & Bates, N. R. (2010). Increased ocean carbon export in the Sargasso Sea linked to climate variability is countered by its enhanced mesopelagic attenuation. *Biogeosciences*, *7*(1), 57–70. https://doi.org/10.5194/bg-7-57-2010
López-Sandoval, D. C., Delgado-Huertas, A., & Agustí, S. (2018). The 13 C method as a robust alternative to 14 C-based measurements of primary productivity in the Mediterranean Sea. *Journal of Plankton Research*, *40*(5), 544–554. https://doi.org/10.1093/plankt/fby031
Love, C. R., Arrington, E. C., Gosselin, K. M., Reddy, C. M., Van Mooy, B. A. S., Nelson, R. K., & Valentine, D. L. (2021). Microbial production and consumption of hydrocarbons in the global ocean. *Nature Microbiology*, *6*(4), 489–498. https://doi.org/10.1038/s41564-020-00859-8
Lyman, J. M., Good, S. A., Gouretski, V. V., Ishii, M., Johnson, G. C., Palmer, M. D., Smith, D. M., & Willis, J. K. (2010). Robust warming of the global upper ocean. *Nature*, *465*(7296), 334–337. https://doi.org/10.1038/nature09043
Madgett, A. S., Yates, K., Webster, L., McKenzie, C., & Moffat, C. F. (2019). Understanding marine food web dynamics using fatty acid signatures and stable isotope ratios: Improving contaminant impacts assessments across trophic levels. *Estuarine,*

Coastal and Shelf Science, *227*(July), 106327. https://doi.org/10.1016/j.ecss.2019.106327

Mann, E. L., & Chisholm, S. W. (2000). Iron limits the cell division rate of Prochlorococcus in the eastern equatorial Pacific. *Limnology and Oceanography*, *45*(5), 1067–1076. https://doi.org/10.4319/lo.2000.45.5.1067

Martinez, S., Grover, R., Baker, D. M., & Ferrier-Pagès, C. (2022). Symbiodiniaceae Are the First Site of Heterotrophic Nitrogen Assimilation in Reef-Building Corals. *MBio*, *13*(5), e0160122. https://doi.org/10.1128/mbio.01601-22

Martiny, A. C., Kathuria, S., & Berube, P. M. (2009). Widespread metabolic potential for nitrite and nitrate assimilation among Prochlorococcus ecotypes. *Proceedings of the National Academy of Sciences of the United States of America*, *106*(26), 10787–10792. https://doi.org/10.1073/pnas.0902532106

Matthews, J. L., Sproles, A. E., Oakley, C. A., Grossman, A. R., Weis, V. M., & Davy, S. K. (2016). Menthol-induced bleaching rapidly and effectively provides experimental aposymbiotic sea anemones (Aiptasia sp.) for symbiosis investigations. *Journal of Experimental Biology*, *219*(3), 306–310. https://doi.org/10.1242/jeb.128934

Maynard, J. A., Anthony, K. R. N., Marshall, P. A., & Masiri, I. (2008). Major bleaching events can lead to increased thermal tolerance in corals. *Marine Biology*, *155*(2), 173–182. https://doi.org/10.1007/s00227-008-1015-y

McGenity, T. J., Crombie, A. T., & Murrell, J. C. (2018). Microbial cycling of isoprene, the most abundantly produced biological volatile organic compound on Earth. *ISME Journal*, *12*(4), 931–941. https://doi.org/10.1038/s41396-018-0072-6

Mieog, J. C., Olsen, J. L., Berkelmans, R., Bleuler-Martinez, S. A., Willis, B. L., & van Oppen, M. J. H. (2009). The roles and interactions of symbiont, host and environment in defining coral fitness. *PLoS ONE*, *4*(7). https://doi.org/10.1371/journal.pone.0006364

Mies, M., Güth, A. Z., Tenório, A. A., Banha, T. N. S., Waters, L. G., Polito, P. S., Taniguchi, S., Bícego, M. C., & Sumida, P. Y. G. (2018). In situ shifts of predominance between autotrophic and heterotrophic feeding in the reef-building coral Mussismilia hispida: an approach using fatty acid trophic markers. *Coral Reefs*, *37*(3), 677–689. https://doi.org/10.1007/s00338-018-1692-z

Mills, M. M., Lipschultz, F., & Sebens, K. P. (2004). Particulate matter ingestion and associated nitrogen uptake by four species of scleractinian corals. *Coral Reefs*, *23*(3), 311–323. https://doi.org/10.1007/s00338-004-0380-3

Mills, M. M., & Sebens, K. P. (2004). Ingestion and assimilation of nitrogen from benthic sediments by three species of coral. *Marine Biology*, *145*(6), 1097–1106. https://doi.org/10.1007/s00227-004-1398-3

Mocking, R. J. T., Assies, J., Lok, A., Ruhé, H. G., Koeter, M. W. J., Visser, I., Bockting, C. L. H., & Schene, A. H. (2012). Statistical methodological issues in handling of fatty acid data: Percentage or concentration, imputation and indices. *Lipids*, *47*(5), 541–547. https://doi.org/10.1007/s11745-012-3665-2

Monismith, S. G., Herdman, L. M. M., Ahmerkamp, S., & Hench, J. L. (2013). Wave transformation and wave-driven flow across a steep coral reef. *Journal of Physical Oceanography*, *43*(7), 1356–1379. https://doi.org/10.1175/JPO-D-12-0164.1

Monroig, Ó., Tocher, D. R., & Navarro, J. C. (2013). Biosynthesis of polyunsaturated fatty acids in marine invertebrates: Recent advances in molecular mechanisms. *Marine*

Drugs, *11*(10), 3998–4018. https://doi.org/10.3390/md11103998
Muscatine, L. (1973). Nutrition of Corals. *Biology and Geology of Coral Reefs*, *2*, 77–115.
Muscatine, L., & Porter, J. W. (1977). Reef Corals: Mutualistic Symbioses Adapted to Nutrient-Poor Environments. *BioScience*, *27*(7), 454–460. https://doi.org/10.2307/1297526
Muscatine, L., Porter, J. W., & Kaplan, I. R. (1989). Resource partitioning by reef corals as determined from stable isotope composition - I. δ 13 C of zooxanthellae and animal tissue vs depth. *Marine Biology*, *100*(2), 185–193. https://doi.org/10.1007/BF00391957
N., P. M., H., V., M., H., M., S., A., S. H., & A., Y. S. M. (2011). Biometrical characters of Artemia from four Iranian regions. *Iranian Journal of Fisheries Sciences*, *10*(2), 293–303.
Nakamura, T., & Van Woesik, R. (2001). Water-flow rates and passive diffusion partially explain differential survival of corals during the 1998 bleaching event. *Marine Ecology Progress Series*, *212*(2), 301–304. https://doi.org/10.3354/meps212301
National Research Council. (2003). *Oil in the Sea III*. https://doi.org/10.17226/10388
Nazemroaya, S., Sahari, M., & Rezaei, M. (2011). Identification of fatty acid in mackerel (Scomberomorus commersoni) and shark (Carcharhinus dussumieri) fillets and their changes during six month of frozen storage at -18°C. *Journal of Agriculture Science and Technology*, *13*, 553–566.
Neall, V. E., & Trewick, S. A. (2008). Review. The age and origin of the Pacific islands: A geological overview. *Philosophical Transactions of the Royal Society B: Biological Sciences*, *363*(1508), 3293–3308. https://doi.org/10.1098/rstb.2008.0119
Nelson, C. E., Alldredge, A. L., McCliment, E. A., Amaral-Zettler, L. A., & Carlson, C. A. (2011). Depleted dissolved organic carbon and distinct bacterial communities in the water column of a rapid-flushing coral reef ecosystem. *ISME Journal*, *5*(8), 1374–1387. https://doi.org/10.1038/ismej.2011.12
Neubauer, P., & Jensen, O. P. (2015). Bayesian estimation of predator diet composition fromfatty acids and stable isotopes. *PeerJ*, *2015*(3), 1–19. https://doi.org/10.7717/peerj.920
Newsome, S. D., Martinez del Rio, C., Bearshop, S., & Phillips, D. L. (2007). A niche for isotopic ecology. *Frontiers in Ecology and the Environment*, *5*(8), 429–436. https://doi.org/10.1890/060150.01
Nie, Y., Chi, C. Q., Fang, H., Liang, J. L., Lu, S. L., Lai, G. L., Tang, Y. Q., & Wu, X. L. (2014). Diverse alkane hydroxylase genes in microorganisms and environments. *Scientific Reports*, *4*(4968). https://doi.org/10.1038/srep04968
Odum, H., & Odum, E. (1955). Trophic structure and productivity of a windward coral reef community on Eniwetok Atoll. *Ecological Monographs*, *25*, 291–320.
Papina, M., Meziane, T., & Woesik, R. van. (2003). Symbiotic zooxanthellae provide the host-coral Montipora digitata with polyunsaturated fatty acids. *Comaparative Biochemist and Physiology*, *135*, 493–502. https://doi.org/10.1016/S1096-4959
Patten, N. L., Wyatt, A. S. J., Lowe, R. J., & Waite, A. M. (2011). Uptake of picophytoplankton, bacterioplankton and virioplankton by a fringing coral reef community (Ningaloo Reef, Australia). *Coral Reefs*, *30*(3), 555–567. https://doi.org/10.1007/s00338-011-0777-8
Penin, L., Adjeroud, M., Schrimm, M., & Lenihan, H. S. (2007). High spatial variability in coral bleaching around Moorea (French Polynesia): patterns across locations and water

depths. *Comptes Rendus - Biologies*, *330*(2), 171–181. https://doi.org/10.1016/j.crvi.2006.12.003

Pethybridge, H. R., Choy, C. A., Polovina, J. J., & Fulton, E. A. (2018). Improving Marine Ecosystem Models with Biochemical Tracers. *Annual Review of Marine Science*, *10*(1), 199–228. https://doi.org/10.1146/annurev-marine-121916-063256

Petillo, D., Hultin, H. O., Krzynowek, J., & Autio, W. R. (1998). Kinetics of Antioxidant Loss in Mackerel Light and Dark Muscle. *Journal of Agricultural and Food Chemistry*, *46*(10), 4128–4137. https://doi.org/10.1021/jf980364z

Polovina, J. J., Howell, E. A., & Abecassis, M. (2008). Ocean's least productive waters are expanding. *Geophysical Research Letters*, *35*(3), 2–6. https://doi.org/10.1029/2007GL031745

Post, D. M. (2002). Using Stable Isotopes to Estimate Trophic Position: Models, Methods, and Assumptions. *Ecology*, *83*(3), 703. https://doi.org/10.2307/3071875

Price, J. T., McLachlan, R. H., Jury, C. P., Toonen, R. J., & Grottoli, A. G. (2021). Isotopic approaches to estimating the contribution of heterotrophic sources to Hawaiian corals. *Limnology and Oceanography*, *66*(6), 2393–2407. https://doi.org/10.1002/lno.11760

Prince, R. C., Amande, T. J., & McGenity, T. J. (2018). Prokaryotic Hydrocarbon Degraders. In *Handbook of Hydrocarbon and Lipid Microbiology* (pp. 1–41). https://doi.org/10.1007/978-3-319-60053-6_15-1

Pupier, C. A., Mies, M., Fine, M., Bastos Francini-Filho, R., Pereira Brandini, F., Zambotti-Villela, L., Colepicolo, P., & Ferrier-Pagès, C. (2021). Lipid biomarkers reveal the trophic plasticity of octocorals along a depth gradient. *Limnology and Oceanography*, *66*(5), 2078–2087. https://doi.org/10.1002/lno.11746

Radice, V. Z., Brett, M. T., Fry, B., Fox, M. D., Hoegh-Guldberg, O., & Dove, S. G. (2019). Evaluating coral trophic strategies using fatty acid composition and indices. *PLoS ONE*, *14*(9). https://doi.org/10.1371/journal.pone.0222327

Radice, V. Z., Hoegh-Guldberg, O., Fry, B., Fox, M. D., & Dove, S. G. (2019). Upwelling as the major source of nitrogen for shallow and deep reef-building corals across an oceanic atoll system. *Functional Ecology*, *33*(6), 1120–1134. https://doi.org/10.1111/1365-2435.13314

Repeta, D. J., Ferrón, S., Sosa, O. A., Johnson, C. G., Repeta, L. D., Acker, M., Delong, E. F., & Karl, D. M. (2016). Marine methane paradox explained by bacterial degradation of dissolved organic matter. *Nature Geoscience*, *9*(12), 884–887. https://doi.org/10.1038/ngeo2837

Reshkin, S. J., & Knauer, G. A. (1979). Light stimulation of phosphate uptake in natural assemblages of phytoplankton. *Limnology and Oceanography*, *24*(6), 1121–1124. https://doi.org/10.4319/lo.1979.24.6.1121

Revel, J., Massi, L., Mehiri, M., Boutoute, M., Mayzaud, P., Capron, L., & Sabourault, C. (2016). Differential distribution of lipids in epidermis, gastrodermis and hosted Symbiodinium in the sea anemone Anemonia viridis. *Comparative Biochemistry and Physiology -Part A : Molecular and Integrative Physiology*, *191*, 140–151. https://doi.org/10.1016/j.cbpa.2015.10.017

Reynaud, S., Martinez, P., Houlbrèque, F., Billy, I., Allemand, D., & Ferrier-Pagès, C. (2009). Effect of light and feeding on the nitrogen isotopic composition of a zooxanthellate coral: Role of nitrogen recycling. *Marine Ecology Progress Series*, *392*, 103–110. https://doi.org/10.3354/meps08195

Ribalet, F., Swalwell, J., Clayton, S., Jiménez, V., Sudek, S., Lin, Y., Johnson, Z. I., Worden, A. Z., & Armbrust, E. V. (2015). Light-driven synchrony of Prochlorococcus growth and mortality in the subtropical Pacific gyre. *Proceedings of the National Academy of Sciences of the United States of America*, *112*(26), 8008–8012. https://doi.org/10.1073/pnas.1424279112

Richards, Z. T., & van Oppen, M. J. H. (2012). Rarity and genetic diversity in indo-pacific acropora corals. *Ecology and Evolution*, *2*(8), 1867–1888. https://doi.org/10.1002/ece3.304

Rudy, M. D., Kainz, M. J., Graeve, M., Colombo, S. M., & Arts, M. T. (2016). Handling and storage procedures have variable effects on fatty acid content in fishes with different lipid quantities. *PLoS ONE*, *11*(8). https://doi.org/10.1371/journal.pone.0160497

Safuan, C. D. M., Samshuri, M. A., Jaafar, S. N., Tan, C. H., & Bachok, Z. (2021). Physiological Response of Shallow-Water Hard Coral Acropora digitifera to Heat Stress via Fatty Acid Composition. *Frontiers in Marine Science*, *8*(September), 1–13. https://doi.org/10.3389/fmars.2021.715167

Saunois, M., R. Stavert, A., Poulter, B., Bousquet, P., G. Canadell, J., B. Jackson, R., A. Raymond, P., J. Dlugokencky, E., Houweling, S., K. Patra, P., Ciais, P., K. Arora, V., Bastviken, D., Bergamaschi, P., R. Blake, D., Brailsford, G., Bruhwiler, L., M. Carlson, K., Carrol, M., … Zhuang, Q. (2020). The global methane budget 2000-2017. *Earth System Science Data*, *12*(3), 1561–1623. https://doi.org/10.5194/essd-12-1561-2020

Schneider, C. A., Rasband, W. S., & Eliceiri, K. W. (2012). NIH Image to ImageJ: 25 years of image analysis. *Nature Methods*, *9*(7), 671–675. https://doi.org/10.1038/nmeth.2089

Schoepf, V., Grottoli, A. G., Levas, S. J., Aschaffenburg, M. D., Baumann, J. H., Matsui, Y., & Warner, M. E. (2015). Annual coral bleaching and the long-term recovery capacity of coral. *Proceedings of the Royal Society B: Biological Sciences*, *282*(1819). https://doi.org/10.1098/rspb.2015.1887

Schwiesow, M. W., Moreno Samayoa, A., Torres, J., Leimbach, A., Santiago-Rivera, G., & Tepper, C. S. (2021). Symbiodinium Distribution Patterns in Millepores in the Caribbean: South Water Cay, Belize and San Salvador, The Bahamas. *Marine Science*, *9*(1), 1–10. https://doi.org/10.5923/j.ms.20210901.01

Sebens, K. P., Witting, J., & Helmuth, B. (1997). Effects of water flow and branch spacing on particle capture by the reef coral Madracis mirabills (Duchassaing and Michelotti). *Journal of Experimental Marine Biology and Ecology*, *211*(1), 1–28. https://doi.org/10.1016/S0022-0981(96)02636-6

Seemann, J., Sawall, Y., Auel, H., & Richter, C. (2013). The use of lipids and fatty acids to measure the trophic plasticity of the coral stylophora subseriata. *Lipids*, *48*(3), 275–286. https://doi.org/10.1007/s11745-012-3747-1

Seifert, R., Delling, N., Richnow, H. H., Kempe, S., Hefter, J., & Michaelis, W. (1999). Ethylene and methane in the upper water column of the subtropical Atlantic. *Biogeochemistry*, *44*(1), 73–91. https://doi.org/10.1023/A:1006090917059

Skinner, C., Mill, A. C., Fox, M. D., Newman, S. P., Zhu, Y., Kuhl, A., & Polunin, N. V. C. (2021). Offshore pelagic subsidies dominate carbon inputs to coral reef predators. *Science Advances*, *7*(8). https://doi.org/10.1126/sciadv.abf3792

Sorokin, Y. I. (1991). Parameters of productivity and metabolism of coral reef ecosystems off central Vietnam. *Estuarine, Coastal and Shelf Science*, *33*(3), 259–280.

https://doi.org/10.1016/0272-7714(91)90056-H
Speare, K. E., Adam, T. C., Winslow, E. M., Lenihan, H. S., & Burkepile, D. E. (2022). Size-dependent mortality of corals during marine heatwave erodes recovery capacity of a coral reef. *Global Change Biology*, *28*(4), 1342–1358. https://doi.org/10.1111/gcb.16000
Stahl, A. (2021). *Identifying Novel Isotopic Tracers of Marine Primary Producers to Study Food Web Carbon Cycles* (Issue 1996).
Starzak, D. E., Quinnell, R. G., Nitschke, M. R., & Davy, S. K. (2014). The influence of symbiont type on photosynthetic carbon flux in a model cnidarian-dinoflagellate symbiosis. *Marine Biology*, *161*(3), 711–724. https://doi.org/10.1007/s00227-013-2372-8
Stat, M., & Gates, R. D. (2011). Clade D Symbiodinium in Scleractinian Corals: A "Nugget" of Hope, a Selfish Opportunist, an Ominous Sign, or All of the Above? *Journal of Marine Biology*, *2011*, 1–9. https://doi.org/10.1155/2011/730715
Stat, M., Morris, E., & Gates, R. D. (2008). Functional diversity in coral-dinoflagellate symbiosis. *Proceedings of the National Academy of Sciences of the United States of America*, *105*(27), 9256–9261. https://doi.org/10.1073/pnas.0801328105
Stimson, J., & Kinzie, R. A. (1991). The temporal pattern and rate of release of zooxanthellae from the reef coral Pocillopora damicornis (Linnaeus) under nitrogen-enrichment and control conditions. *Journal of Experimental Marine Biology and Ecology*, *153*(1), 63–74. https://doi.org/10.1016/S0022-0981(05)80006-1
Suggett, D. J., Warner, M. E., Smith, D. J., Davey, P., Hennige, S., & Baker, N. R. (2008). PHOTOSYNTHESIS AND PRODUCTION OF HYDROGEN PEROXIDE BY SYMBIODINIUM (PYRRHOPHYTA) PHYLOTYPES WITH DIFFERENT THERMAL TOLERANCES(1). *Journal of Phycology*, *44*(4), 948–956. https://doi.org/10.1111/j.1529-8817.2008.00537.x
Sunagawa, S., Coelho, L. P., Chaffron, S., Kultima, J. R., Labadie, K., Salazar, G., Djahanschiri, B., Zeller, G., Mende, D. R., Alberti, A., Cornejo-Castillo, F. M., Costea, P. I., Cruaud, C., D'Ovidio, F., Engelen, S., Ferrera, I., Gasol, J. M., Guidi, L., Hildebrand, F., … Bork, P. (2015). Structure and function of the global ocean microbiome. *Science*, *348*(6237). https://doi.org/10.1126/science.1261359
T. Banaszak, A., LaJeunesse, T. C., & Trench, R. K. (2000). The synthesis of mycosporine-like amino acids (MAAS) by cultured, symbiotic dinoflagellates. *Journal of Experimental Marine Biology and Ecology*, *249*(2), 219–233. https://doi.org/10.1016/S0022-0981(00)00192-1
Taipale, S., Strandberg, U., Peltomaa, E., Galloway, A. W. E., Ojala, A., & Brett, M. T. (2013). Fatty acid composition as biomarkers of freshwater microalgae: Analysis of 37 strains of microalgae in 22 genera and in seven classes. *Aquatic Microbial Ecology*, *71*(2), 165–178. https://doi.org/10.3354/ame01671
Tanaka, Y., Miyajima, T., Koike, I., Hayashibara, T., & Ogawa, H. (2006). Translocation and conservation of organic nitrogen within the coral-zooxanthella symbiotic system of Acropora pulchra, as demonstrated by dual isotope-labeling techniques. *Journal of Experimental Marine Biology and Ecology*, *336*(1), 110–119. https://doi.org/10.1016/j.jembe.2006.04.011
Tanaka, Y., Suzuki, A., & Sakai, K. (2018). The stoichiometry of coral-dinoflagellate symbiosis: Carbon and nitrogen cycles are balanced in the recycling and double

translocation system. *ISME Journal*, *12*(3), 860–868. https://doi.org/10.1038/s41396-017-0019-3

Teece, M. A., Estes, B., Gelsleichter, E., & Lirman, D. (2011). Heterotrophic and autotrophic assimilation of fatty acids by two scleractinian corals, montastraea faveolata and porites astreoides. *Limnology and Oceanography*, *56*(4), 1285–1296. https://doi.org/10.4319/lo.2011.56.4.1285

Thurber, A. R. (2007). Diets of Antarctic sponges: Links between the pelagic microbial loop and benthic metazoan food web. *Marine Ecology Progress Series*, *351*(January), 77–89. https://doi.org/10.3354/meps07122

Titlyanov, E. A., Titlyanova, T. V, Yamazato, K., & Woesik, R. Van. (2001). Journal of Experimental … 2001 Simon.pdf. *Journal of Experimental Marine Biology and Ecology*, *257*, 163–181.

Titlyanov, E., Bil', K., Fomina, I., Titlyanova, T., Leletkin, V., Eden, N., Malkin, A., & Dubinsky, Z. (2000). Effects of dissolved ammonium addition and host feeding with Artemia salina on photoacclimation of the hermatypic coral Stylophora pistillata. *Marine Biology*, *137*(3), 463–472. https://doi.org/10.1007/s002270000370

Tolosa, I., Treignier, C., Grover, R., & Ferrier-Pagès, C. (2011a). Impact of feeding and short-term temperature stress on the content and isotopic signature of fatty acids, sterols, and alcohols in the scleractinian coral Turbinaria reniformis. *Coral Reefs*, *30*(3), 763–774. https://doi.org/10.1007/s00338-011-0753-3

Tolosa, I., Treignier, C., Grover, R., & Ferrier-Pagès, C. (2011b). Impact of feeding and short-term temperature stress on the content and isotopic signature of fatty acids, sterols, and alcohols in the scleractinian coral Turbinaria reniformis. *Coral Reefs*, *30*(3), 763–774. https://doi.org/10.1007/s00338-011-0753-3

Treignier, C., Grover, R., Ferrier-Pagès, C., & Tolosa, I. (2008). Effect of light and feeding on the fatty acid and sterol composition of zooxanthellae and host tissue isolated from the scleractinian coral Turbinaria reniformis. *Limnology and Oceanography*, *53*(6), 2702–2710. https://doi.org/10.4319/lo.2008.53.6.2702

Tremblay, P., Gori, A., Maguer, J. F., Hoogenboom, M., & Ferrier-Pagès, C. (2016). Heterotrophy promotes the re-establishment of photosynthate translocation in a symbiotic coral after heat stress. *Scientific Reports*, *6*(December), 1–14. https://doi.org/10.1038/srep38112

Valentine, D. L., Mezić, I., Maćešić, S., Črnjarić-Žic, N., Ivić, S., Hogan, P. J., Fonoberov, V. A., & Loire, S. (2012). Dynamic autoinoculation and the microbial ecology of a deep water hydrocarbon irruption. In *Proceedings of the National Academy of Sciences of the United States of America* (Vol. 109, Issue 50, pp. 20286–20291). https://doi.org/10.1073/pnas.1108820109

Valentine, D. L., & Reddy, C. M. (2015). Latent hydrocarbons from cyanobacteria. *Proc. Nati. Acad. Sci. USA*, *112*(44), 13434–13435. https://doi.org/10.1073/pnas.1518485112

Van Mooy, B. A. S., Moutin, T., Duhamel, S., Rimmelin, P., & Van Wambeke, F. (2008). Phospholipid synthesis rates in the eastern subtropical South Pacific Ocean. *Biogeosciences*, *5*(1), 133–139. https://doi.org/10.5194/bg-5-133-2008

Van Oppen, M. J. H., Palstra, F. P., Piquet, A. M. T., & Miller, D. J. (2001). Patterns of coral-dinoflagellate associations in Acropora: Significance of local availability and physiology of Symbiodinium strains and host-symbiont selectivity. *Proceedings of the Royal Society B: Biological Sciences*, *268*(1478), 1759–1767.

https://doi.org/10.1098/rspb.2001.1733
Vaulot, D., Marie, D., Olson, R. J., & Chisholm, S. W. (1995). Growth of Prochlorococcus, a photosynthetic prokaryote, in the equatorial Pacific Ocean. *Science*, *268*(5216), 1480–1482. https://doi.org/10.1126/science.268.5216.1480
Venn, A. A., Loram, J. E., & Douglas, A. E. (2008). Photosynthetic symbioses in animals. *Journal of Experimental Botany*, *59*(5), 1069–1080. https://doi.org/10.1093/jxb/erm328
Veron, J. (2000). *Corals of the World: Australian Institute of Marine Sciences*.
Wall, C. B., Kaluhiokalani, M., Popp, B. N., Donahue, M. J., & Gates, R. D. (2020). Divergent symbiont communities determine the physiology and nutrition of a reef coral across a light-availability gradient. *ISME Journal*, *14*(4), 945–958. https://doi.org/10.1038/s41396-019-0570-1
Wall, C. B., Ritson-Williams, R., Popp, B. N., & Gates, R. D. (2019). Spatial variation in the biochemical and isotopic composition of corals during bleaching and recovery. *Limnology and Oceanography*, *64*(5), 2011–2028. https://doi.org/10.1002/lno.11166
Wall, C. B., Wallsgrove, N. J., Gates, R. D., & Popp, B. N. (2021). Amino acid δ13C and δ15N analyses reveal distinct species-specific patterns of trophic plasticity in a marine symbiosis. *Limnology and Oceanography*, *66*(5), 2033–2050. https://doi.org/10.1002/lno.11742
Wang, J. T., Chen, Y. Y., Tew, K. S., Meng, P. J., & Chen, C. A. (2012). Physiological and Biochemical Performances of Menthol-Induced Aposymbiotic Corals. *PLoS ONE*, *7*(9), 23–26. https://doi.org/10.1371/journal.pone.0046406
White, H. K., Marx, C. T., Valentine, D. L., Sharpless, C., Aeppli, C., Gosselin, K. M., Kivenson, V., Liu, R. M., Nelson, R. K., Sylva, S. P., & Reddy, C. M. (2019). Examining inputs of biogenic and oil-derived hydrocarbons in surface waters following the deepwater horizon oil spill. *ACS Earth and Space Chemistry*, *3*(7), 1329–1337. https://doi.org/10.1021/acsearthspacechem.9b00090
Williams, G. J., Sandin, S. A., Zgliczynski, B. J., Fox, M. D., Gove, J. M., Rogers, J. S., Furby, K. A., Hartmann, A. C., Caldwell, Z. R., Price, N. N., & Smith, J. E. (2018). Biophysical drivers of coral trophic depth zonation. *Marine Biology*, *165*(4). https://doi.org/10.1007/s00227-018-3314-2
Wyatt, A. S. J., Leichter, J. J., Washburn, L., Kui, L., Edmunds, P. J., & Burgess, S. C. (2023). Hidden heatwaves and severe coral bleaching linked to mesoscale eddies and thermocline dynamics. *Nature Communications*, *14*(1), 1–17. https://doi.org/10.1038/s41467-022-35550-5
Wyatt, A. S. J., Lowe, R. J., Humphries, S., & Waite, A. M. (2010). Particulate nutrient fluxes over a fringing coral reef: Relevant scales of phytoplankton Production and mechanisms of supply. *Marine Ecology Progress Series*, *405*(Hatcher 1997), 113–130. https://doi.org/10.3354/meps08508
Wyatt, A. S. J., Lowe, R. J., Humphries, S., & Waite, A. M. (2013). Particulate nutrient fluxes over a fringing coral reef: Source-sink dynamics inferred from carbon to nitrogen ratios and stable isotopes. *Limnology and Oceanography*, *58*(1), 409–427. https://doi.org/10.4319/lo.2013.58.1.0409
Xiang, T., Lehnert, E., Jinkerson, R. E., Clowez, S., Kim, R. G., DeNofrio, J. C., Pringle, J. R., & Grossman, A. R. (2020). Symbiont population control by host-symbiont metabolic interaction in Symbiodiniaceae-cnidarian associations. *Nature Communications*, *11*(1), 1–9. https://doi.org/10.1038/s41467-019-13963-z

Yakimov, M. M., Denaro, R., Genovese, M., Cappello, S., D'Auria, G., Chernikova, T. N., Timmis, K. N., Golyshin, P. N., & Giluliano, L. (2005). Natural microbial diversity in superficial sediments of Milazzo Harbor (Sicily) and community successions during microcosm enrichment with various hydrocarbons. *Environmental Microbiology*, *7*(9), 1426–1441. https://doi.org/10.1111/j.1462-5822.2005.00829.x

Yakimov, M. M., Timmis, K. N., & Golyshin, P. N. (2007). Obligate oil-degrading marine bacteria. In *Current Opinion in Biotechnology* (Vol. 18, Issue 3, pp. 257–266). https://doi.org/10.1016/j.copbio.2007.04.006

Yellowlees, D., Rees, T. A. V., & Leggat, W. (2008). Metabolic interactions between algal symbionts and invertebrate hosts. *Plant, Cell and Environment*, *31*(5), 679–694. https://doi.org/10.1111/j.1365-3040.2008.01802.x

Yetsko, K., Ross, M., Bellantuono, A., Merselis, D., Lanetty, M. R., & Gilg, M. R. (2020). Genetic differences in thermal tolerance among colonies of threatened coral Acropora cervicornis: Potential for adaptation to increasing temperature. *Marine Ecology Progress Series*, *646*, 45–68. https://doi.org/10.3354/meps13407

Ziegler, M., Roik, A., Porter, A., Zubier, K., Mudarris, M. S., Ormond, R., & Voolstra, C. R. (2016). Coral microbial community dynamics in response to anthropogenic impacts near a major city in the central Red Sea. *Marine Pollution Bulletin*, *105*(2), 629–640. https://doi.org/10.1016/j.marpolbul.2015.12.045

Zinser, E. R., Lindell, D., Johnson, Z. I., Futschik, M. E., Steglich, C., Coleman, M. L., Wright, M. A., Rector, T., Steen, R., McNulty, N., Thompson, L. R., & Chisholm, S. W. (2009). Choreography of the transcriptome, photophysiology, and cell cycle of a minimal photoautotroph, Prochlorococcus. *PLoS ONE*, *4*(4), 5135. https://doi.org/10.1371/journal.pone.0005135

Zubkov, M. V. (2014). Faster growth of the major prokaryotic versus eukaryotic CO2 fixers in the oligotrophic ocean. *Nature Communications*, *5*. https://doi.org/10.1038/ncomms4776